# Fundamentals of Fluid Mechanics

**MSc course**
**Department of Aeronautics**
**Imperial College London**

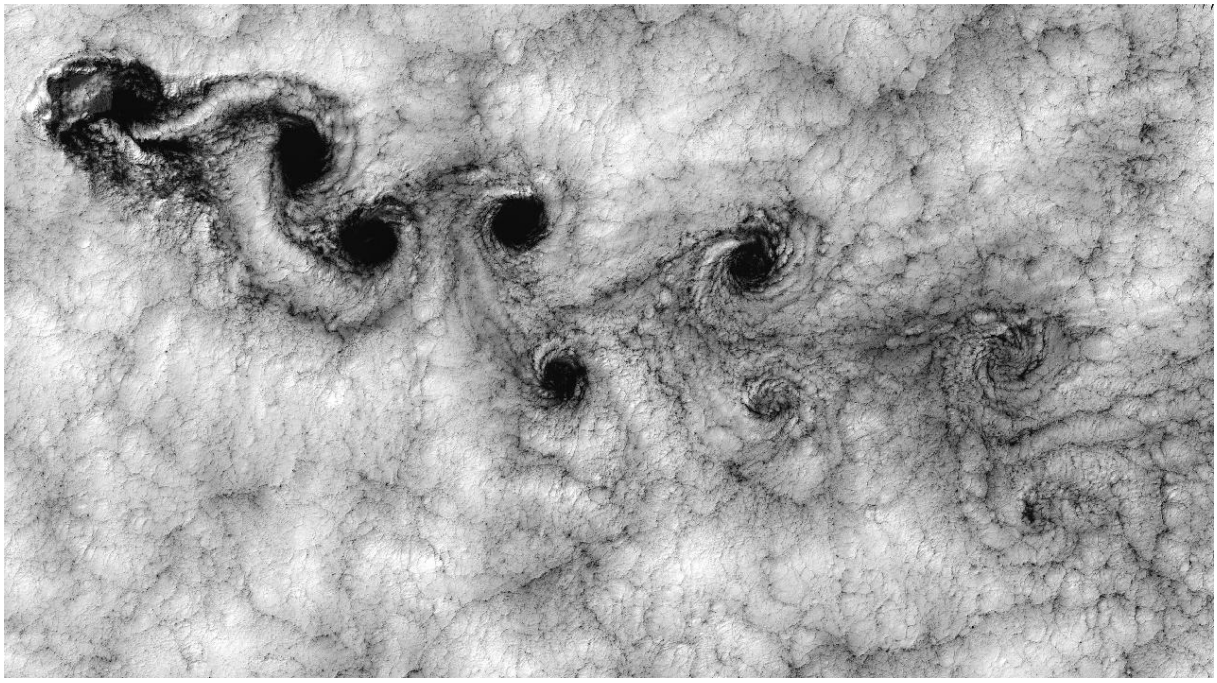

**Lecturer: Dr Cédric Beaume**
c.beaume@imperial.ac.uk
http://www.cbeaume.com

# Chapter 1

# Flow regimes

In this Chapter, we introduce duct flows and the main types of regimes these flows exhibit. We will in particular use the example of circular pipe flow as a qualitative case of study.

## 1.1 Examples of duct flows

### 1.1.1 Oil extraction

Oil reservoirs are found at various depths within the Earth's crust and are generally sandwiched between two layers of shale. Upon finding a natural oil reservoir, several techniques are employed to extract the oil. A schematic of this situation is shown in figure 1.1.

The first and conceptually simplest technique consists in creating an oil well by drilling a long hole into the Earth and placing a duct in it, connecting the reservoir oil to surface storage facilities. The oil reservoir possesses a higher pressure than the atmospheric one, thus the oil is pushed upwards along the duct. During this process, other phenomena start to play a role, such as viscous friction. Indeed, to move up the duct, the oil has to overcome its own resistance to flow against the walls.

When the pressure difference is no longer sufficient to drain oil, other techniques must be employed. Stream injection ranks among the favorite alternatives in which a second hole is created to inject steam. The effect on the oil is two-fold. As the volume of the reservoir is fixed, the addition of steam increases the pressure and pushes the oil further upwards in the duct. In addition, the increase in temperature resulting from the mixing of hot steam with cold oil reduces the viscosity of the latter which helps it go through the duct.

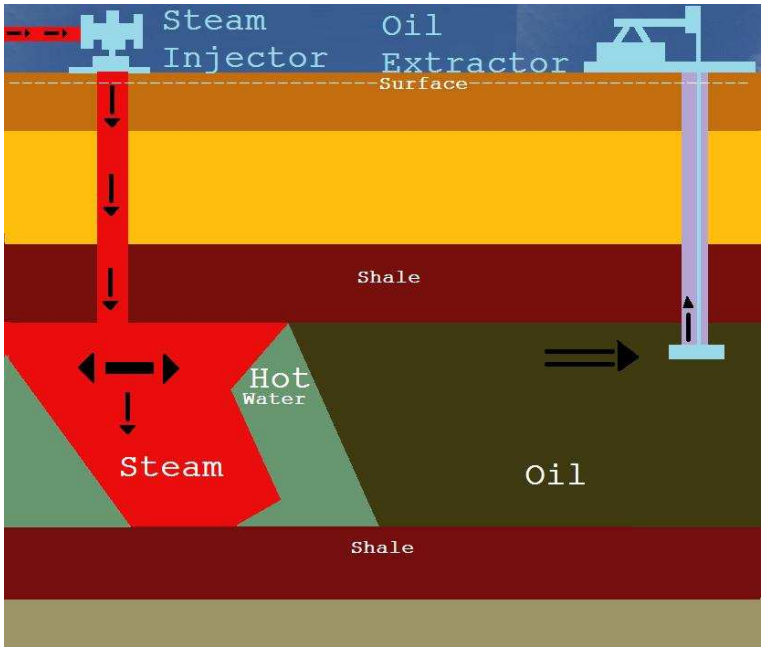


Figure 1.1: Schematic of an oil extraction site showing the oil reservoir sandwiched between two shale layers, an oil extractor and a steam injector.

### 1.1.2 Pipeline transport

Once the oil is extracted, transport systems have to be designed to bring the oil to storage or treatment sites. For large volume transport between two fixed sites, pipelines, such as the Trans-Alaska Pipeline System (TAPS), offer a great solution. This pipeline system was built between 1974 and 1977 to connect the Prudhoe Bay oil field (North in figure 1.2) to Valdez (South in figure 1.2). The pipeline is $1,300$km long, has a diameter of 1.2m and is driven by 11 pump stations, consisting in 4 pumps each, placed along the way. The maximum discharge of TAPS is $300,000\text{m}^3$/day and the construction itself costed about 8 billion 1977 US dollars. I am too afraid to convert this into modern pounds!

The construction and durability of TAPS were not easy to achieve. Engineers had to face many challenges.

For example, the oil extracted is substantially warmer than anything at the surface. This source of heat is dangerous for the permafrost (frozen ground), which may warm up and become unstable. To avoid this, radiators have been placed next to the pipeline. They absorb and dissipate the heat, limiting the impact on the permafrost. Such a radiator is shown in figure 1.3.

An other challenge faced by the designers is that of the seismic activity of Alaska. Indeed, the state of Alaska is known to be one of the most seismologically active regions in the world. To cope with these hazards, several solutions have been implemented to increase the flexibility of the pipeline and to make it less prone to cracks in case of an earthquake. The trajectory of the pipeline is wiggly and not a straight line between

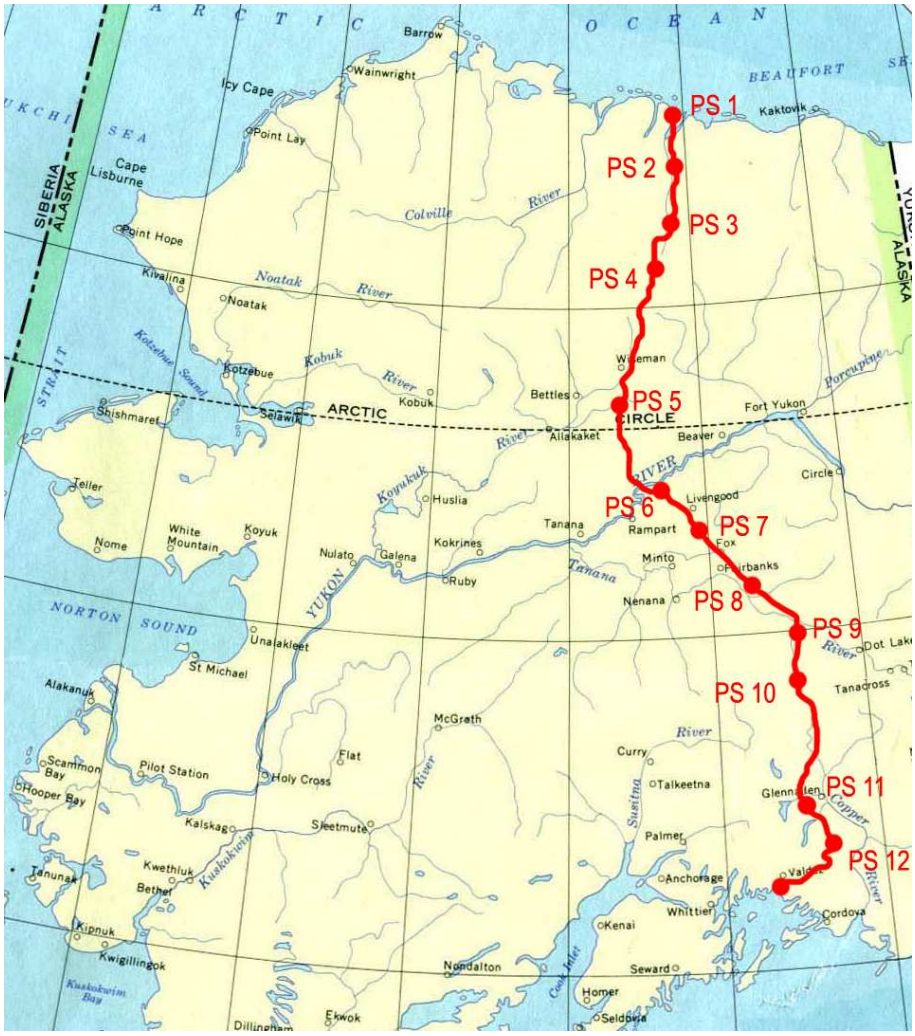


Figure 1.2: Map of the Trans-Alaska Pipeline System shown by the red line, going from Prudhoe Bay (North) to Valdez (South). The red dots labelled PS indicate pump stations (note: PS 11 was never built). More details can be found on `http://www.alyeska-pipe.com/` and `http://en.wikipedia.org/wiki/Trans-Alaska_Pipeline_System`.


Figure 1.3: Picture of the Trans-Alaska Pipeline. A radiator can be seen in the foreground while the wiggly structure of the pipeline is observable in the background. More details can be found on `http://www.alyeska-pipe.com/` and `http://en.wikipedia.org/wiki/Trans-Alaska_Pipeline_System`.

Figure 1.4: Formula 1 pit stop of Jos Verstappen (Benetton). The fuelman released the hose too early and fuel spilt around the car (left). A fraction of a second later, with the engine on, a fire was set (right).

Prudhoe Bay and Valdez to provide flexibility (see figure 1.3). In addition, in the supposedly riskiest zones, the pipeline has been placed on sliders to allow even more flexibility.

### 1.1.3 Other examples

Duct flows appear in an impressively large number of applications. It is by far the most efficient way of transporting fluids from one location to another and is therefore widely used in industry and for domestic and collective purposes.

Such flows are not as simple as they seem: they are viscous and can be time-dependent. These two characteristics create non-trivial interactions with the duct itself and have to be carefully taken into account during design. A bad design will lead to the failure of the duct. A spectacular example of such a failure (human or mechanical) in the world of Formula 1 is shown in figure 1.4. During a pit stop of the team Benetton, the fuelman released the hose too early. Spilling out of the car, the fuel lit up immediatly, providing these impressive images. An accident arising from the breaking of the hose fitting would result in the same consequences. I am sure there are other ways to warm up a driver!

Other applications of duct flows can be found in biological contexts such as the respiratory and circulatory system. The cerebral blood flow in the cortex can be modelled through a complex assembly of ducts, mimicking the vessel network present in the brain. Experimental data coupled with numerical simulations can then provide prediction of the pressure map in the brain (see figure 1.5). Access to these resuls can then be used to predict the risks of blockage or damage of the vessels and thus of brain stroke.

## 1.2 Reynolds's experiment

Osbourne Reynolds (1842–1912), British engineer, University of Manchester.

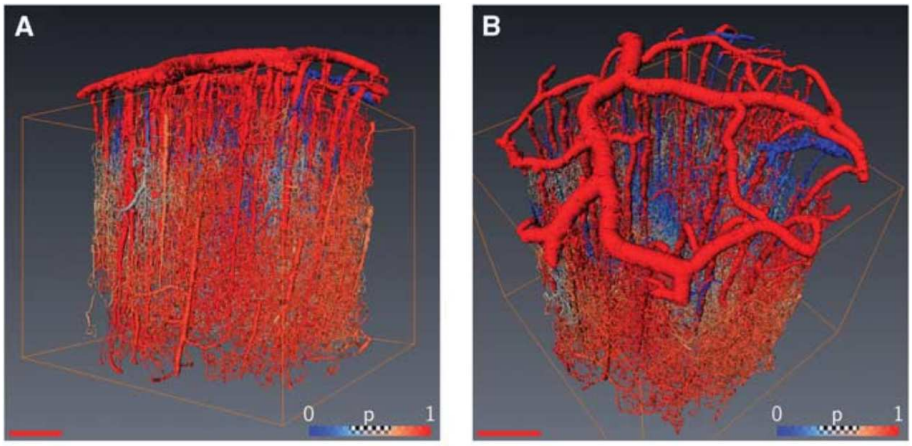


Figure 1.5: Calculation of the pressure in a pipe network obtained from experimental observations of a brain's geometry. Red indicates arteries (blood coming from the heart) while blue indicate veins (blood going back to the heart). After Guibert *et al.*, *J. Cereb. Blood Flow Metab.* **30**, 1860–1873 (2010).

In 1883, Osbourne Reynolds published his famous pipe flow experiment. He placed a pipe within a tank full of water. The water entered in the pipe through a converging cone to decrease the impact of entrance effects and the flow rate is controled by a valve. Aligned with the entrance of the pipe is a needle connected to a dye container. As the desired flow rate is reached, dye is injected within the pipe to trace out the fluid's trajectory. The sketch of the experimental apparatus is shown in figure 1.6.

### 1.2.1 Basic observations

Reynolds made a certain number of observations. In particular, he observed different flow regimes, as indicated by his own drawing in figure 1.7. He observed:

- Laminar flows: the fluid particles follow parallel trajectories. The flow appears smooth and ordered.
- Turbulent flows: the trajectories of fluid particles are no longer parallel. Spatial and temporal complexity appear. Flow data looks erratic and space and unpredictable. You could never succeed in intelligibly defining turbulence but you know it when you see it!

### 1.2.2 The Reynolds number

In addition to making these observations, it is possible to characterise these different regimes in a simple manner. The quantities that influence the flow are:

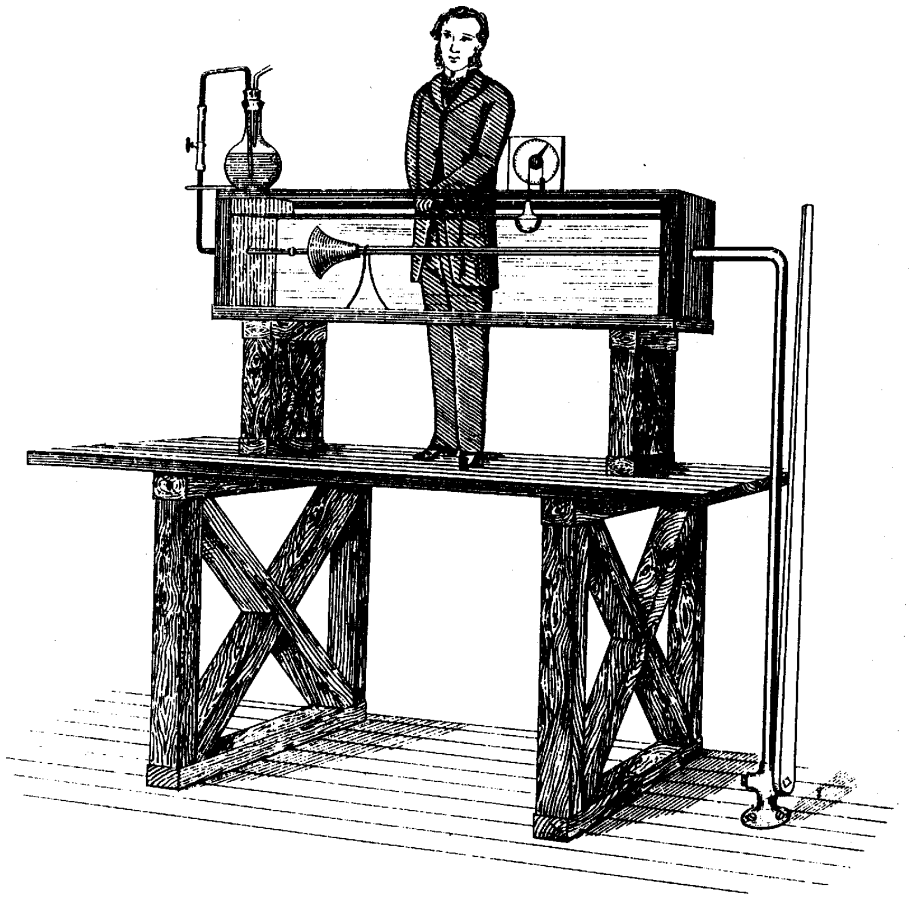

Figure 1.6: Sketch of Reynolds's experiment. After Reynolds, *Phil. Trans. R. Soc. Lond.* **174** (1883).

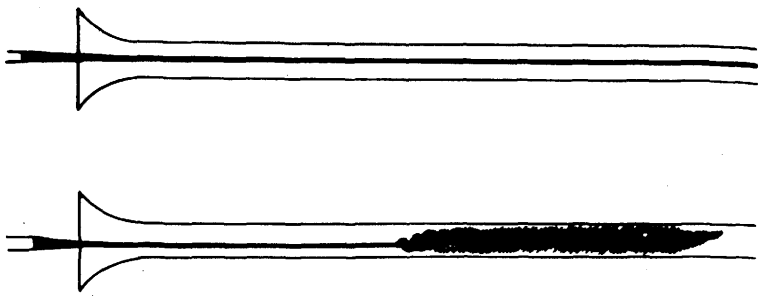

Figure 1.7: Reynolds's observations of laminar (top) and turbulent (bottom) flows. After Reynolds, *Phil. Trans. R. Soc. Lond.* **174** (1883).

- the pipe diameter $l$: $[l] = L$
- the fluid's velocity $u$: $[u] = L.T^{-1}$
- the fluid's density $\rho$: $[\rho] = M.L^{-3}$
- the fluid's dynamic viscosity $\mu$: $\mu = M.L^{-1}.T^{-1}$

We can combine these quantities to obtain a dimensionless number, the Reynolds number:

$$Re = \frac{\rho u l}{\mu}. \tag{1.1}$$

Therefore, to characterise the flow in the Reynolds experiment, only one quantity, the Reynolds number is needed. It follows that, for instance, doubling the velocity of the flow will have the same effect as decreasing the fluid's viscosity by half.

### 1.2.3 Laminar, transitional and turbulent flows

Figure 1.8 shows typical pictures obtained from pipe flow experiments. They allow to identify three regimes and their relation to the Reynolds number:

- Laminar flows: $0 \leq Re \lesssim 1000$
- Transitional flows: $1000 \lesssim Re \lesssim 4000$
- Turbulent flows: $4000 \lesssim Re$

Figure 1.8 provides spatial representations of the different flows at a fixed time. A complementary representation (temporal representation at a fixed spatial point) is sketched in figure 1.9.

The laminar regime is characterised by parallel trajectories and a time-independent pointwise velocity. Note that in figure 1.9, the velocity is shown as slightly varying to emphasize the experimental character of the study. These variations do not matter as any small disturbance of the laminar flow eventually vanishes. The flow is as simple as it can get.

In the turbulent regimes, the dye is no longer tracing a straight line but displays seamingly unstructured wiggles of different amplitudes. This translates into very complex temporal variations mixing low and high frequencies.

In between these two regimes, we find transitional flows, as exemplified in the second snapshot of figure 1.8. Transitional flows are constituted of locations where the dye describes straight lines (the flow appears laminar) interspersed by turbulent zones where the dye fluctuates in a similar way to turbulent flows (figure 1.9 central panel).

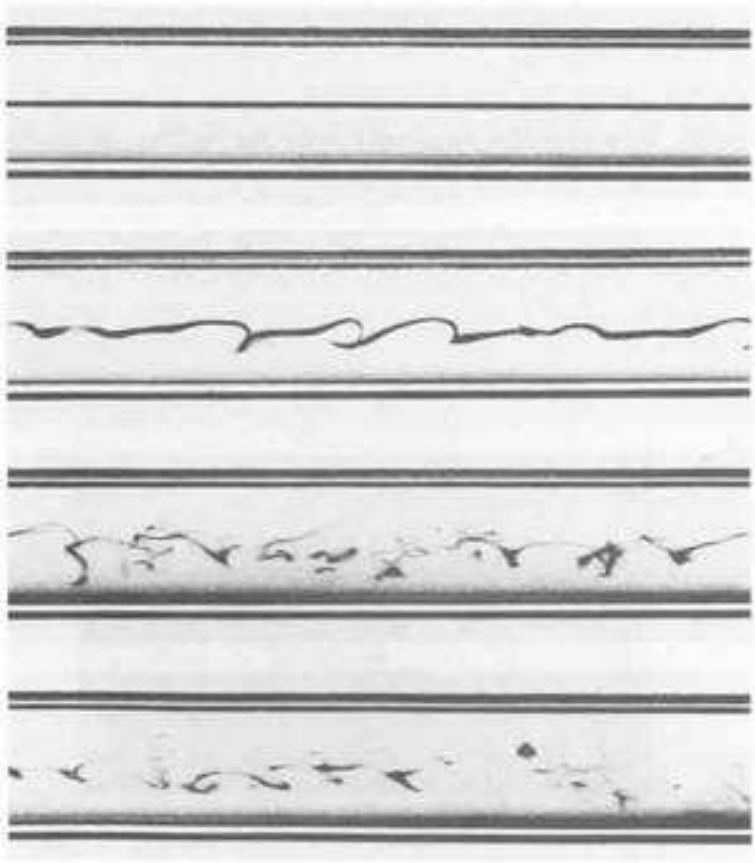

Figure 1.8: Photographs of pipe flow visualised using dye injection in the centerline. The Reynolds number is increased from top to bottom and the successive snapshots represent: laminar flow, transitional flow, turbulent flow, turbulent flow. After Van Dyke, *An Album of Fluid Motion* (1982).

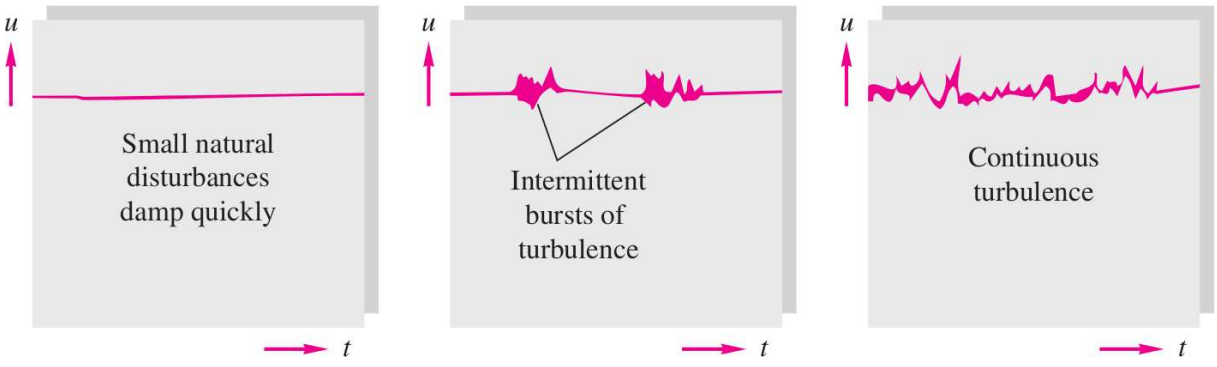


Figure 1.9: Sketch of the temporal variations of the streamwise velocity at a fixed location in the pipe. From left to right: laminar, transitional and turbulent regimes. After White, *Fluid Mechanics* (2011).

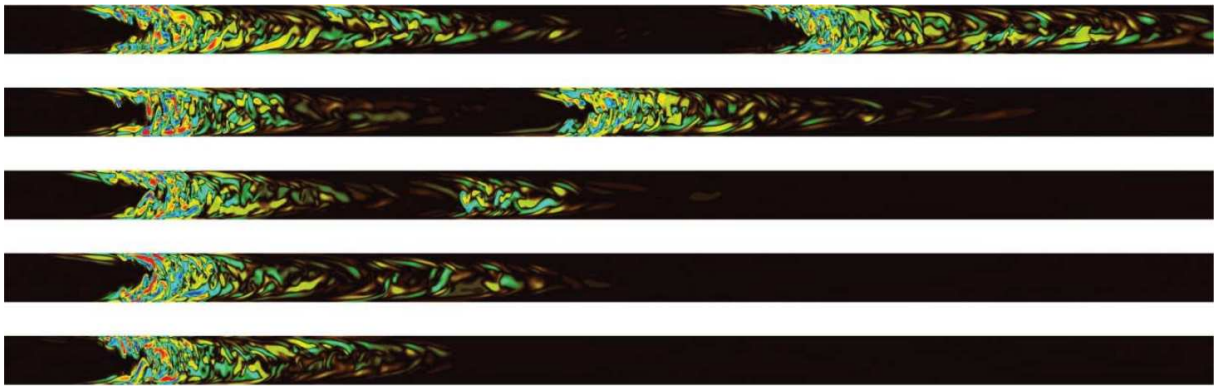

Figure 1.10: Visualisation of a puff going through a pipe and splitting. Time goes from bottom to top and the quantity represented is the streamwise vorticity, red (resp. blue) representing positive (resp. negative) values. The Reynolds number is 2300. After Avila *et al.*, *Science* **333**, 192 (2011).

### 1.2.4 Bursts and puffs

The intermittent bursts of turbulence displayed in the transitional regime are the signature of the passage of turbulent puffs. They can be observed by direct numerical simulation, like in figure 1.10 for $Re = 2300$. Such puffs are created by small perturbations and are turbulent regions surrounded by laminar flow. The upstream edge of the puff is well-defined, however the downstream edge is elongated and fuzzy.

Puffs typically evolve in two different ways. They can either vanish and the flow decays down to the laminar state or split, leading to an increasingly large turbulent fraction in the flow. Puffs decay rapidly in the laminar regime and split frequently in the turbulent regime, but they remain long-lived in the transitional one.

Avila *et al.* compared the mean lifetime of a puff before decay to that before splitting in pipe flow as a function of the Reynolds number. The results are shown in figure 1.11 and confirm that the puffs are long-lived over a wide range of Reynolds numbers. Lastly, the important result coming out of this figure is that there is an intersection between the decay and splitting lifetime curves. This intersection provides a well-defined legitimate threshold between laminar and turbulent flows: $Re_c \approx 2040$.

### 1.2.5 Examples

Water ($\rho \approx 10^3 \text{kg.m}^{-3}$, $\mu \approx 10^{-3} \text{kg.m}^{-1}.\text{s}^{-1}$) running out of the tap:

$$u \approx 1 \text{m.s}^{-1}, \qquad l \approx 10^{-2} \text{m} \tag{1.2}$$

$$\Rightarrow Re \approx 10^4, \tag{1.3}$$

yielding a turbulent flow.

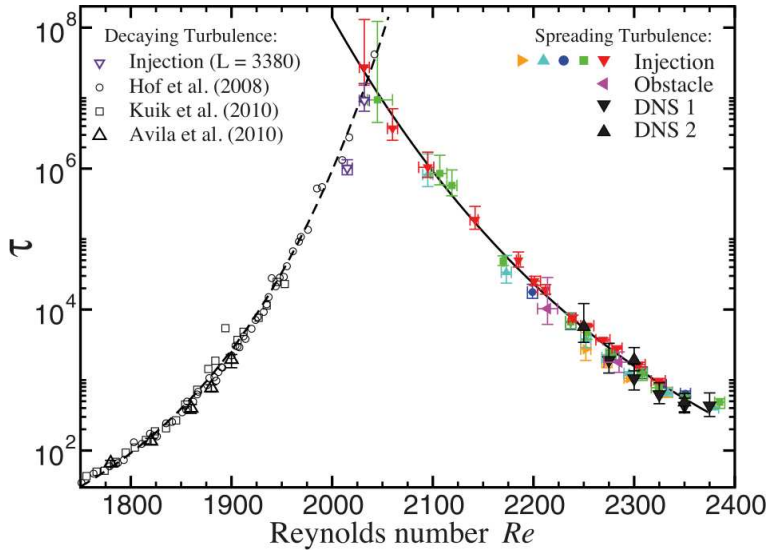


Figure 1.11: Mean lifetime of a puff before decay or splitting in pipe flow as a function of the Reynolds number. After Avila *et al.*, *Science* **333**, 192 (2011).

Air ($\rho \approx 1.2\text{kg.m}^{-3}$, $\mu \approx 1.8.10^{-5}\text{kg.m}^{-1}.\text{s}^{-1}$) in your mouth when you blow:

$$u \approx 1\text{m.s}^{-1}, \qquad l \approx 10^{-2}\text{m} \tag{1.4}$$

$$\Rightarrow Re \approx 700, \tag{1.5}$$

yielding a laminar flow. Note that as the flow exits your mouth into the room, it becomes turbulent as $l$ dramatically increases. The same flow in your lungs ($l \approx 10^{-3}\text{m}$) will also be laminar. Indeed, mass conservation implies that $u \approx 10\text{m.s}^{-1}$ providing the same value for the Reynolds number.

## 1.3 Other considerations

Most of the flows considered in this and the following Chapters are fully characterised using the simple Reynolds number. These flows provide a deep insight into basic fluid dynamics but rely on a certain number of assumptions, like the consideration of Newtonian fluids, incompressible flows, the absence of external forces, etc. We describe here some physics we have left out.

### 1.3.1 Rheology

We have introduced the dynamic (or absolute) viscosity $\mu$: $[\mu] = M.L^{-1}.T^{-1}$, that measures the fluid's resistance to flow. When an object moves into a fluid, or conversely the fluid moves past an object, a normal gradient of velocity is created due to the fluid sticking at the wall and not slipping along it. In the context of Newtonian fluids, this gradient of

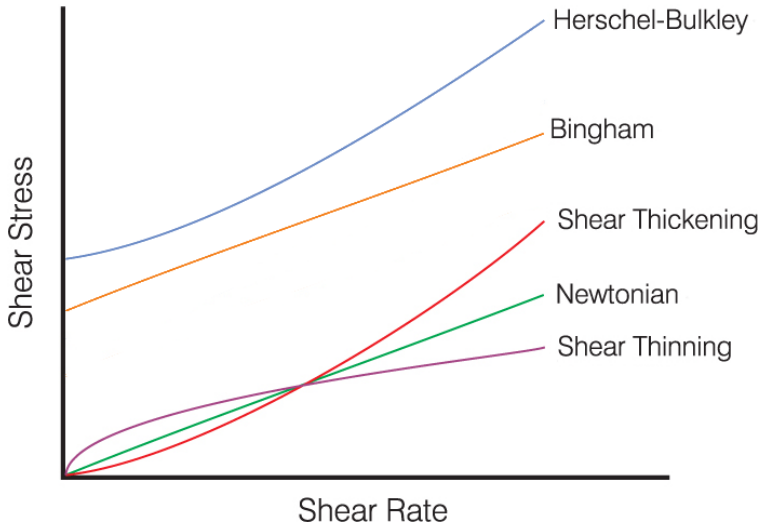


Figure 1.12: Rheological diagram showing the shear stress $\tau$ as a function of the shear rate $\partial_n u$ for several types of fluids.

velocity (also called shear or strain rate) is proportional to the wall shear stress:

$$\tau = \mu \partial_n u, \tag{1.6}$$

where the coefficient of proportionality is the dynamic viscosity. The shear stress-strain rate law for air and water are successfully approximated by a linear curve passing through the origin, they are Newtonian fluids. Unfortunately, not all fluids are that simple.

A sketch of some different types of rheological laws (shear stress $\tau$ versus shear rate $\partial_n u$) is shown in figure 1.12. Some fluids like ketchup become less and less viscous as they are stirred. They are shear thinning. Some other fluids like corn starch are are shear thickening: they get much harder to strain as they receive more stress. Other fluids have a threshold stress below which they behave like solids and above which their rheological law is linear. This is the case of mayonnaise: if you hang the open container upside down, it will not flow. An additional force is needed on the container to create a flow. Unfortunately, it's not sufficient to burn the calories you will eat... Tooth paste has a similar behavior. They form the class of Bingham fluids. Some other fluids behave in an even more complicated manner, like Herschel–Bulkley fluids (e.g. paint) or even time-dependent visco-elastic fluids (e.g. polymers).

All the fluids considered here and in the following Chapters are Newtonian fluids, therefore, the dynamic viscosity $\mu$ will be considered as constant.

### 1.3.2 Compressibility

Large values of the Reynolds number might coincide with high velocities, but some care must be taken. Indeed, if the flow approaches the speed of sound, the fluid becomes

compressible. This is best quantified using the Mach number:

$$Ma = \frac{u}{c}, \tag{1.7}$$

where $c$ is the speed of sound. Using this new dimensionless number, the following regimes are observed:

- $0 \leq Ma \lesssim 0.3$: incompressible flows
- $0.3 \lesssim Ma \leq 1$: compressible subsonic flows
- $1 \leq Ma$: supersonic flows

For $Ma \lesssim 0.3$, the fluid's density remains constant anywhere and at any time. If the Mach number is increased beyond 0.3, compressible effects start to become important and the density of the fluid changes in time and space, leading to contractions and dilatations. For $Ma \geq 1$, the flow is said supersonic and discontinuities of the pressure field appear: shock waves.

All the flows considered in this and the following Chapters are incompressible flows, therefore we restrict ourselves to flows where $u \leq 0.3\,c$ and for which the density $\rho$ is constant.

# Chapter 2

# Laminar flows

We have seen in Chapter 1 that several regimes of flow exist. We focus in this Chapter on laminar flows and will pay special attention to pipe flow.

## 2.1 Framework

### 2.1.1 The Navier–Stokes equation

Claude-Louis Navier (1785–1836), French engineer
George Gabriel Stokes (1819–1903), British mathematical physicist

The Navier–Stokes equation describes the motion of fluids under external forces. It writes:

$$\rho \left[\partial_t \mathbf{u} + (\mathbf{u} \cdot \nabla)\, \mathbf{u}\right] = -\nabla p + \mu \nabla^2 \mathbf{u} + \mathbf{f}, \tag{2.1}$$

where $\mathbf{u}$ is the (three-dimensional) velocity field, $p$ is the pressure, $\rho$ is the fluid's density, $t$ is the time, $\mu$ the fluid's dynamic viscosity and $\mathbf{f}$ the external body forces.

The left-hand-side of the Navier–Stokes equation (2.1) represents inertia. It involves the rate of change of the velocity with time $\partial_t \mathbf{u}$ as well as advection $(\mathbf{u} \cdot \nabla)\, \mathbf{u}$. The latter term quantifies how the fluid is transported by the flow velocity. In an equation such as the heat equation, this term applies to the temperature $T$, reads $(\mathbf{u} \cdot \nabla)\, T$ and quantifies how temperature is transported by the flow velocity.

The right-hand-side represents all the forces acting on the fluid. In addition to the external forces $\mathbf{f}$ that we will not take into account in this Chapter, the other terms come from the divergence of the stress tensor. They include the pressure gradient $-\nabla p$ that translates the fact that the fluid is attracted to low pressure regions and the viscous force $\mu \nabla^2 \mathbf{u}$ quantifying the internal friction between in the fluid.

### 2.1.2 Incompressibility

As the mass of the fluid is conserved, we can write the continuity equation:

$$\partial_t \rho + \nabla \cdot (\rho \mathbf{u}) = 0, \tag{2.2}$$

or

$$\partial_t \rho + (\mathbf{u} \cdot \nabla)\, \rho + \rho\, (\nabla \cdot \mathbf{u}) = 0. \tag{2.3}$$

As we consider incompressible flows, the density does not vary with time or position and the continuity equation simplifies into the incompressibility constraint:

$$\nabla \cdot \mathbf{u} = 0, \tag{2.4}$$

which implies that given a control volume, the quantity of incoming fluid is equal to that exiting the control volume.

### 2.1.3 Additional hypotheses

In this Chapter, we focus exclusively on laminar flows. We recall that we defined such flows in Chapter 1 by saying that the fluid follows parallel trajectories and is as simple as it can get. We will then make some assumptions to simplify the equations in a consistent manner with the above definition. In particular, we will assume:

- stationarity: $\partial_t \equiv 0$
- unidirectionality: the flow is parallel to the walls
- symmetry: the flow is further simplified using the symmetries of the geometry

## 2.2 Pipe flow

### 2.2.1 Cylindrical coordinates

A sketch of the geometry and the coordinates we will use is shown in figure 2.1.

Some important relationships to keep in mind are the definition of the new coordinates:

$$r = \sqrt{x^2 + y^2}, \qquad \theta = \tan^{-1} \frac{y}{x}, \qquad z = z, \tag{2.5}$$

or

$$x = r \cos\theta, \qquad y = r \sin\theta, \qquad z = z. \tag{2.6}$$

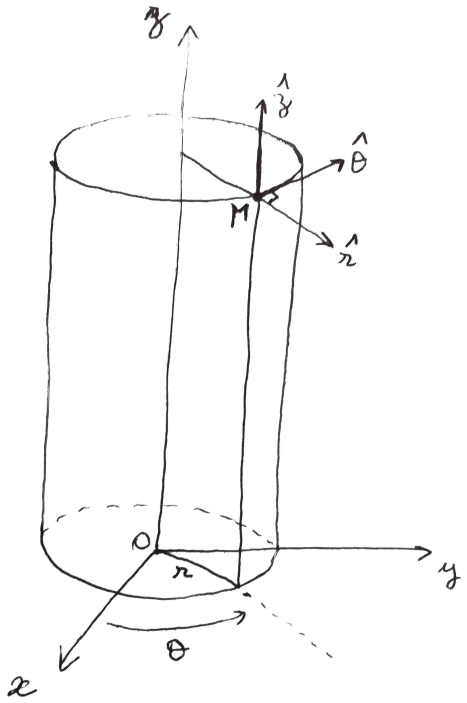


Figure 2.1: Sketch of the cylindrical geometry associated with pipes.

In this new coordinate system, the line element writes:

$$ds = dr\,\hat{\mathbf{r}} + rd\theta\,\hat{\theta} + dz\,\hat{\mathbf{z}}, \tag{2.7}$$

and hence, the gradient operator writes:

$$\nabla = \partial_r \hat{\mathbf{r}} + \frac{1}{r}\partial_\theta \hat{\theta} + \partial_z \hat{\mathbf{z}}. \tag{2.8}$$

Lastly, it is important to remember that unlike with Cartesian coordinates, here, the directions change with $\theta$ and as a consequence:

$$\partial_\theta \hat{\mathbf{r}} = \hat{\theta}, \qquad \partial_\theta \hat{\theta} = -\hat{\mathbf{r}}. \tag{2.9}$$

### 2.2.2 Governing equations

In cylindrical coordinates, the velocity field reads:

$$\mathbf{u} = u_r\,\hat{\mathbf{r}} + u_\theta\,\hat{\theta} + u_z\,\hat{\mathbf{z}}. \tag{2.10}$$

To obtain the governing equations in cylindrical coordinates, we proceed step by step. First, we work on the incompressibility condition:

$$\nabla \cdot \mathbf{u} = 0 \tag{2.11}$$

$$\Rightarrow \quad \left(\partial_r \hat{\mathbf{r}} + \frac{1}{r}\partial_\theta \hat{\theta} + \partial_z \hat{\mathbf{z}}\right) \cdot \left(u_r\, \hat{\mathbf{r}} + u_\theta\, \hat{\theta} + u_z\, \hat{\mathbf{z}}\right) = 0 \tag{2.12}$$

$$\Rightarrow \quad \partial_r u_r + \frac{1}{r} u_r + \frac{1}{r}\partial_\theta u_\theta + \partial_z u_z = 0 \tag{2.13}$$

$$\Rightarrow \quad \frac{1}{r}\left(\partial_r (r u_r)\right) + \frac{1}{r}\partial_\theta u_\theta + \partial_z u_z = 0 \tag{2.14}$$

For the Navier–Stokes equation, we start by expressing the advection term:

$$(\mathbf{u} \cdot \nabla)\, \mathbf{u} \quad = \left(u_r \partial_r + \frac{u_\theta}{r}\partial_\theta + u_z \partial_z\right)\left(u_r\, \hat{\mathbf{r}} + u_\theta\, \hat{\theta} + u_z\, \hat{\mathbf{z}}\right) \tag{2.15}$$

$$\begin{aligned} &= u_r \partial_r u_r\, \hat{\mathbf{r}} + u_r \partial_r u_\theta\, \hat{\theta} + u_r \partial_r u_z\, \hat{\mathbf{z}} \ldots \\ &\qquad + \frac{u_\theta}{r}\partial_\theta u_r\, \hat{\mathbf{r}} + \frac{u_\theta}{r} u_r\, \hat{\theta} + \frac{u_\theta}{r}\partial_\theta u_\theta\, \hat{\theta} - \frac{u_\theta}{r} u_\theta\, \hat{\mathbf{r}} + \frac{u_\theta}{r}\partial_\theta u_z\, \hat{\mathbf{z}} \ldots \\ &\qquad + u_z \partial_z u_r\, \hat{\mathbf{r}} + u_z \partial_z u_\theta\, \hat{\theta} + u_z \partial_z u_z\, \hat{\mathbf{z}} \end{aligned} \tag{2.16}$$

$$\begin{aligned} &= \left(u_r \partial_r u_r + \frac{u_\theta}{r}\partial_\theta u_r - \frac{u_\theta^2}{r} + u_z \partial_z u_r\right) \hat{\mathbf{r}} \ldots \\ &\qquad + \left(u_r \partial_r u_\theta + \frac{u_r u_\theta}{r} + \frac{u_\theta}{r}\partial_\theta u_\theta + u_z \partial_z u_\theta\right) \hat{\theta} \ldots \\ &\qquad + \left(u_r \partial_r u_z + \frac{u_\theta}{r}\partial_\theta u_z + u_z \partial_z u_z\right) \hat{\mathbf{z}}. \end{aligned} \tag{2.17}$$

Then, we work on the Laplacian:

$$\nabla^2 \quad = \nabla \cdot \nabla \tag{2.18}$$

$$= \left(\partial_r \hat{\mathbf{r}} + \frac{1}{r}\partial_\theta \hat{\theta} + \partial_z \hat{\mathbf{z}}\right) \cdot \left(\partial_r \hat{\mathbf{r}} + \frac{1}{r}\partial_\theta \hat{\theta} + \partial_z \hat{\mathbf{z}}\right) \tag{2.19}$$

$$= \partial_r^2 + \frac{1}{r}\partial_r + \frac{1}{r^2}\partial_\theta^2 + \partial_z^2 \tag{2.20}$$

$$= \frac{1}{r}\partial_r\left(r \partial_r\right) + \frac{1}{r^2}\partial_\theta^2 + \partial_z^2, \tag{2.21}$$

which yields:

$$\nabla^2\mathbf{u} = \left(\frac{1}{r}\partial_r\left(r\partial_r\right) + \frac{1}{r^2}\partial_\theta^2 + \partial_z^2\right)\left(u_r\hat{\mathbf{r}} + u_\theta\hat{\theta} + u_z\hat{\mathbf{z}}\right) \tag{2.22}$$

$$\begin{aligned} &= \frac{1}{r}\partial_r\left(r\partial_r u_r\right)\hat{\mathbf{r}} + \frac{1}{r}\partial_r\left(r\partial_r u_\theta\right)\hat{\theta} + \frac{1}{r}\partial_r\left(r\partial_r u_z\right)\hat{\mathbf{z}}\ldots \\ &\qquad + \frac{1}{r^2}\partial_\theta^2 u_r\hat{\mathbf{r}} - \frac{u_r}{r^2}\hat{\mathbf{r}} + \frac{2}{r^2}\partial_\theta u_r\hat{\theta} + \frac{1}{r^2}\partial_\theta^2 u_\theta\hat{\theta} - \frac{u_\theta}{r^2}\hat{\theta} - \frac{2}{r^2}\partial_\theta u_\theta\hat{\mathbf{r}} + \frac{1}{r^2}\partial_\theta^2 u_z\hat{\mathbf{z}}\ldots \\ &\qquad + \partial_z^2 u_r\hat{\mathbf{r}} + \partial_z^2 u_\theta\hat{\theta} + \partial_z^2 u_z\hat{\mathbf{z}} \end{aligned} \tag{2.23}$$

$$\begin{aligned} &= \left[\frac{1}{r}\partial_r\left(r\partial_r u_r\right) + \frac{1}{r^2}\partial_\theta^2 u_r - \frac{u_r}{r^2} - \frac{2}{r^2}\partial_\theta u_\theta + \partial_z^2 u_r\right]\hat{\mathbf{r}}\ldots \\ &\qquad + \left[\frac{1}{r}\partial_r\left(r\partial_r u_\theta\right) + \frac{2}{r^2}\partial_\theta u_r + \frac{1}{r^2}\partial_\theta^2 u_\theta - \frac{u_\theta}{r^2} + \partial_z^2 u_\theta\right]\hat{\theta}\ldots \\ &\qquad + \left[\frac{1}{r}\partial_r\left(r\partial_r u_z\right) + \frac{1}{r^2}\partial_\theta^2 u_z + \partial_z^2 u_z\right]\hat{\mathbf{z}}. \end{aligned} \tag{2.24}$$

We can combine these expressions to write the Navier–Stokes equation in cylindrical coordinates:

$$\begin{aligned} \rho\left[\partial_t u_r + u_r\partial_r u_r + \frac{u_\theta}{r}\partial_\theta u_r - \frac{u_\theta^2}{r} + u_z\partial_z u_r\right] &= -\partial_r p\ldots \\ &\quad + \mu\left[\frac{1}{r}\partial_r\left(r\partial_r u_r\right) + \frac{1}{r^2}\partial_\theta^2 u_r - \frac{u_r}{r^2} - \frac{2}{r^2}\partial_\theta u_\theta + \partial_z^2 u_r\right], \end{aligned} \tag{2.25}$$

$$\begin{aligned} \rho\left[\partial_t u_\theta + u_r\partial_r u_\theta + \frac{u_r u_\theta}{r} + \frac{u_\theta}{r}\partial_\theta u_\theta + u_z\partial_z u_\theta\right] &= -\frac{1}{r}\partial_\theta p\ldots \\ &\quad + \mu\left[\frac{1}{r}\partial_r\left(r\partial_r u_\theta\right) + \frac{2}{r^2}\partial_\theta u_r + \frac{1}{r^2}\partial_\theta^2 u_\theta - \frac{u_\theta}{r^2} + \partial_z^2 u_\theta\right], \end{aligned} \tag{2.26}$$

$$\begin{aligned} \rho\left[\partial_t u_z + u_r\partial_r u_z + \frac{u_\theta}{r}\partial_\theta u_z + u_z\partial_z u_z\right] &= -\partial_z p\ldots \\ &\quad + \mu\left[\frac{1}{r}\partial_r\left(r\partial_r u_z\right) + \frac{1}{r^2}\partial_\theta^2 u_z + \partial_z^2 u_z\right]. \end{aligned} \tag{2.27}$$

### 2.2.3 Solution

The pipe is constituted of no-slip walls, i.e., the fluid particles in contact with the walls remain static. This boundary condition writes:

$$\mathbf{u}(r = R) = \mathbf{0}, \tag{2.28}$$

where $R$ is the radius of the pipe ($r = 0$ being its center). Based on Section 2.1.3, we make the further assumptions:

- $u_r = 0$: no radial motion
- $u_\theta = 0$: no spiraling motion

- $\partial_\theta \mathbf{u} = \mathbf{0}$: axisymmetric flow

The first two hypotheses lead to the velocity being unidirectional and the third one indicates it does not vary with $\theta$: $\mathbf{u} = u_z(r, z)\hat{\mathbf{z}}$.

We now examine what remains from equations (2.25)–(2.27) once the above hypotheses are used. The incompressibility constraints simplifies into:

$$\partial_z u_z = 0, \tag{2.29}$$

which, together with the above hypotheses reduces the velocity to:

$$\mathbf{u} = u_z(r)\hat{\mathbf{z}}. \tag{2.30}$$

The Navier–Stokes equation in the radial and in the azimuthal direction (2.25) and (2.26) yields:

$$\partial_r p = \partial_\theta p = 0, \tag{2.31}$$

which gives:

$$p = p(z). \tag{2.32}$$

Lastly, the Navier–Stokes equation in the streamwise direction reduces to:

$$0 = -\partial_z p + \frac{\mu}{r}\partial_r \left(r\partial_r u_z\right). \tag{2.33}$$

We note that, upon derivation of equation (2.33) with respect to $z$: $\partial_z^2 p = 0$ and therefore that the gradient of pressure is a constant independent of the location in the flow. We integrate equation (2.33) twice:

$$\partial_r \left(r\partial_r u_z\right) = \frac{r\,\partial_z p}{\mu} \tag{2.34}$$

$$\Rightarrow \quad \partial_r u_z = \frac{r\,\partial_z p}{2\mu} + \frac{k_1}{r} \tag{2.35}$$

$$\Rightarrow \quad u_z = \frac{r^2 \partial_z p}{4\mu} + k_1 \ln r + k_2, \tag{2.36}$$

where $k_1$ and $k_2$ are real constants of integration to be determined. To avoid a singularity at the center of the pipe $r = 0$, it is necessary to fix $k_1 = 0$. The other constant is determined using the boundary condition:

$$u_z(R) = 0 \tag{2.37}$$

$$\Rightarrow \quad k_2 = -\frac{R^2 \partial_z p}{4\mu}. \tag{2.38}$$

Therefore, the laminar pipe flow, also known as Poiseuille flow follows a quadratic law:

$$u_z = \frac{R^2 \partial_z p}{4\mu}\left(\frac{r^2}{R^2} - 1\right), \tag{2.39}$$

ans is sketched in figure 2.2 for negative pressure gradients.

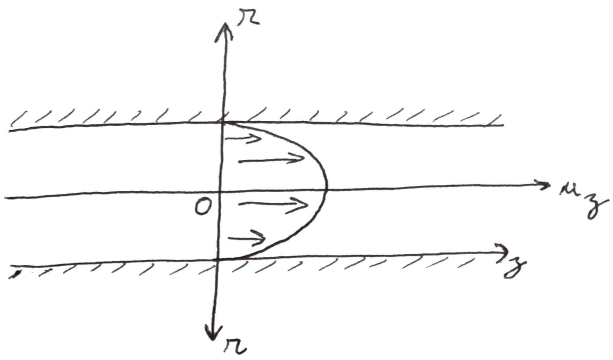


Figure 2.2: Laminar pipe flow: Poiseuille flow.

### 2.2.4 Some characteristic quantities

It is obvious based on the symmetries of the solution that its maximum is reached at the center of the pipe:

$$u_{zmax} = u_z(0) = -\frac{R^2 \partial_z p}{4\mu}, \tag{2.40}$$

showing that the flow goes against the gradient of pressure, from the high pressure to the low pressure regions. We will use the convention that $\partial_z p < 0$ in what follows so that the fluid goes from left to right: $u_z > 0$.

The average velocity can be calculated as follows:

$$u_{zavg} = \frac{1}{A} \int u_z dA, \tag{2.41}$$

where $A$ is the pipe section and $dA = r dr d\theta$. It follows:

$$\begin{aligned} u_{zavg} &= \frac{1}{\pi R^2} \int_0^{2\pi} \int_0^R \frac{R^2 \partial_z p}{4\mu} \left( \frac{r^2}{R^2} - 1 \right) r dr d\theta && (2.42) \\ &= \frac{\partial_z p}{2\mu} \int_0^R \left( \frac{r^3}{R^2} - r \right) dr && (2.43) \\ &= -\frac{R^2 \partial_z p}{8\mu}, && (2.44) \end{aligned}$$

which can be expressed as a function of the maximum velocity:

$$u_{zavg} = \frac{1}{2} u_{zmax}. \tag{2.45}$$

We can also calculate the flow rate:

$$\begin{aligned} Q &= A u_{zavg} && (2.46) \\ &= -\frac{\pi R^4 \partial_z p}{8\mu}. && (2.47) \end{aligned}$$

If the pipe has length $L$, we can introduce the total pressure drop in the pipe: $\triangle p = -\partial_z p L$ to get

$$Q = \frac{\pi R^4 \triangle p}{8\mu L}. \tag{2.48}$$

Lastly, we can express the wall shear stress $\tau_w$:

$$\tau_w = \mu |\partial_n u_z|_R, \tag{2.49}$$

where $\partial_n$ denotes the derivative normal to the wall. In the present case, we have:

$$\tau_w = \mu |\partial_r u_z|_R \tag{2.50}$$

$$= -\frac{\partial_z p R}{2}. \tag{2.51}$$

Note that the wall shear stress of laminar pipe flow can be related to the average velocity (and therefore to the flow rate):

$$\tau_w = \frac{4\mu u_{zavg}}{R}. \tag{2.52}$$

## 2.3 Other cases of interest

### 2.3.1 Non-viscous pipe flow

Leonhard Euler (1707–1783), Swiss mathematician

Inviscid flows are governed by the Euler equation, which are nothing else but the Navier–Stokes equation without the viscous term:

$$\rho \left[\partial_t \mathbf{u} + (\mathbf{u} \cdot \nabla)\, \mathbf{u}\right] = -\nabla p. \tag{2.53}$$

The incompressibility constraint is, however, unchanged:

$$\nabla \cdot \mathbf{u} = 0. \tag{2.54}$$

Because the fluid is non viscous, the no-slip boundary condition does not make sense: the fluid cannot stick to the wall. Instead, a free-slip boundary condition where the wall is considered unpenetrable and stress-free can be imposed:

$$u_r(R) = 0, \qquad \partial_r u_\theta|_R = 0, \qquad \partial_r u_z|_R = 0. \tag{2.55}$$

The incompressibility constraint simplifies into:

$$\partial_z u_z = 0 \tag{2.56}$$

$$\Rightarrow \quad u_z = \text{cst}, \tag{2.57}$$

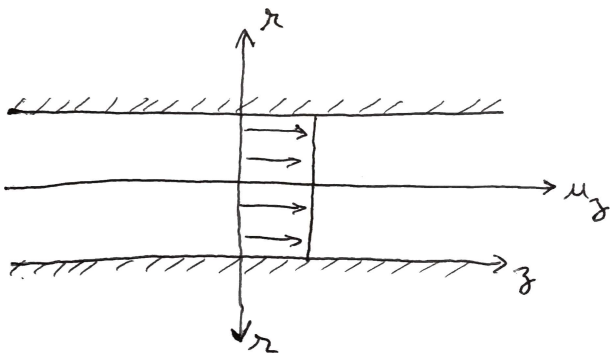

Figure 2.3: Inviscid laminar pipe flow: plug flow.

providing a different kind of flow: plug flow (figure 2.3).

The velocity being constant, its maximum and average values are equal and trivially obtained:

$$u_{zmax} = u_{zavg} = u_z. \tag{2.58}$$

The flow rate is:

$$Q = Au_z = \pi R^2 u_z. \tag{2.59}$$

Lastly, the fluid being non-viscous, there is no friction at the wall and therefore no wall shear stress.

### 2.3.2 Channel flow

Jean Léonard Marie Poiseuille (1797–1869), French physicist, École polytechnique

We study now channel flow, i.e., a three-dimensional flow confined between two parallel plates and driven similarly to pipe flow by a pressure gradient. A sketch of the configuration is shown in figure 2.4.

This time, we work in Cartesian coordinates and therefore write:

$$\mathbf{u} = u_x\hat{\mathbf{x}} + u_y\hat{\mathbf{y}} + u_z\hat{\mathbf{z}}. \tag{2.60}$$

The presence of no-slip walls dictates the following boundary condition:

$$\mathbf{u}(y = \pm h) = \mathbf{0}. \tag{2.61}$$

We look for a laminar solution under the following hypotheses:

- $u_y = 0$: no wall-normal flow
- $u_z = 0$: the velocity is unidirectional and therefore projected onto $x$

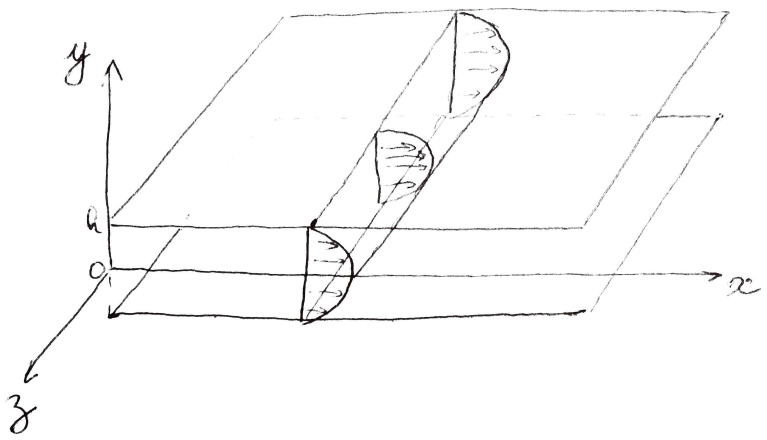


Figure 2.4: Sketch of channel flow between two parallel plates and driven by a pressure gradient in the $x$ direction.

- $\partial_z u_x = 0$: the flow is spanwise invariant

The first two hypotheses lead to the velocity having only one non-vanishing component while the third one indicates it only varies in the streamwise and wall-normal directions: $\mathbf{u} = u_x(x, y)\hat{\mathbf{x}}$.

We recall the writing of the incompressibility constraint in Cartesian coordinates:

$$\partial_x u_x + \partial_y u_y + \partial_z u_z = 0, \tag{2.62}$$

and of the Navier–Stokes equation:

$$\rho\left[\partial_t u_x + u_x\partial_x u_x + u_y\partial_y u_x + u_z\partial_z u_x\right] = -\partial_x p + \mu\left[\partial_x^2 u_x + \partial_y^2 u_x + \partial_z^2 u_x\right], \tag{2.63}$$
$$\rho\left[\partial_t u_y + u_x\partial_x u_y + u_y\partial_y u_y + u_z\partial_z u_y\right] = -\partial_y p + \mu\left[\partial_x^2 u_y + \partial_y^2 u_y + \partial_z^2 u_y\right], \tag{2.64}$$
$$\rho\left[\partial_t u_z + u_x\partial_x u_z + u_y\partial_y u_z + u_z\partial_z u_z\right] = -\partial_z p + \mu\left[\partial_x^2 u_z + \partial_y^2 u_z + \partial_z^2 u_z\right]. \tag{2.65}$$

The incompressibility constraint (2.62) yields:

$$\partial_x u_x = 0, \tag{2.66}$$

which, together with the starting hypotheses provides:

$$\mathbf{u} = u_x(y)\hat{\mathbf{x}}. \tag{2.67}$$

The Navier–Stokes equation in the wall-normal and spanwise directions (2.64) and (2.65) give:

$$\partial_y p = \partial_z p = 0, \tag{2.68}$$

thus:

$$p = p(x). \tag{2.69}$$

Eventually, the Navier–Stokes equation in the streamwise direction (2.63) gives:

$$0 = -\partial_x p + \mu \partial_y^2 u_x, \tag{2.70}$$

which is solved in the same fashion as for pipe flow. The solution reads

$$u_x = \frac{\partial_x p}{2\mu} y^2 + k_1 y + k_2, \tag{2.71}$$

where $k_1$ and $k_2$ are solved for using the boundary conditions:

$$\frac{\partial_x p}{2\mu} h^2 + k_1 h + k_2 = 0, \tag{2.72}$$

$$\frac{\partial_x p}{2\mu} h^2 - k_1 h + k_2 = 0, \tag{2.73}$$

yielding:

$$k_1 = 0, \qquad k_2 = -\frac{\partial_x p\, h^2}{2\mu}. \tag{2.74}$$

The trivial laminar flow in a channel, also called plane Poiseuille flow, then reads:

$$u_x = \frac{\partial_x p\, h^2}{2\mu} \left( \frac{y^2}{h^2} - 1 \right). \tag{2.75}$$

## 2.4 Gaining in generality

To gain in generality, we can non-dimensionalise the equations. We introduce $\mathcal{L}$, $\mathcal{U}$, $\mathcal{L}/\mathcal{U}$, and $\mathcal{P}$ as dimensional units of length, velocity, time and pressure. We therefore write:

$$(x, y, z) = \mathcal{L}(x', y', z'), \tag{2.76}$$

$$u = \mathcal{U} u', \tag{2.77}$$

$$t = \frac{\mathcal{L}}{\mathcal{U}} t', \tag{2.78}$$

$$p = \mathcal{P} p', \tag{2.79}$$

where the dimensionless quantities are denoted with a prime.

Upon substitution in the Navier–Stokes equations, we obtain:

$$\frac{\rho \mathcal{U}^2}{\mathcal{L}} \left[ \partial_{t'} u' + (u' \cdot \nabla') u' \right] = -\frac{\mathcal{P}}{\mathcal{L}} \nabla' p' + \frac{\mu \mathcal{U}}{\mathcal{L}^2} \nabla'^2 u'. \tag{2.80}$$

We can define the pressure scale to be a dynamic pressure scale: $\mathcal{P} = \rho \mathcal{U}^2$ and introduce the Reynolds number: $Re = \rho \mathcal{U} \mathcal{L} / \mu$. The resulting equation is:

$$\partial_{t'} u' + (u' \cdot \nabla') u' = -\nabla' p' + \frac{1}{Re} \nabla'^2 u'. \tag{2.81}$$

To solve this equation, only one number is required: the Reynolds number, as opposed to the original dimensional equation that required two ($\rho$ and $\mu$).

# Chapter 3

# Viscous losses

In this Chapter, we discuss general results on the losses due to viscous effects in pipe flow.

## 3.1 Pressure drop

### 3.1.1 Experimental evidence

Gotthilf Hagen (1797–1884), German engineer

In 1839, Hagen studied water flows in long brass pipes and hinted at the possible existence of two different regimes of viscous flows: laminar and turbulent.

He characterised, in particular, laminar flows through the following law:

$$\triangle p = k \frac{LQ}{R^4} + \text{entrance effects}, \tag{3.1}$$

where $k = \text{cst}$, $L$ is the length of the pipe, $Q$ the flow rate and $R$ the radius of the pipe.

As he increased $Q$ beyond a certain threshold, Hagen observed that this law broke down, and deduced the existence of a second regime. This experimental observations are easily reproduced and the results sketched in figure 3.1.

### 3.1.2 Dimensional analysis

We consider a laminar flow in a horizontal pipe for which density and gravity effects are negligible. The pressure drop $\triangle p$ has dimension $[\triangle p] = M.L^{-1}.T^{-2}$. The relevant quantities to characterise the pressure drop are:

- the flow rate $Q$: $[Q] = L^3.T^{-1}$

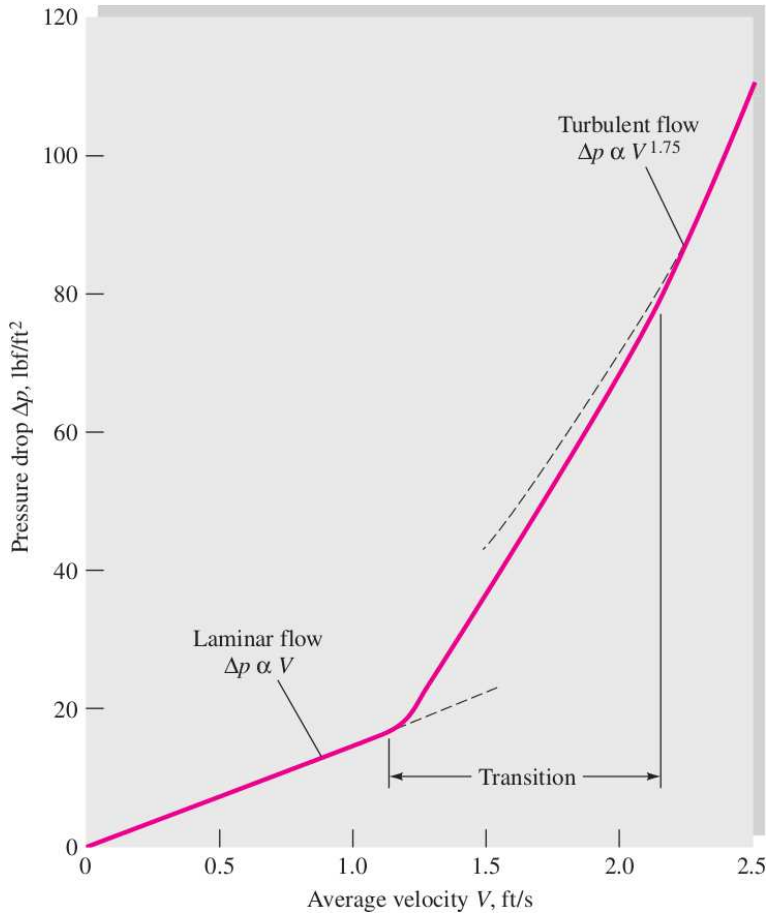


Figure 3.1: Relationship between the pressure drop $\triangle p$ and the average velocity $V$ in a pipe with radius 3mm and length 3m. After White, *Fluid Mechanics* (2011).

- the pipe length $L$: $[L] = L$
- the pipe radius $R$: $[R] = L$
- the fluid's dynamic viscosity $\mu$: $[\mu] = M.L^{-1}.T^{-1}$

As the pressure gradient is constant along the pipe and the flow fully characterised by the radial direction only, we can write

$$\frac{\triangle p}{L} = \mathcal{F}(Q, R, \mu), \tag{3.2}$$

where $\mathcal{F}$ indicate the dependence of the left-hand-side on the variables between parentheses only.

We note that the left-hand-side has dimension proportional to a mass $M$ and that only the dynamic viscosity has dimension proportional to a mass. We can then divide by the dynamic viscosity to get rid of this dimension.

$$\frac{\triangle p}{\mu L} = \mathcal{F}(Q, R). \tag{3.3}$$

The dimension of the left-hand-side is now proportional to the inverse of a length, so we can multiply it by $R$ to get rid of the length dimension. Similarly, $Q$ has dimension proportional to cube lengths so we can divide it by $R^3$. The resulting relationship reads

$$\frac{R\triangle p}{\mu L} = \mathcal{F}\left(\frac{Q}{R^3}\right). \tag{3.4}$$

At this stage, both the left-hand-side and the right-hand-side terms are both homogeneous to the inverse of a time. Upon dividing the one by the other, we obtain the following relationship:

$$\frac{R^4\triangle p}{\mu L Q} = \text{cst}, \tag{3.5}$$

which provides the following pressure drop law:

$$\triangle p = \text{cst}\, \mu \frac{LQ}{R^4}. \tag{3.6}$$

This law is very similar to that obtained experimentally by Hagen. In particular, it shows that Hagen's constant $k$ is homogeneous to a dynamic viscosity.

### 3.1.3 Theoretical answer

We recall that for laminar pipe flow, the streamwise velocity reads

$$u = \frac{R^2\partial_z p}{4\mu}\left(\frac{r^2}{R^2} - 1\right), \tag{3.7}$$

giving the following flow rate:

$$Q = -\frac{\pi R^4 \partial_z p}{8\mu} = \frac{\pi R^4 \triangle p}{8\mu L}. \tag{3.8}$$

Using expression (3.8) we can express the pressure drop. We obtain

$$\triangle p = \frac{8}{\pi}\,\mu\,\frac{LQ}{R^4}. \tag{3.9}$$

This expression sheds additional light on the nondimensional constant found using dimensional analysis and proves the relevance of Hagen's formula to laminar pipe flows.

## 3.2 Head loss

Don't worry, you won't lose yours!

### 3.2.1 The Bernoulli equation

Daniel Bernoulli (1700–1782), Swiss mathematical physicist, University of Basel

In viscous flows, the energy is not conserved. The occurrence of friction at the walls dissipates energy and the system is said dissipative. As the energy is not conserved, the Bernoulli equation is no longer valid as formulated but can be corrected to take into account viscous losses as we shall see.

Consider the flow in the inclined pipe shown in figure 3.2. For an incompressible inviscid flow along a streamline, the Bernoulli equation writes

$$p + \frac{1}{2}\rho u^2 + \rho g z = \text{cst}, \tag{3.10}$$

where $p$ is the pressure, $\rho$ is the density of the fluid, $u$ its steamwise velocity, $g$ the gravitational acceleration and $z$ the altitude. For practical reasons, we can write this law in terms of a height that is usually called head:

$$\frac{p}{\rho g} + \frac{u^2}{2g} + z = \text{cst}. \tag{3.11}$$

We consider a control volume delimited by section 1 and section 2 in figure 3.2. As a result of the friction between the fluid and the wall, the energy and head decrease between these two sections. We take this into account by adding a term to the Bernoulli equation that we write between section 1 and section 2 and obtain the viscous Bernoulli equation:

$$\frac{p_1}{\rho g} + \frac{u_1^2}{2g} + z_1 = \frac{p_2}{\rho g} + \frac{u_2^2}{2g} + z_2 + h_f, \tag{3.12}$$

where $h_f$ is called head loss and accounts for the viscous dissipation. The equivalent loss of energy per unit volume is $\rho g h_f$.

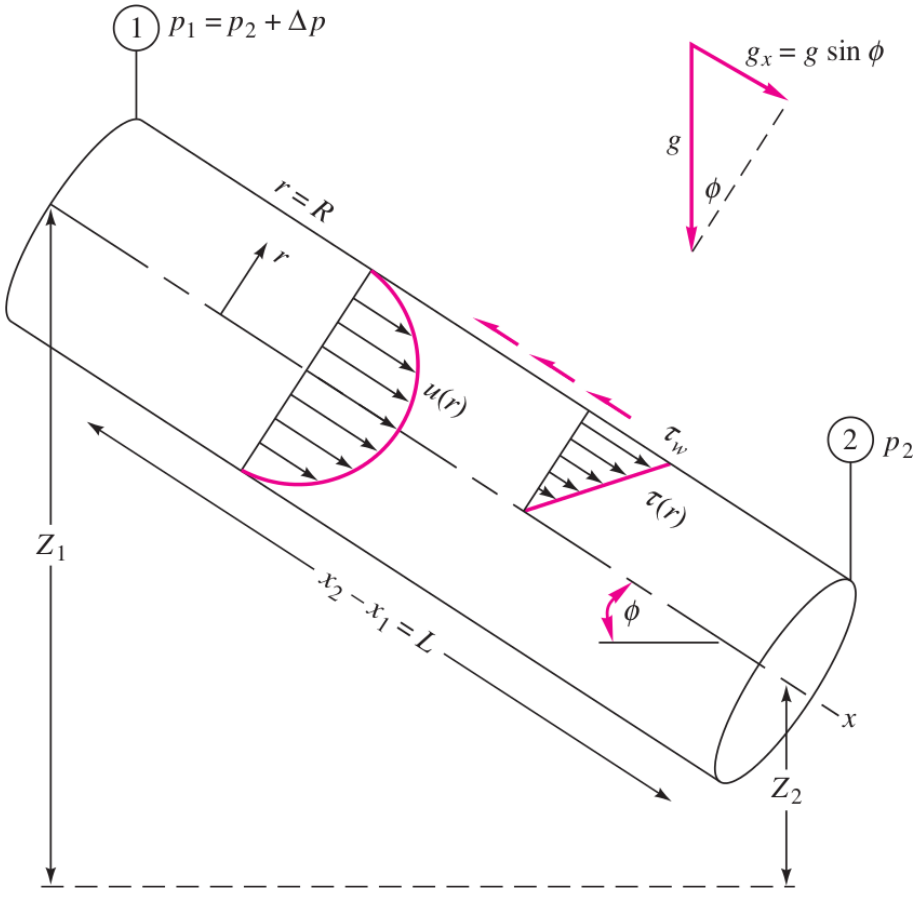


Figure 3.2: Sketch of an inclined pipe. After White, *Fluid Mechanics* (2011).

### 3.2.2 Application to pipe flow

The Bernoulli equation (3.12) is generic for incompressible flows. We can apply it to pipe flow. In the case of laminar pipe flow, the velocity of the fluid is invariant with the streamwise direction $x$, so $u_1 = u_2$. We can then express the head loss:

$$h_f = \frac{p_1 - p_2}{\rho g} + z_1 - z_2, \tag{3.13}$$

$$\Rightarrow \quad h_f = \frac{\triangle p}{\rho g} + \triangle z. \tag{3.14}$$

We can independently apply the momentum flux equation for the control volume represented in figure 3.2:

$$\Sigma F_x = \rho \pi R^2 (u_{2avg}^2 - u_{1avg}^2). \tag{3.15}$$

The left-hand-side includes all the forces in the $x$ direction, while the right hand side represents the difference in mass flux between the two opposite sections of the control volume. There are three forces acting on the fluid in the $x$ direction:

- pressure: $\triangle p \pi R^2$
- weight: $\rho L \pi R^2 \sin(\phi) g$
- shear: $-\tau_w 2\pi R L$

Additionally, the fluid's velocity is constant along $x$, so $u_{2avg} = u_{1avg}$. We obtain:

$$\triangle p \pi R^2 + \rho L \pi R^2 \sin(\phi) g - \tau_w 2\pi R L = 0. \tag{3.16}$$

By noting that $L \sin(\phi) = \triangle z$, expression (3.16) can be simplified into:

$$\triangle p \pi R^2 + \rho \triangle z \pi R^2 g - \tau_w 2\pi R L = 0, \tag{3.17}$$

to yield:

$$\frac{\triangle p}{\rho g} + \triangle z = \frac{2\tau_w L}{\rho g R}. \tag{3.18}$$

We can then express the head loss the following ways:

$$h_f = \frac{2\tau_w L}{\rho g R} = \frac{4\tau_w L}{\rho g d}, \tag{3.19}$$

$$h_f = \frac{8\mu u_{avg} L}{\rho g R^2} = \frac{32\mu u_{avg} L}{\rho g d^2}, \tag{3.20}$$

where we have defined $d$ to be the diameter of the pipe and have used the laminar wall shear relation $\tau_w = 4\mu u_{avg}/R$.

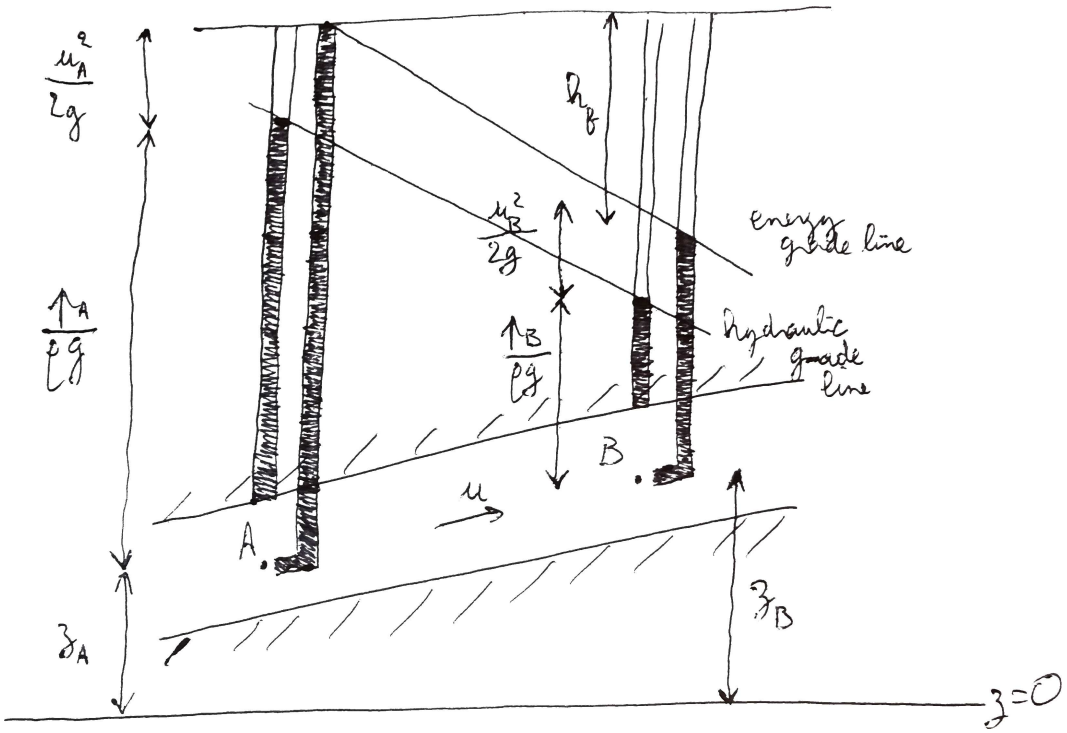


Figure 3.3: Physical interpretation of head loss, together with hydraulic and energy grade lines.

### 3.2.3 Physical interpretation

Enough pressure? This section is for you!

We can experimentally observe (or mentally imagine) quantities related to the Bernoulli equation (3.12). Tubes directly connected to the side of the pipe allow to directly observe the pressure head $p/\rho g$. When this quantity is summed with the altitude $z$ and tracked along the pipe, we obtain the hydraulic grade line. The use of Pitot tubes provides additional information: as they are oriented in the direction of the flow, they are sensitive to the fluid's velocity and include the kinetic head $u^2/2g$. The line obtained by summing the kinetic head together with the pressure head and the altitude is called energy grade line.

When viscous effects are non-negligible, the head loss can be observed as loss of pressure and therefore as a drop for both lines. This situation is depicted in figure 3.3.

### 3.2.4 General formulae

Julius Weisbach (1806–1871), German mathematician
Lewis Moody (1880–1953), American engineer, Princeton

The theory introduced so far is only valid for laminar flows but flows are often observed turbulent in applications. The following question naturally arose: how to get an expression

that will be universally valid?

In 1850, Weisbach used physical intuition to lead the way to a unifying theory. He realised that the head loss was proportional to $L/d$ (see expression (3.19)) and also approximately proportional to $u_{avg}^2$ experimentally for turbulent flows (note that Hagen's experiment provides an exponent of about 1.75). He then suggested the following relationship:

$$h_f = f\frac{L}{d}\frac{u_{avg}^2}{2g}, \tag{3.21}$$

where $f$ is a non-dimensional parameter called Darcy friction factor. Still out of physical intuition, he precised that the friction factor depend on the Reynolds number, the duct shape and the roughness of the wall for turbulent flows.

For a laminar flow in a pipe, we can combine expression (3.20) with relation (3.21):

$$\frac{32\mu u_{avg}L}{\rho g d^2} = f_{lam}\frac{L}{d}\frac{u_{avg}^2}{2g}, \tag{3.22}$$

$$\Rightarrow f_{lam} = \frac{64\mu u_{avg}Ldg}{\rho g d^2 L u_{avg}^2}, \tag{3.23}$$

$$\Rightarrow f_{lam} = \frac{64\mu}{\rho d u_{avg}}, \tag{3.24}$$

$$\Rightarrow f_{lam} = \frac{64}{Re_d}, \tag{3.25}$$

where $Re_d$ is the Reynolds number based on the diameter of the pipe.

For turbulent flows, things are expectedly more complicated. In fact, no purely theoretical law is known and progress has mainly come by experimentally ways. In 1939, Colebrook provided an interpolation formula of empirical data:

$$\frac{1}{f^{1/2}} = -2\log\left(\frac{\epsilon/d}{3.7} + \frac{2.51}{Re_d f^{1/2}}\right). \tag{3.26}$$

In this formula, $\epsilon/d$ quantifies the relative roughness of the walls, with $\epsilon$ being related to the size of the disturbance from a smooth wall. For a perfectly smooth pipe, $\epsilon/d = 0$. This value increases as the walls get rougher. Figure 3.4 provides a visual definition of these quantities.

Colebrook's formula (3.26) is transcendental and cannot be solved by hand. Hence, in 1944, Moody plotted what is now known as the Moody chart (figure 3.5) to provide directly readable data. This chart is nowadays a standard in the engineering world.

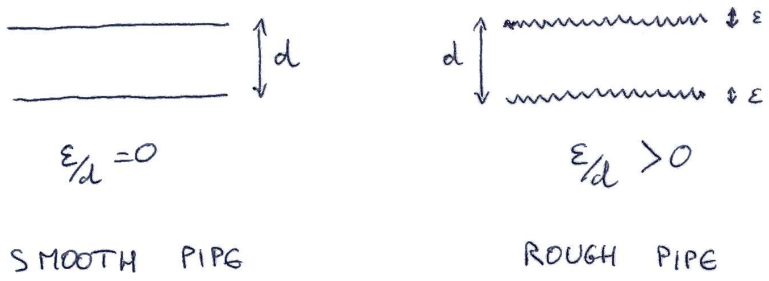


Figure 3.4: Visual definition of the roughness of the walls for a pipe.

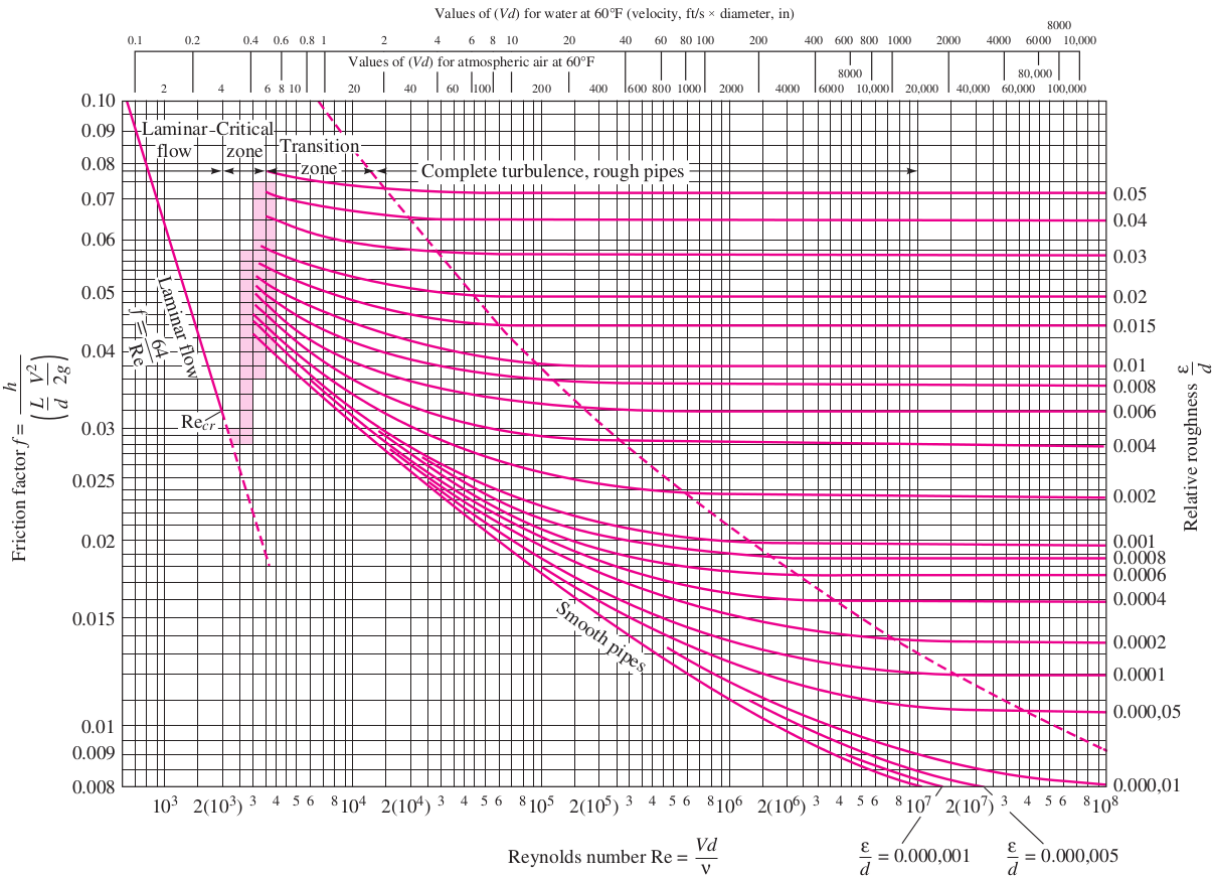


Figure 3.5: The Moody chart representing the friction factor $f$ as a function of the Reynolds number $Re$ and the relative roughness $\epsilon/d$ of the pipe. After White, *Fluid Mechanics* (2011).

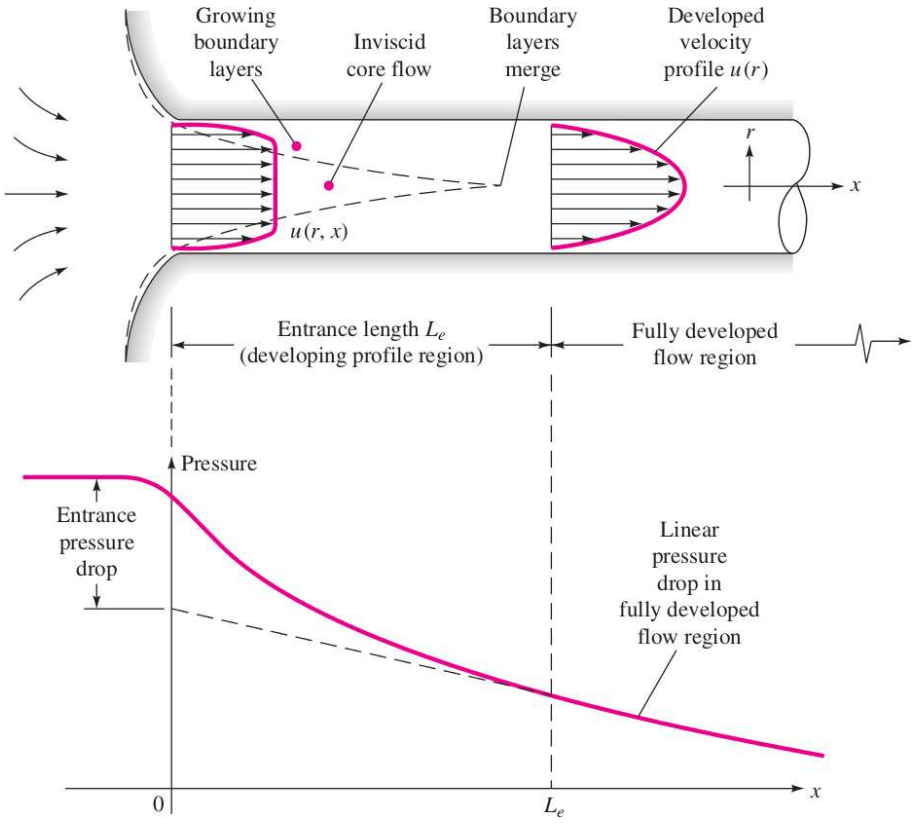


Figure 3.6: Depiction of the entrance region and the accommodation of the fluid to the presence of walls. After White, *Fluid Mechanics* (2011).

## 3.3 Entrance effects

### 3.3.1 When an external flow becomes internal flow

When an experiment is set up, departures from the theory developed in the last section are observed. This was first observed by Hagen and he mostly attributed these departures to entrance effects. These effects arise from the difference in the nature of the flow: away from the pipe, the external flow is homogeneous (therefore, not dissipative, or conservative); the flow within the pipe displays vanishing velocity at the wall due to viscosity. It is dissipative. Thus, there is a region (time if you follow the fluid) where the flow progressively accommodates to the presence of walls. This region is called entrance region and is depicted in figure 3.6.

### 3.3.2 Entrance length

It is important to know how long is the entrance region to determine where the flow is invariantly laminar and therefore where the theory directly applies.

We use dimensional analysis. The entrance length $L_e$ has dimension $[L_e] = L$ and is sensitive to the following quantities:

- the diameter of the pipe $d$: $[d] = L$
- the average fluid velocity $u_{avg}$: $[u_{avg}] = L.T^{-1}$
- the fluid's density $\rho$: $[\rho] = M.L^{-3}$
- the fluid's dynamic viscosity $\mu$: $[\mu] = M.L^{-1}.T^{-1}$

As $[L_e/d] = 1$, we can try to combine the other quantities to get a dimensionless product. We can then write:

$$[u_{avg}]^{\alpha}[\rho]^{\beta}[\mu]^{\gamma}[d]^{\delta} = M^{\beta+\gamma}.L^{\alpha-3\beta-\gamma+\delta}.T^{-\alpha-\gamma}. \tag{3.27}$$

To get a dimensionless group, all exponents need to vanish:

$$\begin{cases} \beta + \gamma = 0, \\ \alpha - 3\beta - \gamma + \delta = 0, \\ -\alpha - \gamma = 0. \end{cases} \tag{3.28}$$

It follows that

$$\alpha = \beta = \delta = -\gamma, \tag{3.29}$$

so the dimensional analysis gives:

$$\left[\frac{L_e}{d}\right] = \left[\frac{\rho u_{avg} d}{\mu}\right]^{\gamma}. \tag{3.30}$$

The group on the right-hand-side is nothing else but the Reynolds number based on the diameter of the pipe $Re_d$. Finally, we obtain:

$$\frac{L_e}{d} = \mathcal{F}(Re_d^{\gamma}), \tag{3.31}$$

where $\mathcal{F}$ indicates a power law.

In fact, the following empirical laws have been established:

- laminar flows: $L_e/d \approx 0.06 Re_d$
- turbulent flows: $L_e/d \approx 1.6 Re_d^{1/4}$

These laws provide again some interesting differences between laminar and turbulent flows: at $Re_d = 2000$, the entrance length of a laminar flow is $L_e = 120d$ while a turbulent flow at $Re_d = 10000$ will yield an entrance length of only $L_e = 16d$.

# Chapter 4

# Fluid-structure interaction

Chapters 1–3 focused on internal flows with a strong emphasis on pipe flow. Unlike these flows which are confined by walls, we are here interested in external flows. Such flows are unbounded and are at the heart of fluid-structure interaction studies.

When an unbounded homogeneous flow approaches a body, viscous effects become important and substantially deform the flow profile. For example, the flow entering a pipe discussed in Chapter 3 yielded a developing region where its nature changed from homogeneous and non-dissipative to a laminar (or turbulent) profile. This developing region created departures from theoretical predictions.

More generally, flows past immersed structures develop boundary layers and wakes which are responsible for generating forces and moments on the obstacle. These features are of prime importance in applications.

## 4.1 Some examples

### 4.1.1 Lift generation

Daniel Bernoulli (1700–1782), Swiss mathematical physicist, University of Basel

The most popular aerodynamics question probably is: how does an aircraft fly? The basic answer is that the airfoil is shaped in such a way as to generate lift. Such a response comes up as very unsatisfactory and we often hear the following more elaborate answer. The airfoil is shaped so that its upper surface is longer than its lower surface. A parcel of fluid arriving at the leading edge then splits into two parcels, one following the upper surface and the other the lower surface. As the fluid has more distance to travel on the upper surface than on the lower surface, it goes faster to have the same transit time. The Bernoulli effect follows: the higher velocity on the upper surface yields a lower pressure and an ascending force is created: the lift.

Although the use of Bernoulli effect is, to some extent, correct, the equal transit time argument is in fact *wrong*. Figure 4.1 shows a series of snapshots for a flow past an airfoil. It is very clear from these that the upper flow is accelerated compared to the lower flow. This happens already at the leading edge, but the lower flow never catches up with the upper one. Consequently, the upper flow reaches the trailing edge first and had a shorter transit time.

As a consequence, the physical mechanism behind lift is not so simple. The introduction of a shape to the airfoil curves the streamlines and produces non-trivial velocity and hence pressure distributions. On the one hand, the fluid is accelerated on the upper surface and slowed down on the lower surface, creating a descending pressure gradient, hence lift. On the other hand, the fluid trajectory is overall deflected downwards when passing the airfoil. This implies that the airfoil creates a descending force onto the fluid, and, by Newton's third law, that the fluid generates an ascending force onto the airfoil. The combination of these two effects is what creates lift.

### 4.1.2 Wingtip vortices

What happens at the tip of the wing when the lower pressure upper surface meets the higher pressure lower surface?

The fluid receives a force from the high pressure area to the low pressure area. Thus, at the tip of the wing, it is attracted to the upper surface and tends to rotate around the wing. This generates wingtip vortices such as the one visualised with smoke in figure 4.2. These vortices are generally strong, long-lived. They are consequently dangerous: flying through such a vortex will create a rolling moment that can destabilize the flight. Many such incidents have happened during takeoff and landing. As a result, airports have decided on quiet periods of one to two minutes between two successive takeoffs or landings to allow for these vortices to dissipate to a less dangerous strength.

### 4.1.3 The V-formation

Nature knows about wingtip generation. Birds are notorious for using wingtip vortices to their advantage. When they follow another bird, they place themselves a little bit on the side to benefit from the lift generated by the wingtip vortices of their leader. The resulting flock layout is a beautiful V-formation as exemplified in figure 4.3. I am afraid nature is still a better engineer than you.

### 4.1.4 Other examples

Examples of flows past immersed bodies and their interaction abounds. The transportation industry is a good example and designing vehicles, increasing their performances (decreasing consumption) is an evergoing challenge.

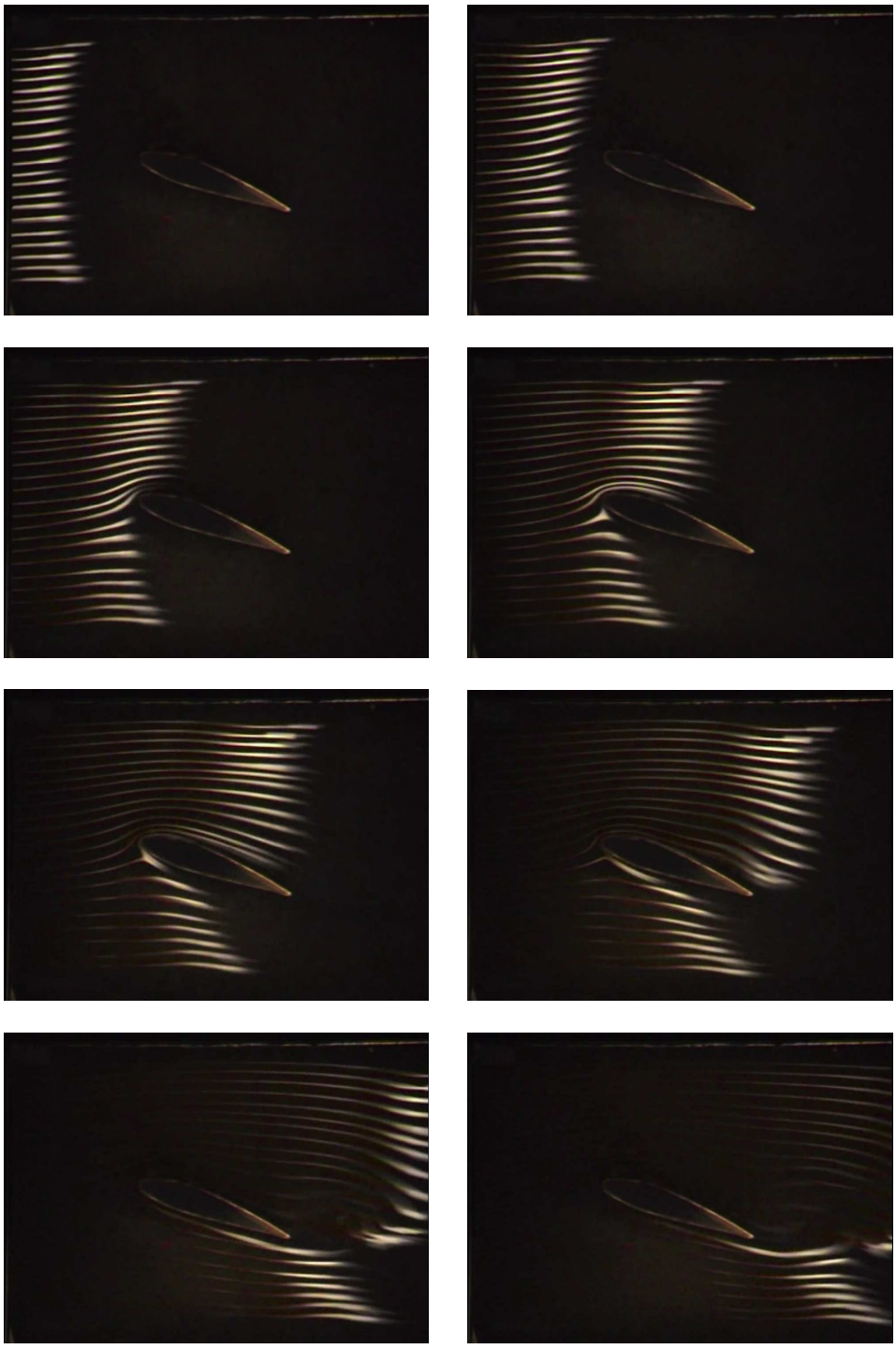

Figure 4.1: Flow past an airfoil visualised through the trajectory of one pulse of smoke. After Babinsky (`http://www.cam.ac.uk/research/news/how-wings-really-work`).

Figure 4.2: Wingtip vortex behind a plane visualised with red smoke.

Figure 4.3: Birds flying in V-formation.

Wind and ocean engineering also present important challenges in the area of fluid-structure interaction. The construction of tall building is necessary to accommodate large professional centres and these tall buildings interact strongly with the wind. Similar issues arise with bridges as we shall see.

In water, it is important to understand fluid-structure interactions to design efficient breakwaters and protect constructions on the shore or beaches. Pilings are also good examples of structures interacting with water and that have to be designed carefully. Lastly, we can take advantage of natural phenomena such as wind and currents by designing structures that will store such energy like wind and water turbines.

## 4.2 Effect of a structure on the fluid

When an external flow goes past an obstacle, it is locally deflected. In addition, due to viscosity, the walls do not allow the fluid to slip along it and the fluid slows down close to the wall generating a boundary layer. Past the structure, a wake results from the inertia of the fluid.

### 4.2.1 Boundary layers

Clos to the wall, the flow is slower than far from it. We can then define a region where the fluid's velocity parallel to the wall is smaller or equal to 99% of the external velocity. We call this region the boundary layer. Note that this convenient definition is not a consensus and different metrics can be used.

Inside the boundary layer, the flow feels the effect of the wall and is gradually slowed down as we approach the wall. The presence of these velocity gradients is a consequence of viscous dissipation. Outside the boundary layer, the flow does not feel the presence of the walls. It remains homogeneous and is considered inviscid. Examples of boundary layers are shown in figure 4.4.

For low values of the Reynolds number, the flow possesses low inertia and displays slow spatial variations around the flat plate. For these reasons, it is referred to as laminar boundary layer. Because spatial variations are slow, the laminar boundary layer occupies a large spatial region.

The velocity in the direction parallel to the wall varies in the direction orthogonal to the wall. As the flow is incompressible, the velocity orthogonal to the wall becomes non-zero. This is called the viscous displacement effect. For laminar boundary layers, this effect is important.

The case of large values of the Reynolds numbers is more complex. As the flow has more inertia, velocity gradients become large allowing the boundary layer to remain confined very close to the wall. We observe two distinct regions in the boundary layer:

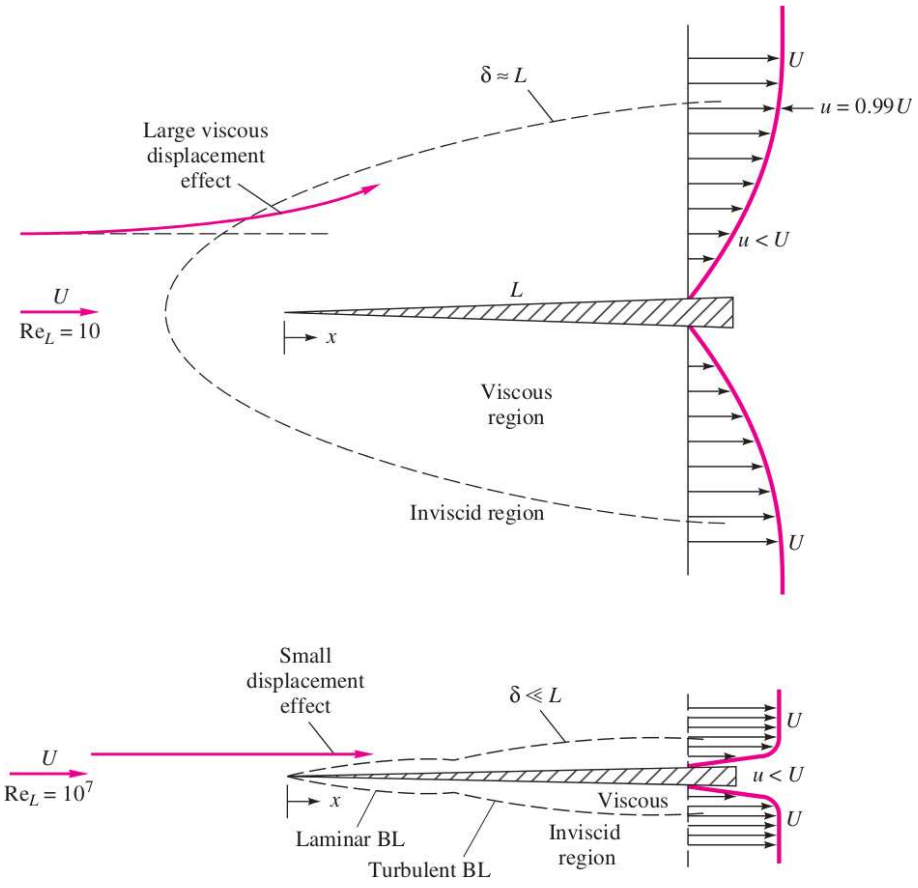


Figure 4.4: Sketch of the flow past a sharp flat plate oriented in the direction of the flow. Two situations are shown: a low-$Re$ flow ($Re_L = 10$) and a high-$Re$ flow ($Re_L = 10^7$) and the associated boundary layers depicted. After White, *Fluid Mechanics* (2011).

the first one is a laminar boundary layer similar to that of low-$Re$ flows but much thinner and a turbulent boundary layer that occurs further away in the streamwise direction and is larger than the laminar boundary layer. These boundary layers are so thin that the viscous displacement is negligible.

Note that for slender bodies at large $Re$, such as airfoils, the boundary layer is so thin and weak when placed parallel to the flow, that the assumption of negligible interaction between the boundary layer and the outer pressure distribution provides good results.

### 4.2.2 Wakes

Time to wake!

Theodore Von Kármán (1881–1963), Hungarian-American aeronautical engineer, California Institute of Technology

Unless inertia is negligible (equivalently viscous effects are overwhelmingly dominant), the gradients of velocity induced by the boundary layer are advected downstream and create a wake past the obstacle. This region can display dramatic departures from the established flow infinitely far away from the obstacle.

Wakes are best introduced using simple geometries. Figure 4.5 shows how the wake past a cylinder is changed when the Reynolds number $Re$ is increased. Several regimes are observed:

- At low $Re$: the flow is steady and symmetric.
- At $Re = \mathcal{O}(10)$: the upstream-downstream symmetry is broken and flow separation occurs. Due to the increased inertia of the fluid, the boundary layers are no longer able to stick to the wall at the back of the cylinder. They separate from the wall and a recirculation zone is created where two counter-rotating vortices live. This wake remains stationary and still preserves the up-down symmetry.
- At $Re = \mathcal{O}(100)$: the up-down symmetry is broken and the wake is now periodic in time. The vortices periodically break away from the back of the cylinder in an alternate fashion and are advected downstream. This type of wake is called *Von Kármán streets*.
- At $Re > \mathcal{O}(1000)$: any simple time-dependence in the wake is lost and it is now turbulent.

It is useful here to point out that as the Reynolds number is increased, different types of turbulent wakes can be observed. At $Re = 5.10^3$ for example, the turbulent wake is detached from the wall and a laminar bubble is observed at the back of the cylinder. This bubble shrinks as the Reynolds number is increased and by $Re = 10^5$, the back of the cylinder has become fully turbulent. As $Re$ is further increased, the turbulent wake

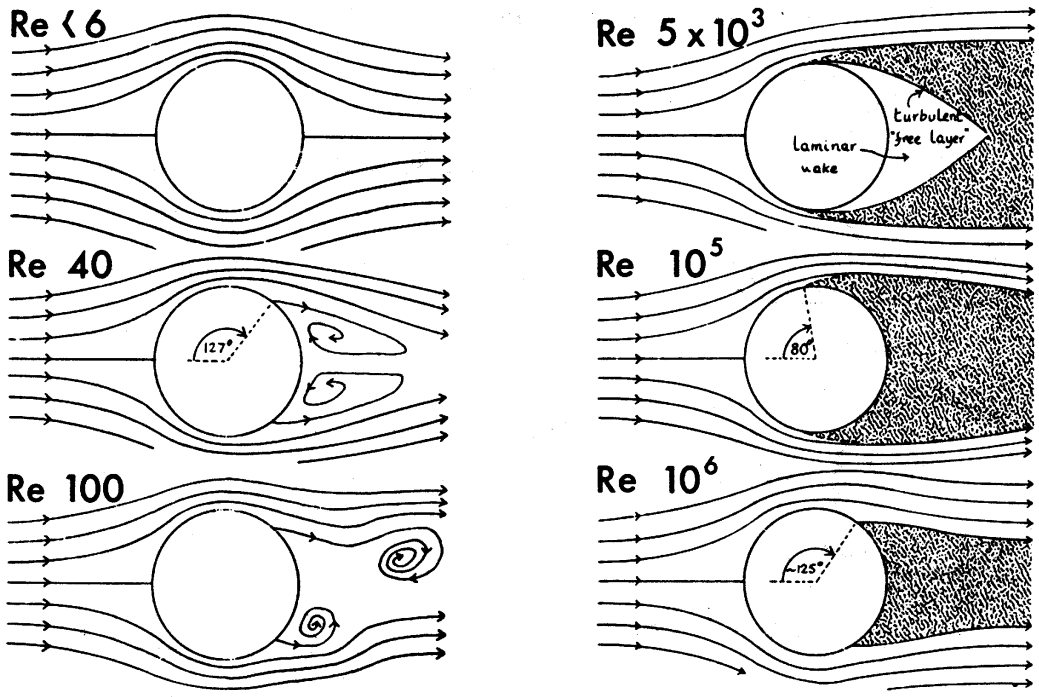


Figure 4.5: Sketch of the wake past a cylinder and the different regimes observed as a function of the Reynolds number $Re = UR/\nu$, where $U$ is the velocity of the fluid infinitely far away from the cylinder, $R$ the cylinder radius and $\nu$ the fluid's kinematic viscosity. After Middleton & Southard, *Mechanics of Sediment Movement*, SEPM Short Course Notes, Vol. 3 (1984).

becomes thinner and thinner and the influence of the cylinder on the flow decreases. This is the result of the fact that the characteristic length for advection becomes incomparably larger than the diameter of the cylinder. Would a dust grain deflect a river?

## 4.3 Effect of the fluid on a structure

We have seen in the previous section how the presence of a structure induces strong disturbances to the flow. In this section, we look at the opposite interaction: the impact of boundary layers and wakes on the structures. The fact that the flow is no longer symmetric around the structure creates a new pressure distribution whose integral over the structure may no longer be zero or trivial. This, in turn, leads to the creation of new forces on the structure.

### 4.3.1 Bend it like Beckham

Heinrich Gustav Magnus (1802–1870), German physicist, University of Berlin

In 1998, during a friendly tournament fixture prior to the FIFA World Cup, Roberto Carlos (Brazil) scored a free kick goal against France. I was furious! The trajectory of the ball mystified Fabien Barthez, the French goalkeeper, who remained still while the ball made its way to the goal. Figure 4.6 shows a few pictures of this goal taken a few tenths of a second apart to provide a sense of the trajectory. The ball is kicked toward the right and after flying past the wall of defenders, turns left to end its course in the nets in a very spectacular manner.

The explanation of such a trajectory lies in the *Magnus effect* and is illustrated in figure 4.7. Rotating the ball accelerates the flow on one side while slowing it down on the other. This difference of velocity breaks the symmetry of the flow and creates a difference of pressure. In turn, this pressure difference creates a lateral force pointing to the side where the flow is accelerated. This is this additional force that bends the trajectory of the ball and that allows surprising effects in many ball games.

### 4.3.2 The Tacoma Narrows bridge

The Tacoma Narrows bridge was a 1.8km long bridge between Tacoma and the Kitsap peninsula in the state of Washington (USA). The bridge opened on July 1st, 1940 and collapsed on November 7th, 1940. A picture before the collapse and one while it was under way are shown in figure 4.8.

During that day of November 7th, 1940, the wind blew steadily at 65km.h$^{-1}$. This not so violent wind (to London standards) interacted in an unexpected manner with the bridge and created a positive feedback loop called *aeroelastic flutter*. The origin of the


Figure 4.6: Pictures of Roberto Carlos's goal for Brazil against France in a friendly fixture before the 1998 FIFA World Cup.

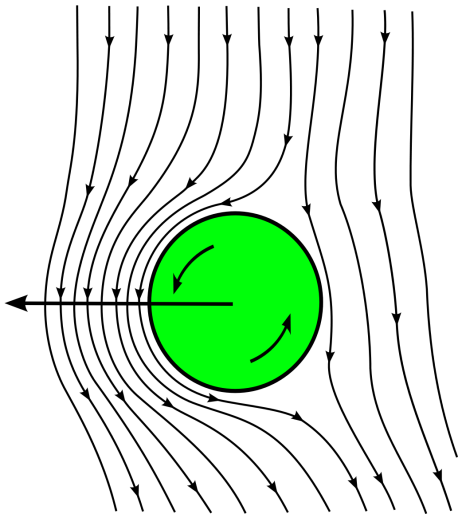

Figure 4.7: Illustration of the Magnus effect using a downward flow past an anti-clockwise rotating sphere. The flow is slowed down on the right as opposed to the left. The pressure is then greater on the right of the sphere and a leftward force is generated.

Figure 4.8: Pictures of the Tacoma Narrows bridge on November 7th, 1940 before and during its collapse. After http://en.wikipedia.org/wiki/Tacoma_Narrows_Bridge_(1940).

this phenomenon is likely the oscillating wake due to a periodic vortex shedding state like the Von Kármán streets. This excited a torsional mode: the centerline of the bridge stood still while the right lane moved up and the left lane moved down. More precisely, it is the second torsional mode that was excited: the midpoint of the bridge remained motionless while the two opposite halves twisted in opposite directions. This torsion enhanced the strength of the wake, which in turn increased the torsion until the collapse of the bridge.

You don't need to blow hard to collapse a bridge!

# Chapter 5

# Boundary layer theory – Integral approach

Boundary layer theory, our best BLT!

As we have seen in Chapter 4, any flow interacting with a structure develops boundary layers. They are due to the fact that the fluid cannot slip along the wall but rather adheres to it, creating velocity gradients orthogonal to the wall.

In this chapter, we consider a steady incompressible two-dimensional flow. This flow is represented in figure 5.1 where the boundary layer thickness is denoted by $\delta$ and varies with the streamwise coordinate $x$. We introduce the control volume delimited by:

- Boundary 1: the segment $(0, 0)$ to $(0, h)$, where $\mathbf{u} = U\hat{\mathbf{x}}$.
- Boundary 2: the streamline $(0, h)$ to $(L, \delta)$, where $\mathbf{u} \cdot \mathbf{n} = \mathbf{0}$.
- Boundary 3: the segment $(L, \delta)$ to $(L, 0)$, where $\mathbf{u} = u(x, y)\hat{\mathbf{x}} + v(x, y)\hat{\mathbf{y}}$.
- Boundary 4: the plate surface and streamline $(L, 0)$ to $(0, 0)$, where $\mathbf{u} = \mathbf{0}$.

In these, the vector $\mathbf{n}$ represents the outward-pointing normal unit vector.

## 5.1 Viscous displacement

### 5.1.1 Physical origin

When a flow is incompressible, the creation of a boundary layer generates orthogonal viscous displacement. The explanation behind this phenomenon lies in the incompressibility constraint. For the flow in figure 5.1 this two-dimensional constraint reads:

$$\partial_x u + \partial_y v = 0. \tag{5.1}$$

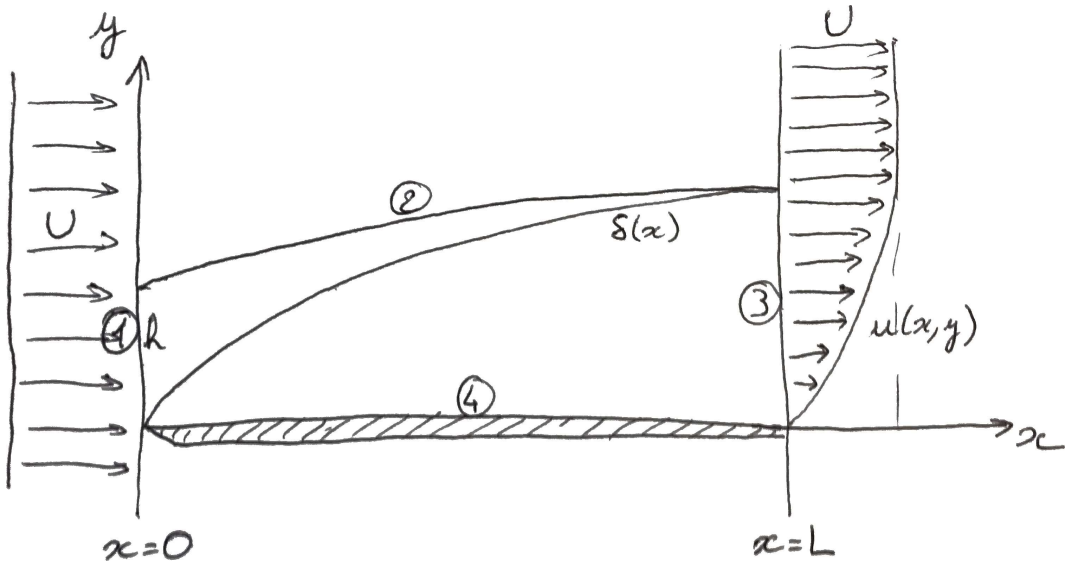


Figure 5.1: Sketch of a developing boundary layer on a flat plate. The control volume used in this lecture is delimited by the boundaries labeled 1, 2, 3 and 4.

Around $x = 0$, the near-wall streamwise velocity $u$ is decreased: $\partial_x u < 0$. To compensate for this and preserve the incompressible character of the flow, $\partial_y v > 0$, creating an orthogonal viscous displacement. The consequence of this displacement is that the streamlines are not parallel to the wall but move away from it.

### 5.1.2 Displacement thickness

To better characterise this effect, we write the conservation of mass between the inlet ($x = 0$, boundary 1) and the outlet ($x = L$, boundary 3):

$$\rho \int_1 (\mathbf{u} \cdot \mathbf{n})\, ds + \rho \int_3 (\mathbf{u} \cdot \mathbf{n})\, ds = 0, \tag{5.2}$$

where $ds$ represents the local line element. On the inlet, $\mathbf{n} = -\hat{\mathbf{x}}$, while on the outlet, $\mathbf{n} = \hat{\mathbf{x}}$. Using these equalities and evaluating the velocities, we get:

$$\rho \int_0^h (-U) dy + \rho \int_0^\delta u dy = 0, \tag{5.3}$$

where $u = u(L, y)$, $\delta$ is the boundary layer thickness at $x = L$ and the point $(0, h)$ with $h = \delta - \delta^*$ is on the same streamline as the $(L, \delta)$. The quantity $\delta^*$ is called displacement thickness and represents the distance by which the wall would have to be moved in the wall normal direction to obtain the same flow rate in an inviscid flow (see figure 5.1 for a graphical representation of these quantities and figure 5.2 for an explanation). The density of the fluid being constant,

$$Uh = \int_0^\delta u dy. \tag{5.4}$$

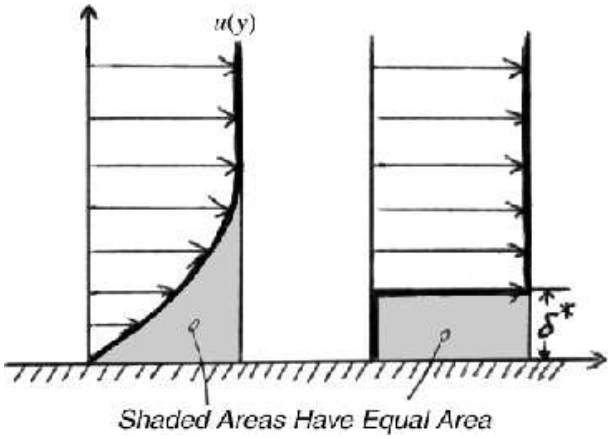


Figure 5.2: Left: actual viscous boundary layer. Right: analogy with an inviscid flow displaying the same flow rate. The wall-normal delay $\delta^*$ necessary to obtain the same flow rate is called displacement thickness.

To express the displacement thickness $\delta^*$ at $x = L$, we write $u = U + u - U$. Expression (5.4) yields:

$$Uh = \int_0^\delta (U + u - U)\, dy, \tag{5.5}$$

$$\Rightarrow Uh = U\delta + \int_0^\delta (u - U)\, dy, \tag{5.6}$$

which, using $\delta = h + \delta^*$, simplifies into:

$$h = h + \delta^* + \int_0^\delta \left(\frac{u}{U} - 1\right) dy, \tag{5.7}$$

$$\Rightarrow \delta^* = \int_0^\delta \left(1 - \frac{u}{U}\right) dy. \tag{5.8}$$

Therefore, if the wall is a slip wall (inviscid flow), i.e. $u \equiv U$, the displacement thickness $\delta^* = 0$, a result we expect as no viscous boundary layer develops in an inviscid flow. The displacement thickness is therefore a consequence of the fact that locally, the streamwise velocity is decreased: $u < U$.

## 5.2 Friction drag

Theodore Von Kármán (1881–1963), Hungarian-American aeronautical engineer, California Institute of Technology

### 5.2.1 Drag as a boundary layer effect

We assume constant pressure throughout the domain so that there is no net pressure force. The flow is steady so the conservation of momentum in $\hat{\mathbf{x}}$ writes:

$$\rho \int_1 u(0,y)\,(\mathbf{u}\cdot\mathbf{n})\,ds + \quad \rho \int_2 u(x,y)\,(\mathbf{u}\cdot\mathbf{n})\,ds \ldots$$
$$+\rho \int_3 u(L,y)\,(\mathbf{u}\cdot\mathbf{n})\,ds + \rho \int_4 u(x,0)\,(\mathbf{u}\cdot\mathbf{n})\,ds = \Sigma F_x. \quad (5.9)$$

Boundary 2 is defined as a streamline, so the velocity fully projects onto it and does not have any normal component: $(\mathbf{u}\cdot\mathbf{n}) = 0$. Furthermore, the velocity at the plate surface $u(x,0)$ vanishes and the only force on the fluid is the opposite of the drag force $-D\hat{\mathbf{x}}$. Note that the drag force $D\hat{\mathbf{x}}$ is the force created by the fluid on the plate, so the negative sign is necessary to calculate the force created by the plate on the fluid.

Equation (5.9) simplifies into:

$$\rho \int_0^h U\,(-U)\,dy + \rho \int_0^\delta u\,(u)\,dy = -D. \quad (5.10)$$

Upon evaluating the first integral, we obtain:

$$D = \rho h U^2 - \rho \int_0^\delta u^2 dy. \quad (5.11)$$

Expression (5.11) is not satisfactory in that the height $h$ is not known. To obtain a more useful expression for the drag, we use mass conservation between the inlet and the outlet (relation (5.4)), which, combined with equation (5.11) gives:

$$D = \rho \int_0^\delta u(U-u)dy. \quad (5.12)$$

This result was first derived in Von Kármán, *Z. Angew. Math. Mech.* **1**, 235–236 (1921).

The last interesting quantity to keep track of is the momentum thickness $\theta$:

$$\theta = \frac{D}{\rho U^2} = \int_0^\delta \frac{u}{U}\left(1-\frac{u}{U}\right)dy, \quad (5.13)$$

that represents the characteristic length over which momentum is lost due to the viscous nature of the fluid compared to an inviscid flow. We can then define the shape factor:

$$H = \frac{\delta^*}{\theta}, \quad (5.14)$$

that indicates the wall-normal distance on which the fluid is deflected from the plate compared to that on which gradients of streamwise velocities are felt. A large shape factor indicates a flow near separation.

### 5.2.2 Relation to wall shear stress

We can also understand the drag force as being created by the wall shear stress $\tau_w$ along the place. It follows:

$$D = \int_0^x \tau_w(l) dl. \tag{5.15}$$

or alternately:

$$\tau_w = \partial_x D. \tag{5.16}$$

By differentiating equation (5.13), we obtain:

$$\partial_x \theta = \frac{1}{\rho U^2} \partial_x D, \tag{5.17}$$

that allows us to write an important relation that is valid for laminar and turbulent boundary layers:

$$\tau_w = \rho U^2 \partial_x \theta. \tag{5.18}$$

## 5.3 Some results

Ludwig Prandtl (1875–1953), German aeronautical engineer, University of Göttingen
Heinrich Blasius (1883–1970), German engineer, University of Hamburg

### 5.3.1 Velocity profile

In his studies of laminar boundary layers, Von Kármán assumed that the velocity profile within the boundary layer had a parabolic shape. He wrote:

$$\frac{u(x,y)}{U} \approx \frac{2y}{\delta} - \frac{y^2}{\delta^2}, \qquad 0 \leq y \leq \delta(x). \tag{5.19}$$

Similarly, Prandtl highlighted the fact that turbulent velocity profiles were following a one-seventh power law:

$$\frac{u(x,y)}{U} \approx \left(\frac{y}{\delta}\right)^{1/7}, \qquad 0 \leq y \leq \delta(x). \tag{5.20}$$

These first order approximations are actually very close to reality as shown in figure 5.3. They proved very useful to advance boundary layer theory as we shall see.

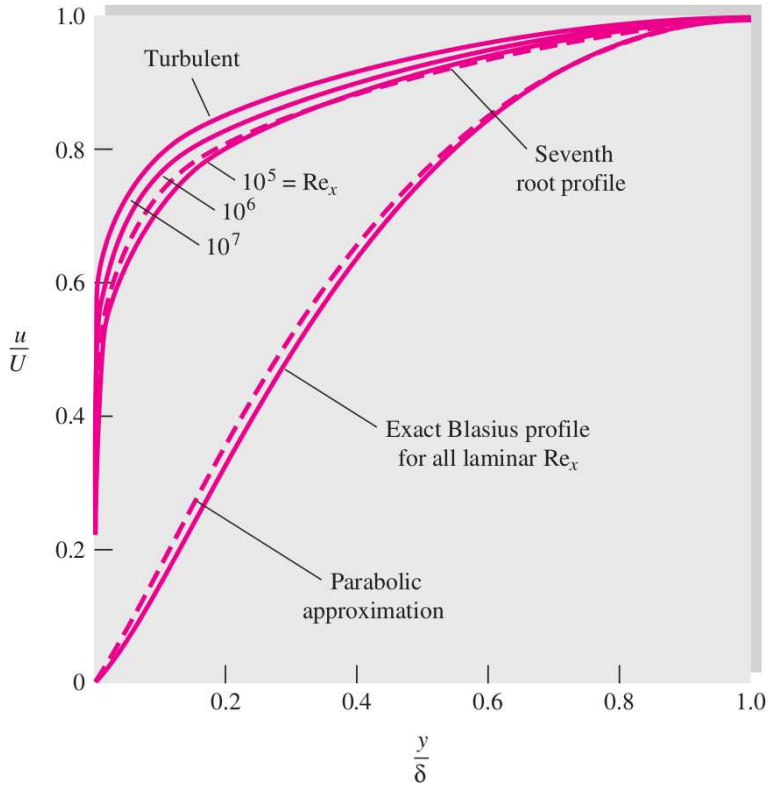


Figure 5.3: Comparison of velocity profiles $u/U$ in the boundary layer $y/\delta < 1$ between the Von Kármán and Prandtl's approximations and the actual laminar and turbulent flows. After White, *Fluid Mechanics* (2011).

### 5.3.2 Laminar results

For laminar flows, some basic insight can be obtained by using Von Kármán's approximation (5.19). We can calculate the momentum thickness using equation (5.13):

$$\theta \approx \int_0^\delta \left(\frac{2y}{\delta} - \frac{y^2}{\delta^2}\right)\left(1 - \frac{2y}{\delta} + \frac{y^2}{\delta^2}\right) dy, \tag{5.21}$$

$$\Rightarrow \quad \theta \approx \int_0^\delta \left(\frac{2y}{\delta} - \frac{5y^2}{\delta^2} + \frac{4y^3}{\delta^3} - \frac{y^4}{\delta^4}\right) dy, \tag{5.22}$$

$$\Rightarrow \quad \theta \approx \delta - \frac{5}{3}\delta + \delta - \frac{1}{5}\delta, \tag{5.23}$$

$$\Rightarrow \quad \theta \approx \frac{2}{15}\delta. \tag{5.24}$$

This provides, together with equation (5.13), the following relation for the drag of a laminar boundary layer:

$$D \approx \frac{2\rho U^2 \delta}{15}. \tag{5.25}$$

The wall shear stress can be expressed in two different ways. The definition writes:

$$\tau_w = \mu\, \partial_y u|_{y=0}, \tag{5.26}$$

$$\Rightarrow \quad \tau_w \approx \mu\ \partial_y \left(\frac{2y}{\delta} - \frac{y^2}{\delta^2}\right)\bigg|_{y=0} \tag{5.27}$$

$$\Rightarrow \quad \tau_w \approx \mu \frac{2U}{\delta}, \tag{5.28}$$

while expression (5.18), combined with result (5.24) yields:

$$\tau_w \approx \rho U^2\, \partial_x \left(\frac{2}{15}\delta\right), \tag{5.29}$$

$$\Rightarrow \quad \tau_w \approx \frac{2\rho U^2}{15}\partial_x \delta. \tag{5.30}$$

Expressions (5.28) and (5.30) can then be combined into:

$$\mu \frac{2U}{\delta} \approx \frac{2\rho U^2}{15}\partial_x \delta, \tag{5.31}$$

which, can be reexpressed and integrated between $x = 0$ (where $\delta = 0$) and an arbitrary length $x$ for which the boundary layer thickness is $\delta$:

$$\int_0^x dx \approx \int_0^\delta \frac{\rho U}{15\mu}\delta\, d\delta, \tag{5.32}$$

$$\Rightarrow \quad x \approx \frac{\rho U \delta^2}{30\mu}. \tag{5.33}$$

The boundary layer thickness can be obtained by multiplying by $x$ and rearranging the terms:

$$x^2 \approx \frac{\rho U \delta^2 x}{30\mu}, \tag{5.34}$$

$$\Rightarrow \quad \left(\frac{\delta}{x}\right)^2 \approx \frac{30\mu}{\rho U x}, \tag{5.35}$$

$$\Rightarrow \quad \frac{\delta}{x} \approx 5.5 Re_x^{-1/2}, \tag{5.36}$$

where we have defined $Re_x = \rho U x/\mu$ as the streamwise Reynolds number. Thus, the laminar boundary layer thickness grows like $x^{1/2}$.

Relation (5.8) provides the displacement thickness:

$$\delta^* \approx \int_0^\delta \left(1 - \frac{2y}{\delta} + \frac{y^2}{\delta^2}\right) dy, \tag{5.37}$$

$$\Rightarrow \quad \delta^* \approx \frac{1}{3}\delta, \tag{5.38}$$

indicating that the orthogonal viscous displacement is felt on a thickness that is only one third of the thickness of the boundary layer, that is

$$\frac{\delta^*}{x} \approx 1.83 Re_x^{-1/2}. \tag{5.39}$$

We can now calculate the shape factor $H$:

$$H = \frac{\delta^*}{\theta}, \tag{5.40}$$

$$\Rightarrow \quad H \approx \frac{\delta}{3} \times \frac{15}{2\delta}, \tag{5.41}$$

$$\Rightarrow \quad H \approx 2.5. \tag{5.42}$$

We can also define a quantity similar to the Darcy friction factor in duct flows, the skin friction coefficient $c_f$:

$$c_f = \frac{2\tau_w}{\rho U^2}, \tag{5.43}$$

which, together with equations (5.28) gives:

$$c_f \approx \frac{4\mu}{\rho U \delta}. \tag{5.44}$$

Upon using result (5.36), we get:

$$c_f \approx 0.73 Re_x^{-1/2}. \tag{5.45}$$

All the results obtained here are good despite the original hypothesis of parabolic flow: they are within 10% of the results from Blasius, *PhD thesis*, Göttingen (1908).

### 5.3.3 Validity of the results

The above results are based on the hypothesis that the boundary layer is thin enough so that the coupling with the outer flow is negligible. This theory breaks down as soon as $\delta/x = \mathcal{O}(1)$. To get an idea of the constraint this poses, we write that the domain of validity of boundary layer theory is

$$\frac{\delta}{x} < 0.1. \tag{5.46}$$

Expression (5.36) gives

$$5.5 Re_x^{-1/2} < 0.1, \tag{5.47}$$

$$\Rightarrow \quad 3025 < Re_x, \tag{5.48}$$

So the theory developed here is valid only for streamwise Reynolds numbers greater than 3025. For smaller Reynolds numbers, the interaction with the outer flow is important and leads to departures from these results.

Conversely, at a threshold Reynolds number, the boundary layer becomes turbulent and the results above do not hold. This critical value of the Reynolds number is $Re_c \approx 3 \times 10^6$. This value corresponds to the relative boundary layer thickness

$$\frac{\delta}{x} \approx 3.2 \times 10^{-3}. \tag{5.49}$$

The boundary layer then becomes turbulent and results are generally obtained numerically or experimentally. Usually, the surfaces are not perfectly polished and transition occurs earlier, sometimes at Reynolds numbers as low as $10^5$.

### 5.3.4 Turbulent results

In the turbulent case, some more assumptions than the Prandtl one-seventh power law (5.20) have to be made. This is out of the scope of this lecture but we will give some results obtained by a similar first-order approach to that used for laminar flows.

The momentum thickness can be directly deduced from equation (5.13):

$$\theta \approx \int_0^\delta \left(\frac{y}{\delta}\right)^{1/7} \left[1 - \left(\frac{y}{\delta}\right)^{1/7}\right] dy, \tag{5.50}$$

$$\Rightarrow \quad \theta \approx \int_0^\delta \left[\left(\frac{y}{\delta}\right)^{1/7} - \left(\frac{y}{\delta}\right)^{2/7}\right] dy, \tag{5.51}$$

$$\Rightarrow \quad \theta \approx \frac{7\,\delta^{8/7}}{8\,\delta^{1/7}} - \frac{7\,\delta^{9/7}}{9\,\delta^{2/7}}, \tag{5.52}$$

$$\Rightarrow \quad \theta \approx \frac{7}{72}\delta. \tag{5.53}$$

Some intricate algebra is needed to obtain the approximate skin friction law for a turbulent boundary layer flow. The consensus law is:

$$c_f \approx 0.02 Re_\delta^{-1/6}, \tag{5.54}$$

where $Re_\delta = \rho U \delta / \mu$ is the wall-normal Reynolds number.

Using relation (5.43) together with definition (5.18) and the result just obtained, we can obtain an approximate scaling for the Reynolds numbers:

$$c_f = 2\partial_x \theta \approx 0.02 Re_\delta^{-1/6}, \tag{5.55}$$

$$\Rightarrow \quad \frac{7}{36}\partial_x \delta \approx 0.02 Re_\delta^{-1/6}. \tag{5.56}$$

We note here that $\partial_x \delta = d\delta/dx = dRe_\delta/dRe_x$ which yields:

$$\frac{7}{36}\frac{dRe_\delta}{dRe_x} \approx 0.02 Re_\delta^{-1/6}, \tag{5.57}$$

$$\Rightarrow \quad Re_\delta \approx 0.16 Re_x^{6/7}. \tag{5.58}$$

Thus, the boundary layer thickness for a turbulent boundary layer is:

$$\frac{\delta}{x} \approx 0.16 Re_x^{-1/7}. \tag{5.59}$$

Therefore, the boundary layer thickness grows like $x^{6/7}$ for turbulent flows, which represents a faster growth than the $x^{1/2}$ law for the laminar boundary layer.

Using relation (5.58) within expression (5.54), one finds the skin friction coefficient as a function of the streamwise Reynolds number:

$$c_f \approx 0.027 Re_x^{-1/7}, \tag{5.60}$$

indicating that the skin friction coefficient is greater for turbulent boundary layers than for the laminar ones.

The displacement thickness can be directly expressed from the one-seventh power law (5.20) within equation (5.8):

$$\delta^* \approx \int_0^\delta \left[1 - \left(\frac{y}{\delta}\right)^{1/7}\right] dy, \tag{5.61}$$

$$\Rightarrow \quad \delta^* \approx \frac{1}{8}\delta, \tag{5.62}$$

$$\Rightarrow \quad \frac{\delta^*}{x} \approx 0.02 Re_x^{-1/7}, \tag{5.63}$$

proving here a statement we made in Chapter 4 that the viscous displacement thickness for turbulent boundary layers is very small. The shape factor then is

$$H = \frac{\delta^*}{\theta}, \tag{5.64}$$

$$\Rightarrow \quad H \approx \frac{\delta}{8} \times \frac{72}{7\delta}, \tag{5.65}$$

$$\Rightarrow \quad H \approx 1.3, \tag{5.66}$$

a much smaller value than for laminar boundary layers.

# Chapter 6

# Boundary layer theory – Navier–Stokes approach

BLT, second course!

External flows around immersed bodies are usually studied using combinations of experiments and numerical simulations. We have seen in Chapter 5 that some insight can be obtained using integral methods. We have in particular seen that boundary layers involve different scales. Primarily, wall-normal length-scales are much smaller than streamwise ones. We show here how we can take advantage of this observation using the Navier–Stokes equation.

## 6.1 Physical framework

We consider the developing boundary layer sketched in figure 6.1. Such a two-dimensional stationary flow is governed by the following Navier–Stokes equations:

$$\rho\left(u\partial_x u + v\partial_y u\right) = -\partial_x p + \mu\left(\partial_x^2 u + \partial_y^2 u\right), \tag{6.1}$$

$$\rho\left(u\partial_x v + v\partial_y v\right) = -\partial_y p + \mu\left(\partial_x^2 v + \partial_y^2 v\right), \tag{6.2}$$

where $\rho$ is the fluid's density, $u$ is the streamwise ($x$-) velocity, $v$ the wall-normal ($y$-) velocity, $p$ is the pressure and $\mu$ is the fluid's dynamic viscosity. The flow is incompressible, so we pose:

$$\partial_x u + \partial_y v = 0. \tag{6.3}$$

Lastly, the boundary conditions are:

$$u = v = 0 \qquad \text{at } y = 0, \tag{6.4}$$

$$(u, v) \to (U, 0) \qquad \text{at } y \to \infty. \tag{6.5}$$

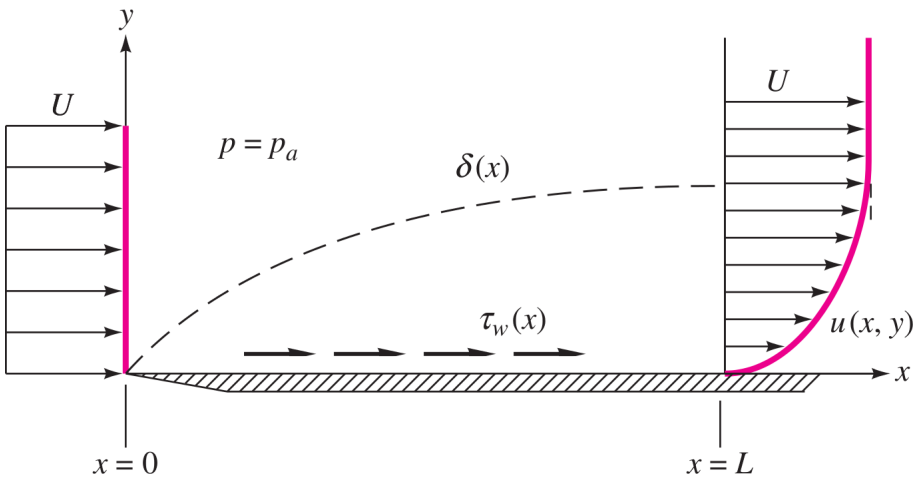


Figure 6.1: Sketch of a developing boundary layer on a flat plate. After White, *Fluid Mechanics* (2011).

## 6.2 Boundary layer equations

### 6.2.1 Scalings

We start by noting that dynamics occur on a (arbitrary) length scale $L$ in the streamwise direction and $\delta$, the boundary layer thickness, in the wall-normal direction. The spatial derivatives then follow the scalings:

$$\partial_x \sim \frac{1}{L}, \qquad \partial_y \sim \frac{1}{\delta}. \tag{6.6}$$

In addition, these length scales are not comparable: $L \gg \delta$. We can thus introduce a small parameter $\epsilon \ll 1$ such that

$$\frac{\delta}{L} = \epsilon. \tag{6.7}$$

The streamwise velocity $u$ is of the same order of magnitude as the velocity infinitely far away from the plate $U$ but the order of magnitude of the wall-normal velocity $v$ is yet to be determined. To that end, we assume that both terms in the incompressibility constraint are of the same order of magnitude:

$$\frac{U}{L} \sim \frac{v}{\delta}, \tag{6.8}$$

which gives:

$$v \sim \frac{U\delta}{L}, \tag{6.9}$$

$$\Rightarrow \quad v \sim \epsilon U, \tag{6.10}$$

implying that the wall-normal velocity is smaller than the streamwise one.

We can now rescale the wall-normal quantities according to the streamwise quantities. We define the rescaled quantities by:

$$x^* = \frac{x}{L}, \tag{6.11}$$
$$y^* = \frac{y}{\delta} = \frac{y}{\epsilon\, L}, \tag{6.12}$$
$$u^* = \frac{u}{U}, \tag{6.13}$$
$$v^* = \frac{v}{\epsilon\, U}, \tag{6.14}$$
$$p^* = \frac{p}{\rho U^2}, \tag{6.15}$$

where the pressure is nondimensionalised in such a way that it remains of the same order of magnitude as the other terms.

Remark: in the case of an incompressible flow, the pressure can be thought of as a mathematical function whose role is to ensure incompressibility.

### 6.2.2 Asymptotic derivation

Using the dimensionless variables, the incompressibility constraint reads:

$$\frac{U}{L}\partial_{x^*}u^* + \frac{\epsilon U}{\epsilon L}\partial_{y^*}v^* = 0, \tag{6.16}$$

yielding:

$$\partial_{x^*}u^* + \partial_{y^*}v^* = 0. \tag{6.17}$$

Similarly, the Navier–Stokes equation becomes:

$$\rho\left(\tfrac{U^2}{L}u^*\partial_{x^*}u^* + \tfrac{U^2}{L}v^*\partial_{y^*}u^*\right) = -\frac{\rho U^2}{L}\partial_{x^*}p^* + \mu\left(\frac{U}{L^2}\partial^2_{x^*}u^* + \frac{U}{\epsilon^2 L^2}\partial^2_{y^*}u^*\right), \tag{6.18}$$
$$\rho\left(\tfrac{\epsilon U^2}{L}u^*\partial_{x^*}v^* + \tfrac{\epsilon U^2}{L}v^*\partial_{y^*}v^*\right) = -\frac{\rho U^2}{\epsilon L}\partial_{y^*}p^* + \mu\left(\frac{\epsilon U}{L^2}\partial^2_{x^*}v^* + \frac{U}{\epsilon L^2}\partial^2_{y^*}v^*\right), \tag{6.19}$$

and simplifies into

$$u^*\partial_{x^*}u^* + v^*\partial_{y^*}u^* = -\partial_{x^*}p^* + \frac{1}{Re_L}\partial^2_{x^*}u^* + \frac{1}{\epsilon^2 Re_L}\partial^2_{y^*}u^*, \tag{6.20}$$
$$u^*\partial_{x^*}v^* + v^*\partial_{y^*}v^* = -\frac{1}{\epsilon^2}\partial_{y^*}p^* + \frac{1}{Re_L}\partial^2_{x^*}v^* + \frac{1}{\epsilon^2 Re_L}\partial^2_{y^*}v^*, \tag{6.21}$$

where we have introduced the Reynolds number $Re_L = \rho UL/\mu$.

We are interested in $Re_L \gg 1$. As $\epsilon \ll 1$, the term $\partial^2_{x^*}u^*/Re_L$ is the smallest in equation (6.20) and $\partial^2_{x^*}v^*/Re_L$ is the smallest in equation (6.21). We drop them.

To keep a balance between advection (left-hand-side) and diffusion (right-hand-side), and therefore retain sensible physics, we impose $\epsilon^2 Re_L = 1$. As a result, the small quantity we have introduced is now related to the Reynolds number:

$$\epsilon = \frac{\delta}{L} = Re_L^{-1/2}, \tag{6.22}$$

a result consistent with the analysis of Von Kármán in Chapter 5.

Consequently, the leading order of system (6.20), (6.21) is:

$$u^* \partial_{x^*} u^* + v^* \partial_{y^*} u^* = -\partial_{x^*} p^* + \partial^2_{y^*} u^*, \tag{6.23}$$

$$\partial_{y^*} p^* = 0, \tag{6.24}$$

where equation (6.24) implies that the pressure does not vary across the boundary layer, but only along it.

We can then express the pressure at any point in the critical layer by applying the Bernoulli equation on a streamline away from the boundary layer. There, no energy is dissipated by viscous forces (the flow is homogeneous) and we have:

$$p + \frac{\rho u^2}{2} = \text{cst}, \tag{6.25}$$

which gives in dimensionless form:

$$p^* + \frac{{u^*}^2}{2} = \text{cst}. \tag{6.26}$$

Outside the boundary layer, the velocity is $u^* = 1$, so we have

$$p^* + \frac{1}{2} = \text{cst}, \tag{6.27}$$

$$\Rightarrow \qquad \partial_{x^*} p^* = 0, \tag{6.28}$$

a relation valid for all $y^*$.

### 6.2.3 Reduced equations

The asymptotic derivation led to remove some subdominant terms from the streamwise momentum equation. The incompressibility constraint remains the same, and as the pressure has now been simplified away, the wall-normal equation is no longer needed. The resulting set of reduced equations for the boundary layer writes

$$\partial_{x^*} u^* + \partial_{y^*} v^* = 0, \tag{6.29}$$

$$u^* \partial_{x^*} u^* + v^* \partial_{y^*} u^* = \partial^2_{y^*} u^*, \tag{6.30}$$

and is to be solved together with the following boundary conditions:

$$u^* = v^* = 0 \qquad \text{at } y^* = 0, \tag{6.31}$$

$$u^* \to 1 \qquad \text{at } y^* \to \infty. \tag{6.32}$$

The second boundary condition for $v$ is not necessary as $v$ is only derived once with respect to $y$ in the above equations.

## 6.3 Asymptotic solution

Heinrich Blasius (1883–1970), German engineer, University of Hamburg

### 6.3.1 Self-similar variables

While studying the dimensional boundary layer equations

$$\partial_x u + \partial_y v = 0, \tag{6.33}$$

$$u\partial_x u + v\partial_y u = \nu\partial_y^2 u, \tag{6.34}$$

where $\nu = \mu/\rho$, Blasius conjectured that the boundary layer is self-similar, i.e., that at any given point along the boundary layer, the velocity profile is the same to a stretching factor on the spatial dimension. He wrote:

$$\eta = y\left(\frac{U}{\nu x}\right)^{1/2}, \qquad \frac{u(x,y)}{U} = f'(\eta), \tag{6.35}$$

where $f(\eta)$ is a dimensionless quantity and $f'(\eta)$ denotes its derivative with respect to the dimensionless wall-normal coordinate $\eta$.

One of the virtues of the rescaling is that the wall-normal direction is rescaled by a quantity proportional to the laminar boundary layer thickness ($\delta/x \approx 5.5Re_x^{-1/2} \Rightarrow \delta \approx 5.5(\nu x/U)^{1/2}$ after Chapter 5). In other words, the laminar boundary layer is mapped onto a rectangle.

### 6.3.2 The Blasius equation

As the flow is incompressible and two-dimensional, we introduce a streamfunction $\psi$ such that

$$u = \partial_y\psi, \qquad v = -\partial_x\psi. \tag{6.36}$$

Such a change of variable is helpful to collapse our two-variable $(u, v)$ problem onto a single variable $(\psi)$ problem: the incompressibility constraint is automatically verified as

$$\partial_x u + \partial_y v = \partial_x(\partial_y\psi) + \partial_y(-\partial_x\psi) = 0. \tag{6.37}$$

More details on streamfunctions will be given in Chapter 7.

Using the streamfunction, the system (6.33), (6.34) reduces down the single equation:

$$\partial_y\psi\,\partial_x\partial_y\psi - \partial_x\psi\,\partial_y^2\psi = \nu\partial_y^3\psi. \tag{6.38}$$

Equation (6.38) has yet to be written in terms of Blasius's variables (6.35). To do so, we note that the definition of the streamfunction (6.36) implies

$$Uf'(\eta) = \partial_\eta\psi\partial_y\eta, \tag{6.39}$$

$$\Rightarrow \quad \psi = U\int_0^\eta \frac{1}{\partial_y\eta} f'(\eta)d\eta, \tag{6.40}$$

providing the new definitions:

$$\psi = U\gamma(x)f(\eta), \qquad \gamma(x) = (\nu x/U)^{1/2}. \tag{6.41}$$

With these new variables, the spatial derivatives of $\psi$ become:

$$\begin{aligned} \partial_x\psi &= U\left(\partial_x\gamma f + \gamma\partial_\eta f\partial_x\eta\right), && (6.42)\\ &= U\left(\gamma' f - \gamma f'\frac{y\gamma'}{\gamma^2}\right), && (6.43)\\ &= U\gamma' f - Uf'\frac{y\gamma'}{\gamma}, && (6.44) \end{aligned}$$

and

$$\begin{aligned} \partial_y\psi &= U\gamma\partial_\eta f\partial_y\eta, && (6.45)\\ &= U\gamma f'\frac{1}{\gamma}, && (6.46)\\ &= Uf', && (6.47) \end{aligned}$$

where $\gamma' = \partial_x\gamma$ and $f' = \partial_\eta f$.

The terms of equation (6.38) therefore become

$$\begin{aligned} \partial_y\psi\,\partial_x\partial_y\psi &= (Uf')\;\partial_x\left(Uf'\right), && (6.48)\\ &= (Uf')\;Uf''\left(-\frac{y\gamma'}{\gamma^2}\right), && (6.49)\\ &= -U^2\frac{y\gamma'}{\gamma^2}f'f'', && (6.50) \end{aligned}$$

$$\begin{aligned} \partial_x\psi\,\partial_y^2\psi &= \left(U\gamma' f - Uf'\frac{y\gamma'}{\gamma}\right)\;\partial_y\left(Uf'\right), && (6.51)\\ &= \left(U\gamma' f - Uf'\frac{y\gamma'}{\gamma}\right)\;U\frac{1}{\gamma}f'', && (6.52)\\ &= U^2\frac{\gamma'}{\gamma}ff'' - U^2\frac{y\gamma'}{\gamma^2}f'f'', && (6.53) \end{aligned}$$

$$\begin{aligned} \nu\partial_y^3\psi &= \nu\partial_y^2\left(Uf'\right), && (6.54)\\ &= \nu U\partial_y\left(\frac{1}{\gamma}f''\right), && (6.55)\\ &= \nu U\frac{1}{\gamma^2}f'''. && (6.56) \end{aligned}$$

In the end, equation (6.38) simplifies into:

$$\begin{aligned} -U^2\frac{y\gamma'}{\gamma^2}f'f'' - \left(U^2\frac{\gamma'}{\gamma}ff'' - U^2\frac{y\gamma'}{\gamma^2}f'f''\right) &= \nu U\frac{1}{\gamma^2}f''', && (6.57)\\ \nu U\frac{1}{\gamma^2}f''' + U^2\frac{\gamma'}{\gamma}ff'' &= 0, && (6.58)\\ f''' + \frac{U\gamma'\gamma}{\nu}ff'' &= 0. && (6.59) \end{aligned}$$

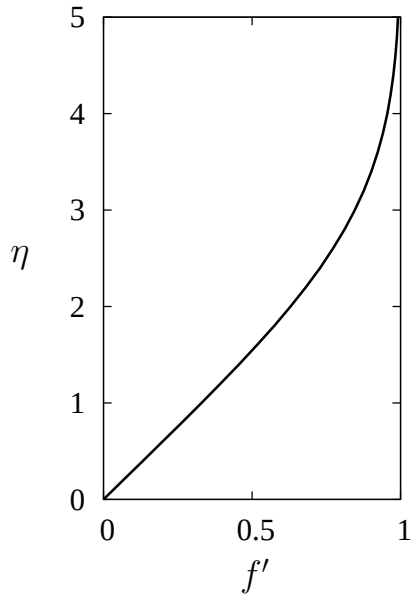


Figure 6.2: Solution of the Blasius equation (6.60) with boundary conditions (6.61) and (6.62). The dimensionless velocity $u/U = f'$ is represented as a function of the dimensionless wall-normal coordinate $\eta = y(U/\nu x)^{1/2}$.

The variable $\gamma$ is easily derived with definition (6.41) and yields $U\gamma'\gamma/\nu = 1/2$. The equation Blasius obtained for the dimensionless quantity $f$ is then

$$f''' + \frac{1}{2} f f'' = 0. \tag{6.60}$$

This equation is complemented with the boundary conditions (6.31) and (6.32) that now write:

$$f' = f = 0, \qquad \eta = 0, \tag{6.61}$$

$$f' \to 1, \qquad \eta \to \infty. \tag{6.62}$$

### 6.3.3 The Blasius boundary layer

Equation (6.60) is generally solved numerically. We show a solution of this equation in figure 6.2.

This laminar boundary layer solution is self-similar: the same profile holds at any given position $x$ along the boundary layer, the only change being a stretching coefficient in the wall-normal direction as $\eta$ is a linear function of $y$ and depends on $x$.

The boundary layer equation (6.60) and this solution are valid for $x \in [0; L_{max}]$ and $\eta \in \mathcal{R}^+$, where $L_{max}$ represents the point at which a change in dynamics occurs that violates one of the hypotheses made. This point can arise due to a transition where the boundary layer becomes turbulent. There, wall-normal velocities become of the same

order as streamwise velocities because of the creation and advection of eddies and the whole analysis carried out in this Chapter breaks down.

Since $u/U \to 1$ as $\eta \to \infty$, we can define the boundary layer thickness as the region in which $u/U \leq 0.99$, or in other words $f' \leq 0.99$. The solution in figure 6.2 provides a boundary layer thickness of $\eta \approx 5.0$. Therefore:

$$\delta \left(\frac{U}{\nu x}\right)^{1/2} \approx 5.0, \tag{6.63}$$

$$\Rightarrow \quad \delta \approx 5.0 \left(\frac{\nu x}{U}\right)^{1/2}, \tag{6.64}$$

$$\Rightarrow \quad \frac{\delta}{x} \approx 5.0 \left(\frac{\nu}{Ux}\right)^{1/2}, \tag{6.65}$$

$$\Rightarrow \quad \frac{\delta}{x} \approx 5.0 Re_x^{-1/2}. \tag{6.66}$$

With this velocity profile known and using definitions introduced in Chapter 5, we can compute the skin friction coefficient:

$$c_f \approx 0.664 Re_x^{-1/2}, \tag{6.67}$$

as well as the displacement thickness:

$$\frac{\delta^*}{x} \approx 1.721 Re_x^{-1/2}. \tag{6.68}$$

The momentum thickness can also be computed from the velocity profile:

$$\frac{\theta}{x} \approx 0.664 Re_x^{-1/2}, \tag{6.69}$$

which eventually gives the shape factor for the Blasius laminar boundary layer:

$$H = \frac{\delta^*}{\theta} \approx 2.59. \tag{6.70}$$

## 6.4 Solution comparison

Table 6.1 provides a comparison of the approximations found in Chapter 5 with the ones obtained by Blasius. Despite the major differences between the approaches, we observe that the error between Von Kármán's integral formulation and Blasius boundary layer theory is rather small: they are at most 10% off for the boundary layer thickness and skin friction coefficient.

| Result | $\delta/x$ | $\delta^*/x$ | $H$ | $c_f$ |
|---|---|---|---|---|
| Blasius laminar | $5.0Re_x^{-1/2}$ | $1.721Re_x^{-1/2}$ | 2.59 | $0.664Re_x^{-1/2}$ |
| Integral laminar | $5.5Re_x^{-1/2}$ | $1.83Re_x^{-1/2}$ | 2.5 | $0.73Re_x^{-1/2}$ |
| Error | 10% | 6% | 3% | 10% |
| Integral turbulent | $0.16Re_x^{-1/7}$ | $0.02Re_x^{-1/7}$ | 1.3 | $0.027Re_x^{-1/7}$ |

Table 6.1: Comparison of boundary layer characteristics for the asymptotic Blasius laminar boundary layer and the integral formulation from Chapter 5. The quantities compared are the boundary layer thickness $\delta$, the displacement thickness $\delta^*$, the shape factor $H$ and the skin friction coefficient $c_f$. Results for turbulent boundary layers, as approximated by the integral method in Chapter 5 are also given for comparison.

# Chapter 7

# Potential flow theory

Flows past immersed bodies generate boundary layers. In cases where the Reynolds number is large enough, the boundary layer becomes thin and we can use asymptotic methods (Chapter 6). Outside these boundary layers, the flow is typically inviscid and irrotational. Such flows are solutions of a Laplace equation and are called potential flows.

Potential flow theory is not only limited to applications to the outer region in boundary layer flows. For very low Reynolds number flows, such as electroosmotic flows or creeping flows, the momentum equation can be reduced to a Laplace equation and potential flow theory applies.

## 7.1 Basic concepts

### 7.1.1 Velocity potential

For an irrotational flow ($\nabla \times \mathbf{u} \equiv \mathbf{0}$), we can define a velocity potential $\phi$ such that

$$\mathbf{u} = \nabla\phi, \tag{7.1}$$

or

$$u = \partial_x\phi, \qquad v = \partial_y\phi, \qquad w = \partial_z\phi. \tag{7.2}$$

The definition of the velocity through the velocity potential ensures the irrotationality of the flow:

$$\nabla \times \mathbf{u} = \nabla \times \nabla\phi = \mathbf{0}. \tag{7.3}$$

The Euler equation for an inviscid flow writes:

$$\rho\left(\partial_t\mathbf{u} + (\mathbf{u}\cdot\nabla)\mathbf{u}\right) = -\nabla p + \rho\mathbf{g}, \tag{7.4}$$

for which we have kept the gravitational acceleration term for the sake of exhaustivity. Using vectorial calculus, we can express the advective term in a different way:

$$\rho\left(\partial_t\mathbf{u}+\frac{1}{2}\nabla(\mathbf{u}\cdot\mathbf{u})+(\nabla\times\mathbf{u})\times\mathbf{u}\right)=-\nabla p+\rho\mathbf{g}. \tag{7.5}$$

As the flow is irrotational, $\nabla\times\mathbf{u}\equiv\mathbf{0}$ and equation (7.5) becomes

$$\rho\left(\partial_t\mathbf{u}+\frac{1}{2}\nabla(\mathbf{u}\cdot\mathbf{u})\right)+\nabla p-\rho\mathbf{g}=0, \tag{7.6}$$

which can be written with the velocity potential as follows:

$$\rho\left(\partial_t\nabla\phi+\frac{1}{2}\nabla(\mathbf{u}\cdot\mathbf{u})\right)+\nabla p-\nabla\left(\rho\mathbf{g}\cdot\mathbf{x}\right)=0, \tag{7.7}$$

where $\mathbf{x}=(x,y,z)$. We now assume $\mathbf{g}=-g\hat{\mathbf{z}}$ and integrate the equation once to get the time-dependent Bernoulli equation:

$$\rho\partial_t\phi+\frac{\rho|\mathbf{u}|^2}{2}+p+\rho gz=\text{cst}, \tag{7.8}$$

where $|\mathbf{u}|^2=\mathbf{u}\cdot\mathbf{u}=|\nabla\phi|^2$.

The incompressibility constraint, expressed with the velocity potential, writes

$$\nabla\cdot\mathbf{u}=0, \tag{7.9}$$
$$\Rightarrow\quad\nabla\cdot\nabla\phi=0, \tag{7.10}$$
$$\Rightarrow\quad\nabla^2\phi=0, \tag{7.11}$$

which is the Laplace equation.

When one solves for a potential flow, the outer boundary conditions are written for the velocity (gradient of the velocity potential) while at the surface of the immersed structure, the boundary condition is a vanishing normal derivative of the velocity potential: $\partial_n\phi=0$. This translates the fact that the immersed structure is an impenetrable boundary. All these boundary conditions turn out to involve derivatives. As a result, the solution to the Laplace equation is not unique and $\phi$ is defined to a constant. A common way to fix this ill-posedness is to set the average of $\phi$ to zero. Such a resetting does not impact the the physical result as the velocity potential only appears through its derivatives.

### 7.1.2 Streamfunction

For a two-dimensional incompressible flow, we can define a streamfunction $\psi$ such that

$$u=\partial_y\psi,\qquad\qquad v=-\partial_x\psi. \tag{7.12}$$

This definition ensures the incompressibility of the flow:

$$\nabla\cdot\mathbf{u}=\partial_x\partial_y\psi-\partial_y\partial_x\psi=0. \tag{7.13}$$

Note that definition (7.12) is not unique. One can define an equivalent streamfunction $\psi'$ through $u = -\partial_y \psi$ and $v = \partial_x \psi$. These two possible definitions are analogous in the sense they provide two streamfunctions only differing by their sign.

If the flow is irrotational, then

$$\nabla \times \mathbf{u} = 0, \tag{7.14}$$

$$\Rightarrow \quad \begin{pmatrix} \partial_x \\ \partial_y \end{pmatrix} \times \begin{pmatrix} \partial_y \psi \\ -\partial_x \psi \end{pmatrix} = 0, \tag{7.15}$$

$$\Rightarrow \quad \nabla^2 \psi = 0, \tag{7.16}$$

which is again the Laplace equation.

The two-dimensional Navier–Stokes equation reads

$$\partial_t u + u\partial_x u + v\partial_y u = -\partial_x p + \partial_x^2 u + \partial_y^2 u, \tag{7.17}$$

$$\partial_t v + u\partial_x v + v\partial_y v = -\partial_y p + \partial_x^2 v + \partial_y^2 v. \tag{7.18}$$

We take the curl of the above equations to obtain:

$$\partial_t \nabla^2 \psi + u\partial_{xy} u + \partial_y u \partial_x u + \partial_y v \partial_y u + v\partial_y^2 u - \partial_x u \partial_x v - u\partial_x^2 v - \partial_x v \partial_y v - v\partial_{xy} v = \nabla^4 \psi, \tag{7.19}$$

where we have used the relation $\nabla \times \mathbf{u} = -\nabla^2 \psi$. Upon correct association of the advective terms, we eventually get:

$$\partial_t \nabla^2 \psi + \partial_y \psi \partial_x \nabla^2 \psi - \partial_x \psi \partial_y \nabla^2 \psi = \nabla^4 \psi. \tag{7.20}$$

Note that this equation is less friendly than equation (7.16).

Equation (7.16) is accompanied with boundary conditions for the velocity (involving derivatives of the streamfunction) for the outer boundaries. The surface of the immersed structure being a streamline, the corresponding boundary condition is $\psi = \text{cst}$. The constant set at the surface of the structure is typically 0 and ensures that the problem is well-posed.

### 7.1.3 Isolines

Lines along which the velocity potential is constant are called potential lines and similarly, lines along which the streamfunction takes a constant value are called streamlines.

Streamlines are tangent to the velocity vector. Indeed:

$$\mathbf{u} \cdot \nabla \psi = u\partial_x \psi + v\partial_y \psi, \tag{7.21}$$

$$= \partial_y \psi \partial_x \psi - \partial_x \psi \partial_y \psi, \tag{7.22}$$

$$= 0, \tag{7.23}$$

indicating that the vector velocity is orthogonal to the vector normal to the streamline.

Conversely, as the velocity is the gradient of the velocity potential, at any point in the flow, the velocity vector is orthogonal to the potential line (this follows from the definition). Differentiating the velocity potential in two dimensions yields:

$$d\phi = \partial_x \phi dx + \partial_y \phi dy, \tag{7.24}$$

where $(dx, dy)$ represents the line element. Along a potential line $d\phi = 0$. Upon substitution of the gradients of $\phi$, we obtain:

$$0 = udx + vdy, \tag{7.25}$$

$$\Rightarrow dy = -\frac{udx}{v}. \tag{7.26}$$

The same calculation can be carried out for the streamfunction with the line element defined as $(dx', dy')$:

$$d\psi = \partial_x \psi dx' + \partial_y \psi dy', \tag{7.27}$$

$$\Rightarrow 0 = -vdx' + udy', \tag{7.28}$$

$$\Rightarrow dy' = \frac{vdx'}{u}. \tag{7.29}$$

Taking the dot product between the potential line element and the streamline element, we find:

$$dx\,dx' + dy\,dy' = dx\,dx' - \frac{udx}{v}\frac{vdx'}{u}, \tag{7.30}$$

$$= dx\,dx' - dx\,dx', \tag{7.31}$$

$$= 0, \tag{7.32}$$

showing that potential lines and streamlines are orthogonal, and proving again that the potential lines are orthogonal to the velocity gradient.

## 7.2 Elementary solutions

We illustrate the use of the velocity potential and of the streamfunction through a few examples of elementary solutions in the absence of a structure. In this section, the flow is two-dimensional, irrotational, incompressible and inviscid and obeys equations (7.11) and (7.16).

As we shall see in Chapter 8, these equations (and associated boundary conditions) are linear and we can therefore add two solutions together to create a third solution. The solutions introduced here thus represent building blocks of potential flow theory.

### 7.2.1 Uniform streams

A uniform stream $\mathbf{u} = U\hat{\mathbf{x}}$ is both incompressible ($\nabla \cdot \mathbf{u} = 0$) and irrotational ($\nabla \times \mathbf{u} = 0$). This flow therefore possesses both a velocity potential and a streamfunction.

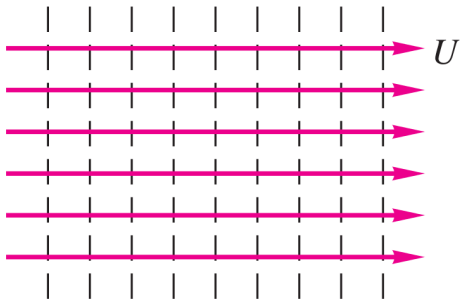


Figure 7.1: Uniform flow $\mathbf{u} = U\hat{\mathbf{x}}$ represented using potential lines ($x = \text{cst}$, dashed lines) and streamlines ($y = \text{cst}$, solid pink lines). After White, *Fluid Mechanics* (2011).

Definition (7.2) yields

$$U = \partial_x \phi, \qquad 0 = \partial_y \phi, \tag{7.33}$$

indicating the velocity potential does not depend on $y$ and that upon integrating the first equation we get

$$\phi = Ux, \tag{7.34}$$

where we have set the constant of integration to zero.

In the same spirit, definition (7.12) yields

$$U = \partial_y \psi, \qquad 0 = \partial_x \psi, \tag{7.35}$$

which shows that the streamfunction is independent of $x$. It follows, upon integration of the first equation:

$$\psi = Uy. \tag{7.36}$$

No immersed structure is present to set the constant of integration, so we set it once again to zero.

The potential lines correspond to $x = \text{cst}$ and the streamlines to $y = \text{cst}$. They are therefore orthogonal as shown in figure 7.1. Finally, it is straighforward to show that both $\phi$ and $\psi$ are harmonic functions, i.e., that they solve $\nabla^2\phi = 0$ and $\nabla^2\psi = 0$.

It might be interesting to consider a flow forming an angle $\alpha$ with the $x$ coordinate. Definitions (7.2) and (7.12) imply:

$$U\cos(\alpha) = \partial_x \phi = \partial_y \psi, \qquad U\sin(\alpha) = \partial_y \phi = -\partial_x \psi, \tag{7.37}$$

which gives the following expressions for the velocity potential and streamfunction:

$$\phi = U(x\cos(\alpha) + y\sin(\alpha)), \qquad \psi = U(y\cos(\alpha) - x\sin(\alpha)). \tag{7.38}$$

### 7.2.2 Sources and sinks

We inject some fluid at the origin ($x = 0, y = 0$) creating an axisymmetric outward flow with no azimuthal velocity. This special point is called source. If, on the contrary, we

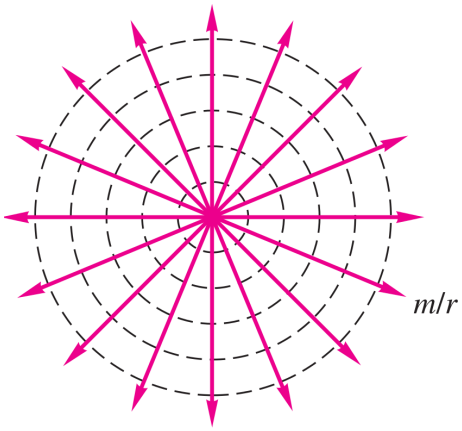


Figure 7.2: Source $\mathbf{u} = Q/2\pi r\hat{\mathbf{r}} = m/r\hat{\mathbf{r}}$ represented using potential lines ($r$ = cst, dashed lines) and streamlines ($\theta$ = cst, solid pink lines). After White, *Fluid Mechanics* (2011).

suck up fluid at this point, the resulting velocity field is pointing inwards and the point is called sink.

In polar coordinates, the velocity components associated with a source or sink are:

$$u_r = \frac{Q}{2\pi r}, \qquad u_\theta = 0, \tag{7.39}$$

where $u_r$ represents the radial velocity, $Q$ the flow rate and $u_\theta$ the azimuthal velocity. Note that the flow rate across a section $r$ = cst in polar coordinates is:

$$Q = \int_0^{2\pi} u_r r d\theta. \tag{7.40}$$

It follows that $Q$ is not a function of $r$.

Definitions (7.2) and (7.12), in polar coordinates, give:

$$\frac{Q}{2\pi r} = \partial_r \phi = \frac{1}{r}\partial_\theta \psi, \qquad 0 = \frac{1}{r}\partial_\theta \phi = -\partial_r \psi, \tag{7.41}$$

which, upon integration give the following forms for the velocity potential and streamfunction:

$$\phi = \frac{Q}{2\pi}\ln r, \qquad \psi = \frac{Q}{2\pi}\theta, \tag{7.42}$$

where, once again, the constants of integration have been dropped.

The potential lines are circles ($r$ = cst) and the streamlines spokes ($\theta$ = cst), as shown in figure 7.2. The Lapace operator applied to the velocity potential and streamfunction in polar coordinates writes

$$\nabla^2\phi = \frac{1}{r}\partial_r\left(r\partial_r\phi\right) + \frac{1}{r^2}\partial_\theta^2\phi = \frac{1}{r}\partial_r\left(\frac{Q}{2\pi}\right) + 0 = 0, \tag{7.43}$$

$$\nabla^2\psi = \frac{1}{r}\partial_r\left(r\partial_r\psi\right) + \frac{1}{r^2}\partial_\theta^2\psi = 0 + \frac{1}{r^2}\partial_\theta\frac{Q}{2\pi} = 0, \tag{7.44}$$

which confirms that both the velocity potential and the streamfunction defined in equation (7.42) are harmonic functions.

The difference between a source and a sink lies in the sign of $Q$: $Q > 0$ defines a source while $Q < 0$ defines a sink.

We can also define sources and sinks that are not located at the origin. Consider such an object of corresponding flow rate $Q$ located at $(x, y) = (a, b)$. Back to Cartesian coordinates, $r = \sqrt{x^2 + y^2}$. If the source/sink is offset, this relationship becomes $r = \sqrt{(x-a)^2 + (y-b)^2}$. The velocity potential from equation (7.42) now writes:

$$\phi = \frac{Q}{2\pi} \ln \left[ \sqrt{(x-a)^2 + (y-b)^2} \right], \tag{7.45}$$

$$\Rightarrow \quad \phi = \frac{Q}{4\pi} \ln \left[ (x-a)^2 + (y-b)^2 \right]. \tag{7.46}$$

Similarly, the angle $\theta$ can be expressed in Cartesian coordinates: $\theta = \tan^{-1} y/x$. The streamfunction corresponding to an offset source or sink then writes:

$$\psi = \frac{Q}{2\pi} \tan^{-1} \left( \frac{y-b}{x-a} \right). \tag{7.47}$$

Remark: it might be easier to think in terms of the source/sink strength $m = Q/2\pi$ rather than the flow rate $Q$.

### 7.2.3 Free vortices

The last elementary potential flow solution we introduce in this lecture is the irrotational vortex. The irrotational or free vortex has vanishing radial velocity and the azimuthal velocity only varies with $r$. We can then write:

$$u_r = 0, \qquad u_\theta = f(r), \tag{7.48}$$

Note that this flow naturally satisfies the incompressibility constraint. As we want it to be irrotational, we impose

$$\nabla \times \mathbf{u} = 0, \tag{7.49}$$

$$\Rightarrow \frac{1}{r} \left[ \partial_r (r u_\theta) - \partial_\theta u_r \right] = 0. \tag{7.50}$$

The solution of equation (7.50), provided the solution form in relations (7.48) is

$$u_r = 0, \qquad u_\theta = \frac{K}{r}, \tag{7.51}$$

where $K$ represents the strength of the vortex.

The definition of the velocity potential and of the streamfunction in polar coordinates writes:

$$0 = \partial_r \phi = \frac{1}{r} \partial_\theta \psi, \qquad \frac{K}{r} = \frac{1}{r} \partial_\theta \phi = -\partial_r \psi, \tag{7.52}$$

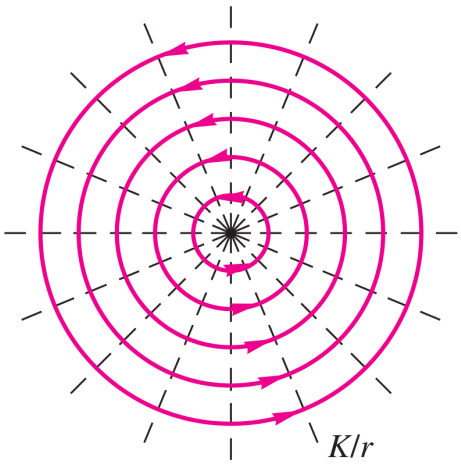


Figure 7.3: Irrotational vortex $\mathbf{u} = K/r\hat{\theta}$ represented using potential lines ($\theta$ = cst, dashed lines) and streamlines ($r$ = cst, solid pink lines). After White, *Fluid Mechanics* (2011).

which yields:

$$\phi = K\theta, \qquad \psi = -K \ln r, \tag{7.53}$$

where once again, the constants of integration have been dropped.

The potential lines associated with this irrotational vortex are spokes: $\theta$ = cst; while the streamlines are circles: $r$ = cst, as shown in figure 7.3.

A similar calculation to that done for the source/sink in equation (7.43) and (7.44) can be carried out here to demonstrate that both the velocity potential and the streamfunction are harmonic functions.

We can also express the velocity potential and streamfunction of an offset free vortex using the same method as for the source/sink. The result for a vortex located at $(x, y) = (a, b)$ is:

$$\phi = K \tan^{-1}\left(\frac{y-b}{x-a}\right), \qquad \psi = -\frac{K}{2} \ln\left[(x-a)^2 + (y-b)^2\right]. \tag{7.54}$$

Note that $K > 0$ defines a anti-clockwise vortex while $K < 0$ defines a clockwise vortex.

## 7.3 Wrap-up

Your potential cheat sheet!

We summarise the definitions and properties of the velocity potential and the streamfunction in table 7.1.

| Function | Velocity potential | Streamfunction |
|---|---|---|
| Definition | $\mathbf{u} = \nabla\phi$ | $u = \partial_y\psi;\ v = -\partial_x\psi$ |
| Dimension | 3D | 2D |
| $\nabla \cdot \mathbf{u} = 0$ | $\nabla^2\phi = 0$ | Automatically satisfied |
| $\nabla \times \mathbf{u} = 0$ | Automatically satisfied | $\nabla^2\psi = 0$ |
| Isoline | $(\phi = \text{cst}) \perp \mathbf{u}$ | $(\psi = \text{cst}) \parallel \mathbf{u}$ |

Table 7.1: Summary of the definition and properties of the velocity potential $\phi$ and streamfunction $\psi$.

| Elementary flow | Velocity potential | Streamfunction |
|---|---|---|
| Uniform stream | $\phi = U(x\cos(\alpha) + y\sin(\alpha))$ | $\psi = U(y\cos(\alpha) - x\sin(\alpha))$ |
| Source/sink | $\phi = \dfrac{Q}{4\pi}\ln\left[(x-a)^2 + (y-b)^2\right]$ | $\psi = \dfrac{Q}{2\pi}\tan^{-1}\left(\dfrac{y-b}{x-a}\right)$ |
| Free vortex | $\phi = K\tan^{-1}\left(\dfrac{y-b}{x-a}\right)$ | $\psi = -\dfrac{K}{2}\ln\left[(x-a)^2 + (y-b)^2\right]$ |

Table 7.2: Summary of the main elementary potential flows. The uniform stream is defined by its velocity $U$ and angle with respect to the $x$-axis: $\alpha$. The source/sink is defined through its flow rate $Q$ while the free vortex is defined through its strength $K$. Both source/sink and free vortex are located at $(x, y) = (a, b)$.

Note that the streamfunction we have introduced in this Chapter is two-dimensional. There exist more complex definitions for the streamfunction that can be used in three dimensions.

The elementary flows introduced in this lecture are also summarised in table 7.2. These flows prove very useful to construct more complicated and realistic models as we shall see in the next lecture.

# Chapter 8

# Superposition of potential flow solutions

We have introduced in Chapter 7 three flows that are incompressible and irrotational: a uniform stream, a source/sink and an irrotational vortex. They represent elementary potential flow solutions as they possess harmonic velocity potential $\phi$ and streamfunction $\psi$:

$$\nabla^2\phi = 0, \tag{8.1}$$
$$\nabla^2\psi = 0. \tag{8.2}$$

As equations (8.1) and (8.2) are linear, it is possible to superpose several elementary potential flow solutions to generate additional potential flows. Indeed, if $\phi_1$ and $\phi_2$ are distinct elementary potential flow solution, then:

$$\nabla^2(\phi_1 + \phi_2) = \nabla^2\phi_1 + \nabla^2\phi_2 = 0 + 0 = 0. \tag{8.3}$$

An identical calculation stands for streamfunctions. In this Chapter, we use this superposition principle to create more complex flows using the three elementary flows previously introduced.

## 8.1 A source and a sink

### 8.1.1 Magnets

We consider a source of strength $m$ (flow rate $Q = 2\pi m$) placed at $(x, y) = (-a, 0)$ combined with a sink of strength $-m$ placed at $(x, y) = (a, 0)$. The velocity and the streamfunction characterising the source are:

$$\phi_{source} = \frac{1}{2} m \ln[(x+a)^2 + y^2], \qquad \psi_{source} = m \tan^{-1} \frac{y}{x+a}, \tag{8.4}$$

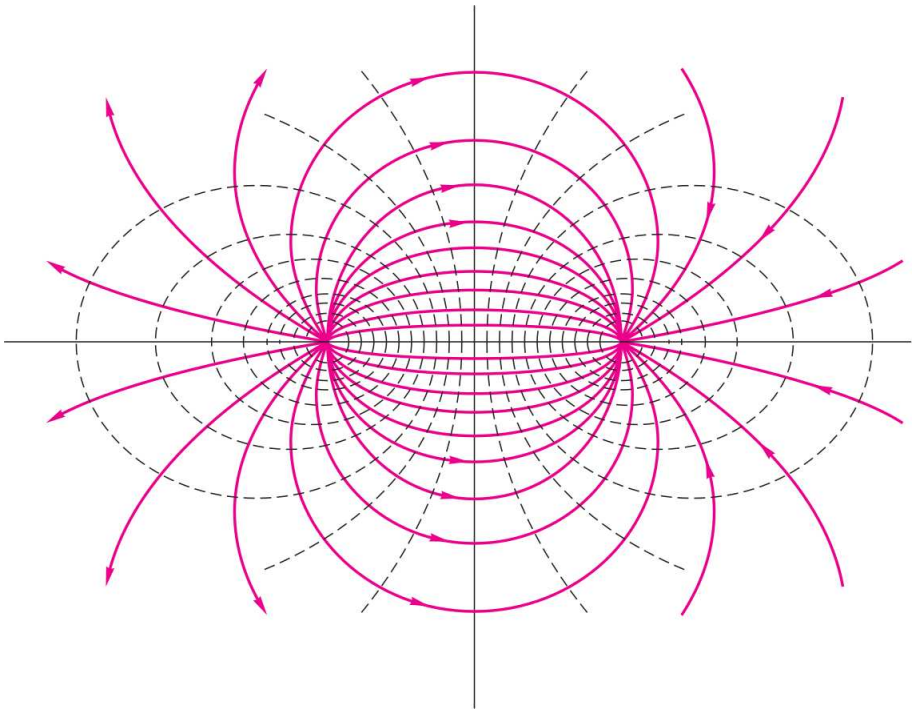

Figure 8.1: Potential flow resulting from the superposition of a source $m$ at $(a, 0)$ and a sink $-m$ at $(-a, 0)$. Solid lines are streamlines while dashes lines are potential lines. The direction of the flow is indicated with the arrows on the streamlines. After White, *Fluid Mechanics* (2011).

while those of the sink are:

$$\phi_{sink} = -\frac{1}{2} m \ln[(x-a)^2 + y^2], \qquad \psi_{sink} = -m \tan^{-1} \frac{y}{x-a}. \tag{8.5}$$

It follows that the composite velocity potential and streamfunction are the sum of the two:

$$\phi = \phi_{source} + \phi_{sink} \quad = \frac{1}{2} m \left( \ln[(x+a)^2 + y^2] - \ln[(x-a)^2 + y^2] \right) \tag{8.6}$$

$$= \frac{1}{2} m \ln \frac{(x+a)^2 + y^2}{(x-a)^2 + y^2}, \tag{8.7}$$

$$\psi = \psi_{source} + \psi_{sink} \quad = m \left( \tan^{-1} \frac{y}{x+a} - \tan^{-1} \frac{y}{x-a} \right) \tag{8.8}$$

$$= -m \tan^{-1} \frac{2ay}{x^2 + y^2 - a^2}. \tag{8.9}$$

The potential lines and streamlines obtained for this configuration are shown in figure 8.1. Note that such a figure is well known to electrodynamicists since the velocity potential (streamfunction) here is analogous to the electric potential (electric current) of a magnet with poles at $(\pm a, 0)$.

Moving the relative position of the sink compared to the source (or vice-versa) does not change the resulting flow. Indeed, a trivial change of coordinate (rotation and homothety)

will always bring us back to this figure. A change in their relative strength will however break the left/right symmetry.

### 8.1.2 The doublet

If we move the source and sink closer to each other, i.e., if $a$ is decreased to a vanishingly small quantity, we obtain another interesting flow: the doublet. The streamfunction writes

$$\psi = \lim_{a\to 0}\left(-m\tan^{-1}\frac{2ay}{x^2+y^2-a^2}\right) \tag{8.10}$$

$$= -\frac{2amy}{x^2+y^2}, \tag{8.11}$$

which tends to zero. To avoid this and preserve a flow, we impose $2am = \lambda = \text{cst}$:

$$\psi = -\frac{\lambda y}{x^2+y^2}. \tag{8.12}$$

We can express the velocity potential similarly to obtain:

$$\phi = \frac{\lambda x}{x^2+y^2}. \tag{8.13}$$

An interesting property of the doublet is the shape of the potential lines and streamlines. Indeed, by multiplying the left- and right-hand-side of relation (8.12) by $(x^2+y^2)/\psi$ and rearranging the terms, we find:

$$x^2 + \left(y + \frac{\lambda}{2\psi}\right)^2 = \left(\frac{\lambda}{2\psi}\right)^2, \tag{8.14}$$

indicating that the streamlines are circles. Their centre lies at $(x, y) = (0, -\lambda/2\psi)$ and they have a radius of $\lambda/2\psi$. Consequently, they all touch the origin $(0, 0)$ and are aligned vertically. A similar result is obtained for the potential lines: by multiplying the left- and right-hand-side of relation (8.13) by $(x^2+y^2)/\phi$ and rearranging the terms, we find:

$$\left(x - \frac{\lambda}{2\phi}\right)^2 + y^2 = \left(\frac{\lambda}{2\phi}\right)^2. \tag{8.15}$$

The potential lines are thus cercles touching the origin $(0, 0)$ and aligned horizontally. These results are illustrated in figure 8.2.

It may also be helpful to think of the doublet in terms of polar coordinates:

$$\phi = \frac{\lambda\cos\theta}{r}, \tag{8.16}$$

$$\psi = -\frac{\lambda\sin\theta}{r}. \tag{8.17}$$

This writing will be particularly helpful for cylinder flows.

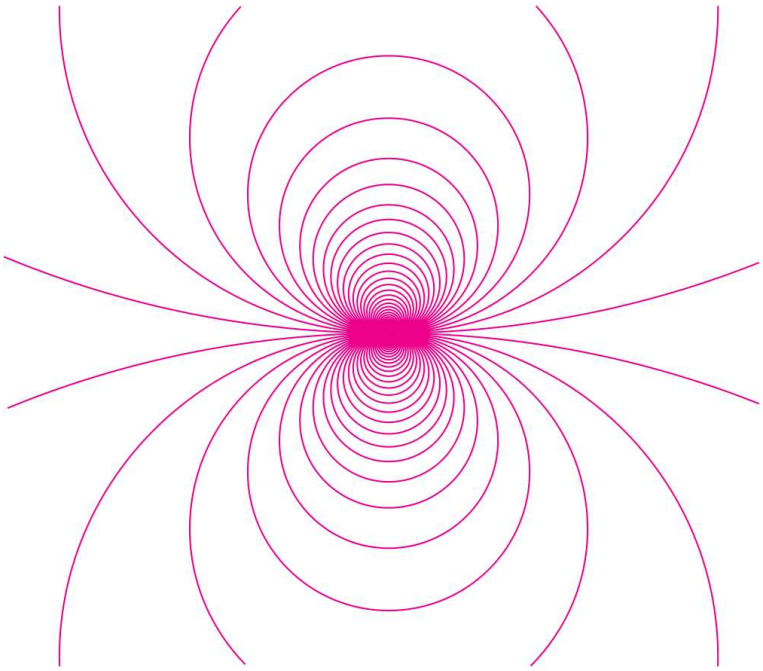

Figure 8.2: Potential flow resulting from the bringing a source $m$ and a sink $-m$ asymptotically close to each other. The product $am$, where $a$ is half the distance between the source and the sink is kept constant. Solid lines represent streamlines. This configuration is called doublet. After White, *Fluid Mechanics* (2011).

## 8.2 A vortex and a sink: tornadoes

Close to ground level, a tornado basically looks like a vortex that is sucking up fluid to higher altitude. We can model this by superposing a sink of strength $m$ and a free vortex of strength $K$ placed both at the origin $(0, 0)$. The resulting potential flow and streamfunction in polar coordinates are:

$$\begin{aligned} \phi &= \phi_{sink} + \phi_{vortex} && (8.18)\\ &= m \ln r + K\theta, && (8.19)\\ \psi &= \psi_{sink} + \psi_{vortex} && (8.20)\\ &= m\theta - K \ln r. && (8.21) \end{aligned}$$

The potential lines and the streamlines obtained from equations (8.19) and (8.21) are shown in figure 8.3. The fluid spirals down to the center, like in a simplified depiction of a tornado.

It is possible to adjust how fast the fluid is drained to the center compared to how many rotations it does by changing the ratio $m/K$. For larger $m/K$, the vortex is weaker and the fluid goes to the center more rapidly. For smaller $m/K$, the sink is weaker and the fluid particles undergo more revolutions around the core of the tornado before reaching it.

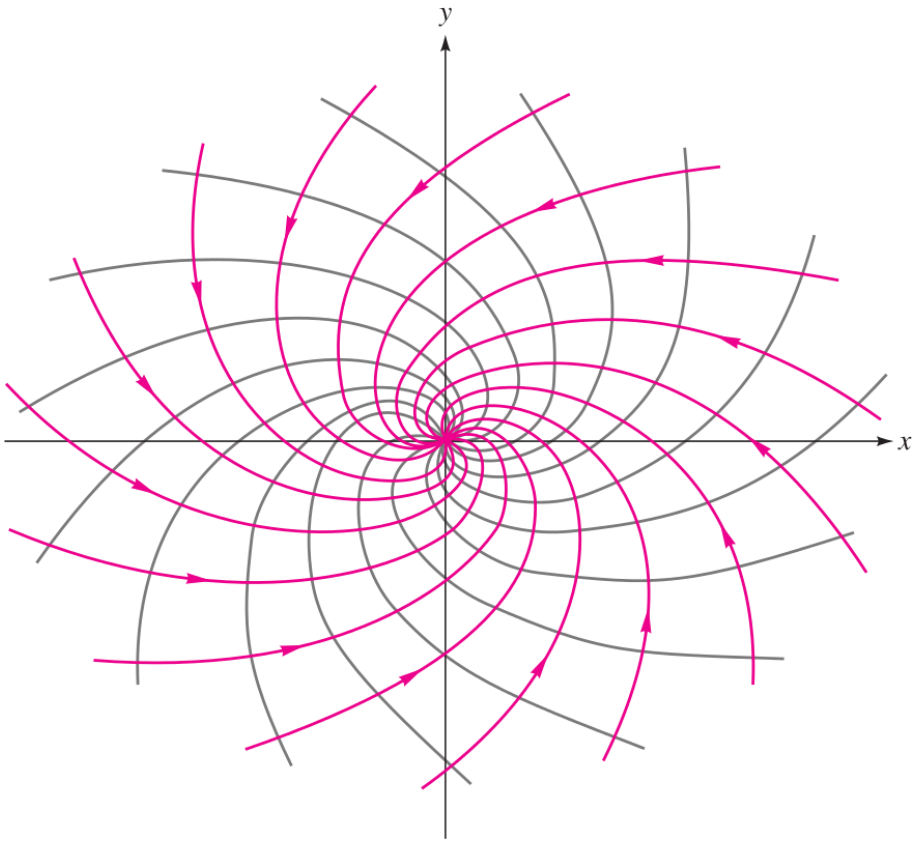


Figure 8.3: Potential flow resulting from the superposition of a sink $m$ at $(0,0)$ and a free vortex $K$ at $(0,0)$. Solid pink lines are streamlines while solid black lines are potential lines. The direction of the flow is indicated with the arrows on the streamlines. After White, *Fluid Mechanics* (2011).

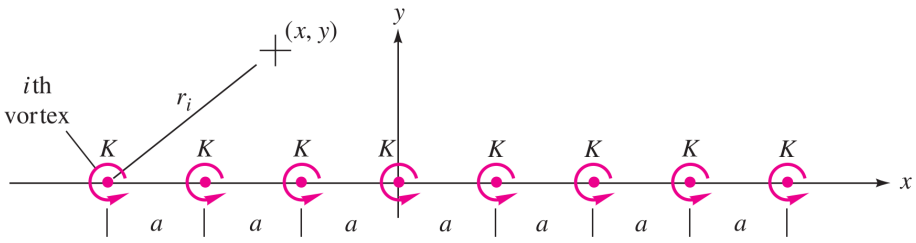


Figure 8.4: Row of vortices of strength $K$ placed at a distance $a$ from each other. After White, *Fluid Mechanics* (2011).

Remark: a real tornado is way more complex. It is a fully three-dimensional flow, viscous, rotational and turbulent. This potential flow here is not meant to model an actual tornado but just provide some low-level modeling for spiraling flows.

## 8.3 Many vortices

### 8.3.1 Cat's eyes

If we create a row of equally strong equispaced free vortices, a fascinating structure arises: the cat's eyes. The associated streamfunction is

$$\psi = -K \sum_{i=1}^{\infty} \ln r_i, \tag{8.22}$$

where we have considered an infinite amount of vortices of strength $K$, and where the distance between the $i$-th vortex and the considered point is $r_i$ as indicated in figure 8.4. After some algebra, the infinite sum in expression (8.22) can be collapsed to a closed-form function:

$$\psi = -\frac{1}{2} K \ln \left[ \frac{1}{2} \left( \cosh \frac{2\pi y}{a} - \cos \frac{2\pi x}{a} \right) \right], \tag{8.23}$$

where $(x, y)$ is the position at which the streamfunction is evaluated. Figure 8.5 shows the streamfunction corresponding to the superposition of such free vortices. The pattern obtained is called *cat's eyes*: the fluid in the vicinity of the vortices rotates around the closest vortex while far enough, it will either go left (above the vortices) or right (below the vortices). Such a pattern is similar to that found in mixing layers and known under the phenomenon called *Kelvin–Helmholtz instability* (see figure 8.6).

### 8.3.2 The vortex sheet

We can see from expression (8.23) that there are two main regions in physical space:

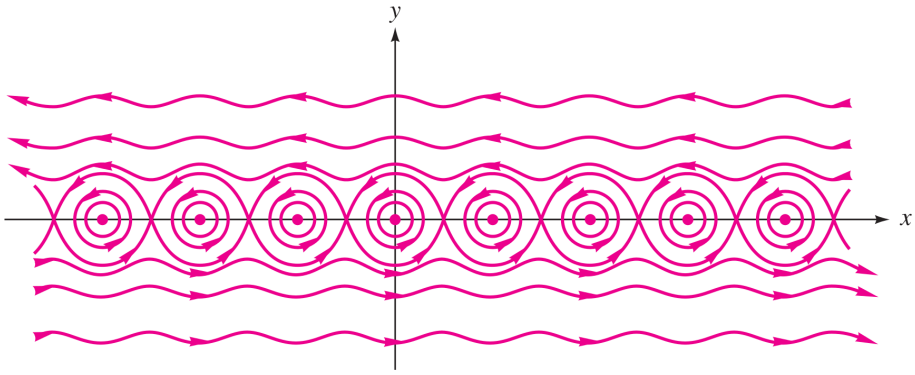


Figure 8.5: Cat's eyes pattern obtained from the configuration shown in figure 8.4. After White, *Fluid Mechanics* (2011).

Figure 8.6: Temporal development of the Kelvin–Helmholtz secondary instability in a sheared fluid constituted of two layers, with the black fluid being three times denser than the white fluid. After Fontane *et al.*, *Phys. Fluids* **20**, 091109 (2008).

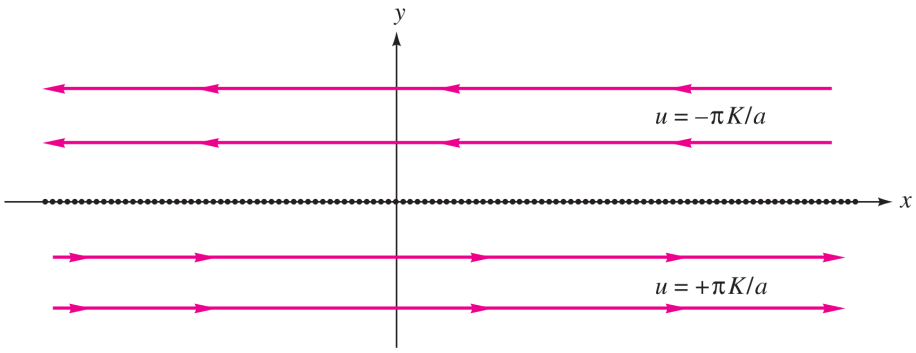


Figure 8.7: Figure 8.5 viewed from afar. The vortices are packed into a continuous vortex sheet. Above (resp. below) the vortex sheet, the flow goes to the left (resp. right). After White, *Fluid Mechanics* (2011).

- For small enough $y$, we are in a vortex region:

$$\psi \approx -\frac{1}{2}K \ln\left[\frac{1}{2}\left(1-\cos\frac{2\pi x}{a}\right)\right]. \tag{8.24}$$

- For large enough $y$, we are in a streaming region:

$$\psi \approx -\frac{1}{2}K \ln\left[\frac{1}{2}\left(\cosh\frac{2\pi y}{a}\right)\right]. \tag{8.25}$$

Therefore, far from the vortices, the flow is dominated by $x$-velocity (the approximated streamfunction only varies with $y$). Upon differentiation, we obtain:

$$\begin{aligned} u &\approx \partial_y \psi && (8.26)\\ &\approx -\frac{1}{2}K\frac{2\pi}{a}\frac{\sinh(2\pi y/a)}{\cosh(2\pi y/a)} && (8.27)\\ &\approx \mp\frac{K\pi}{a}, && (8.28) \end{aligned}$$

where we have used the fact that far away from the vortices, $|y| \gg a$ and therefore $\sinh(2\pi y/a)/\cosh(2\pi y/a) = \tanh(2\pi y/a) \to \pm 1$.

Looked from afar, the vortices are packed so closely that they look like a *vortex sheet*. Above the vortex sheet, the flow is to the left, below, it is to the right. Figure 8.7 illustrate this configuration.

In the equivalent limit of infinitely close vortices, the cat's eyes vertical length goes to zero and there is no $y$-velocity. The resulting flow looks like a uniform stream possessing a velocity jump at $y = 0$. The vortex sheet is a central piece of the modelling of thin lift-generating surfaces like airfoils.

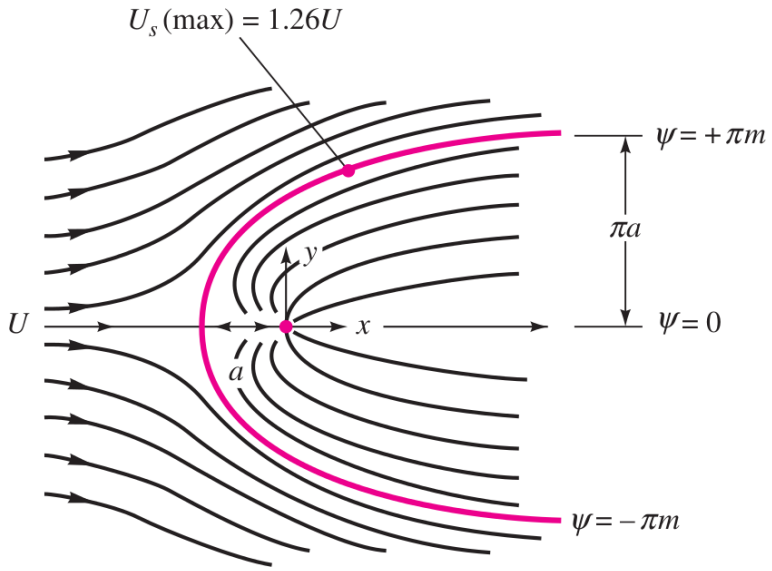


Figure 8.8: Potential flow resulting from the superposition of a uniform stream $U\hat{\mathbf{x}}$ and a source $m$ at $(0, 0)$ represented through its streamlines. The direction of the flow is indicated by the arrows. After White, *Fluid Mechanics* (2011).

## 8.4 The Rankine half-body

William Rankine, (1820–1872), Scottish engineer, University of Glasgow

If we superpose a uniform stream $U\hat{\mathbf{x}}$ and a source of strength $m$ located at the origin, we obtain a particular flow: the Rankine half-body. We recall that the velocity potential and the streamfunction of the uniform stream write:

$$\phi_{stream} = Ux = Ur\cos\theta, \tag{8.29}$$
$$\psi_{stream} = Uy = Ur\sin\theta. \tag{8.30}$$

The superposition therefore yields:

$$\phi = Ur\cos\theta + m\ln r, \tag{8.31}$$
$$\psi = Ur\sin\theta + m\theta. \tag{8.32}$$

The streamlines associated with this superposition are shown in figure 8.8.

There are two stagnation points: the source at $(x, y) = (0, 0)$ and an additional point on the left where the flow injected at the source meets that coming from the uniform stream.

To find the second stagnation point, we write the velocity field from the velocity potential:

$$u = \partial_x\phi = U + \frac{m}{r}\cos\theta, \tag{8.33}$$
$$v = \partial_y\phi = \frac{m}{r}\sin\theta. \tag{8.34}$$

On the line $\theta = \pm\pi$, the $y$-velocity vanishes everywhere, but the $x$-velocity only vanishes at $U - m/r = 0$. The left stagnation point is therefore at $(r, \theta) = (a, \pm\pi)$ or equivalently $(x, y) = (-a, 0)$ where $a = m/U$.

This stagnation point is on the streamline that separates the incoming stream from the source flow (see figure 8.8). It corresponds to:

$$\psi = Ua\sin(\pm\pi) + m(\pm\pi) = \pm m\pi. \tag{8.35}$$

The upper part of the streamline corresponds to $\psi = +m\pi$:

$$m\pi = Ur\sin\theta + m\theta, \tag{8.36}$$

$$\Rightarrow \qquad r = a\frac{\pi - \theta}{\sin\theta}. \tag{8.37}$$

Similarly, the lower streamline corresponds to $\psi = -m\pi$:

$$-m\pi = Ur\sin\theta + m\theta, \tag{8.38}$$

$$\Rightarrow \qquad r = -a\frac{\pi + \theta}{\sin\theta}. \tag{8.39}$$

It is a reflection ($y \to -y$ or $\theta \to -\theta$) of the upper streamline. These streamlines being connected and going to infinity, they can be seen as a solid surface.

The norm of the velocity writes:

$$V = \sqrt{u^2 + v^2} = U\sqrt{1 + \frac{a^2}{r^2} + \frac{2a}{r}\cos\theta}, \tag{8.40}$$

where we have used $m = Ua$.

We can use equation (8.37) to express the norm of the velocity along the upper streamline. Upon setting its derivative to zero, we find the location where the velocity is maximum along the streamline: $\theta \approx 1.1 \approx 63°$. This point is labelled $U_{s,max}$ in figure 8.8 and by symmetric construction, there exists an analogous point along the lower streamline at $\theta \approx -1.1 \approx -63°$. In the context of boundary layers past a body, this is the point after which the surface flow decelerates and creates an increase in pressure. As a consequence, the laminar boundary layer grows thicker and becomes susceptible to separation.

# Chapter 9

# Potential flows around solid bodies

In the previous Chapter, we have superposed several elementary potential flow solutions to construct a series of more complex flows. We have seen that in the context of the superposition of a source and a uniform stream, a streamline separates space into two different regions. This streamline can be seen as a solid body, the Rankine half-body, and the flow assimilated to a potential flow around it. Similarly, we have seen that the vortex sheet was another way to separate space into two different regions and that it can be used as a modelling tool. We focus, in this Chapter, on closed body shapes.

## 9.1 Closed bodies

Due to the superposition principle (see Chapter 8), we can superpose many elementary potential flows together to generate more complex flows. A general rule to construct closed bodies is to superpose a uniform stream, creating the incoming flow, with sources, sinks and vortices. Additionally, to conserve mass, with the outflow created by the sources equal to the net sink inflow. Generally, the presence of the uniform stream creates the incoming flow, the combination of sources and sinks creates the shape of the body and the vortices design shear or velocity differences across the body.

### 9.1.1 Rankine oval

William Rankine, (1820–1872), Scottish engineer, University of Glasgow

The first closed shape we introduce here is obtained by superposing a source-sink pair to a uniform stream with the source-sink pair aligned with the incoming flow. The source $m$ is placed at $(x, y) = (-a, 0)$ and the sink $-m$ at $(x, y) = (a, 0)$. The uniform stream has form $U\hat{\mathbf{x}}$.

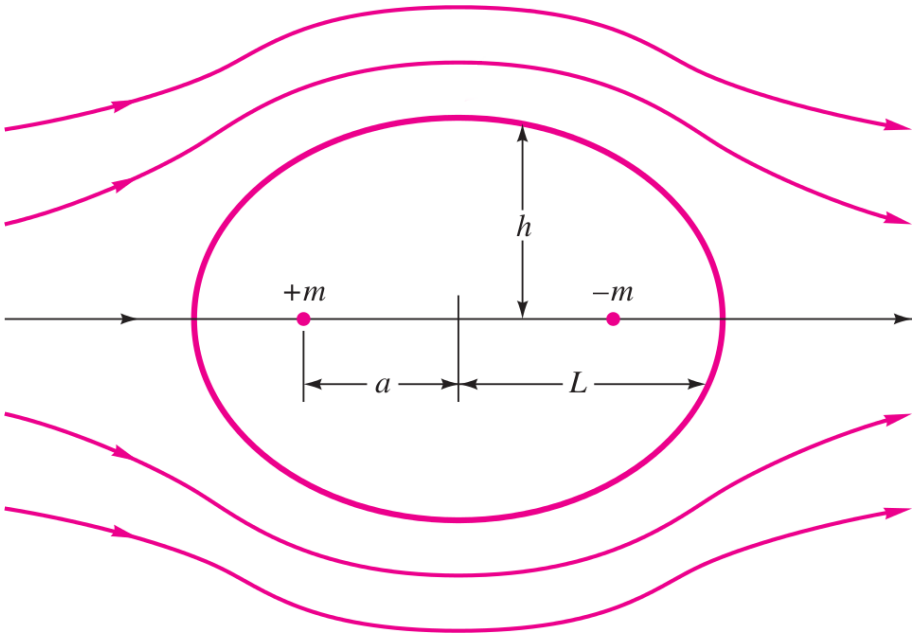


Figure 9.1: Flow generated by the superposition of a source $m$ located at $(x, y) = (-a, 0)$, a sink $-m$ located at $(x, y) = (a, 0)$ and a uniform stream $U\hat{\mathbf{x}}$. This configuration creates a closed streamline around the source-sink pair called Rankine oval. This example is represented for $m/Ua = 1$. After White, *Fluid Mechanics* (2011).

The streamfunction writes:

$$\psi = Uy - m \tan^{-1} \frac{2ay}{x^2 + y^2 - a^2}, \tag{9.1}$$

where the first term represents the contribution from the uniform stream and the second term that of the source-sink pair.

The flow associated with the Rankine oval is shown in figure 9.1. The incoming flow separates after meeting the outflow from the source, creating a stagnation point at $x = -L$. It then goes around the source and comes back together further downstream due to the influence of the sink at $x = a$, creating a second stagnation point at $x = L$. These two stagnation points are connected by two streamlines and thus constitute the leading and trailing edge of a closed body: the *Rankine oval*. Note that the inside of the Rankine oval is not of interest and we do therefore not represent the streamlines there.

To characterise the Rankine oval, we first need to determine the streamline on which these stagnation points occur. Both are at $y = 0$ for which equation (9.1) gives $\psi = 0$. We can now obtain some characteristic quantities related to the Rankine oval by writing that on its surface:

$$0 = Uy - m \tan^{-1} \frac{2ay}{x^2 + y^2 - a^2}. \tag{9.2}$$

We can determine the half-size $L$ of the Rankine oval by positing that $y \ll 1$. Equation

(9.2) gives:

$$Uy \approx m \tan^{-1} \frac{2ay}{L^2 - a^2}, \tag{9.3}$$

$$\Rightarrow \quad Uy \approx m \frac{2ay}{L^2 - a^2}, \tag{9.4}$$

$$\Rightarrow \quad L \approx \sqrt{a^2 + \frac{2am}{U}}, \tag{9.5}$$

$$\Rightarrow \quad \frac{L}{a} \approx \sqrt{1 + \frac{2m}{Ua}}. \tag{9.6}$$

Similarly, we can obtain the half-width $h$ of the Rankine oval by setting $x = 0$. Equation (9.2) yields:

$$\tan \frac{Uh}{m} \approx \frac{2ah}{h^2 - a^2}, \tag{9.7}$$

$$\Rightarrow \quad \tan \left[ \left( \frac{Ua}{m} \right) \frac{h}{a} \right] \approx 2 \frac{h}{a} \left( \frac{1}{(h/a)^2 - 1} \right), \tag{9.8}$$

$$\Rightarrow \quad \frac{h}{a} \approx \frac{1}{2} \left[ \left( \frac{h}{a} \right)^2 - 1 \right] \tan \left[ \left( \frac{Ua}{m} \right) \frac{h}{a} \right]. \tag{9.9}$$

While the length of the Rankine oval is easily computed from equation (9.6), its height has to be solved numerically due to the transcendental character of equation (9.9). We plot in figure 9.2 the reduced aspect ratio of the Rankine oval $L/h - 1$ against the group $Ua/m$. These results indicate a clear dependence of the aspect ratio on the nondimensional group $Ua/m$. In fact, we can roughly estimate the aspect ratio by the following form:

$$\frac{L}{h} \approx 1 + 0.3 \frac{Ua}{m}. \tag{9.10}$$

As a consequence, increasing the speed of the incoming flow, or similarly reducing the strength of the source-sink pair increases the aspect ratio of the Rankine oval: it becomes longer and longer while getting thinner and thinner.

### 9.1.2 Kelvin oval

William Thomson, 1st Baron Kelvin (1824–1907), Irish physicist, University of Glasgow

The aspect ratio of the Rankine oval is given by relation (9.10) and indicate that $L \geq h$. In other words, the long axis of the Rankine oval is always in the direction of the flow. We give here an example of construction of a closed body that is shaped against the flow: the Kelvin oval.

We superpose to the same incoming flow as for the Rankine oval two counter-rotating free vortices. The flow induced by the vortices between the vortices has to be against the

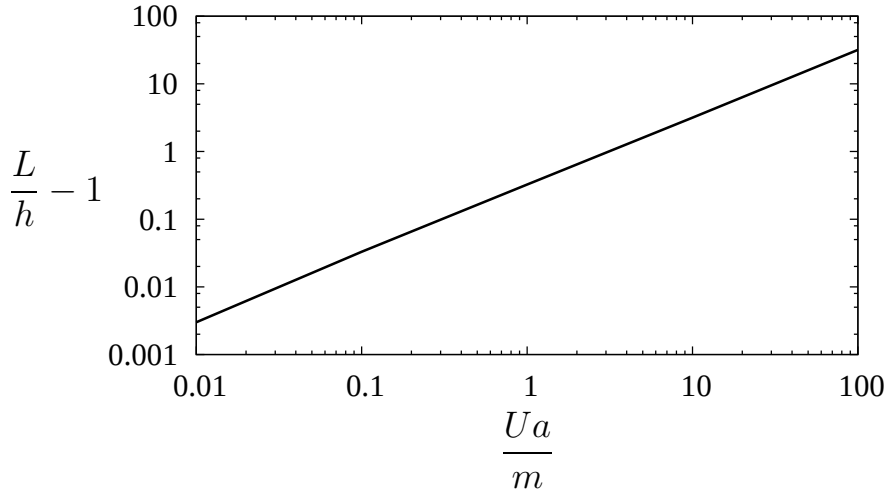


Figure 9.2: Reduced aspect ratio of the Rankine oval $L/h - 1$ against the nondimensional parameter $Ua/m$. Here, $L$ and $h$ are half the length and half the height of the Rankine oval respectively, $U$ is the incoming flow velocity, $a$ half the distance between the source and the sink and $m$ the strength of the source/sink.

incoming flow to create a continuous body. If the vortices are placed at $y = \pm a$ (and $x = 0$), and the uniform stream is rightwards, then the upper vortex should be clockwise (strength $-K$ with $K > 0$) and the lower vortex should be anti-clockwise (strength $K$).

The composite streamfunction reads:

$$\psi = Uy - \frac{1}{2}K \ln \frac{x^2 + (y+a)^2}{x^2 + (y-a)^2}, \tag{9.11}$$

and yields the streamlines represented in figure 9.3. For large values of $K/Ua$, the obtained geometry looks similar to the Rankine oval (see fig 9.1). However, for $K/Ua < 0.75$, the oval gets pinched at $x = 0$ and ends up looking like a figure-8 for $K/Ua = 0.5$.

The symmetry of the configuration indicates that the stagnation points should be on $y = 0$, where the vortex induced flow meets the incoming one. As a result, the streamlines reaching these stagnation points are characterised by $\psi = 0$, giving the following equality on the streamline:

$$0 = Uy - \frac{1}{2}K \ln \frac{x^2 + (y+a)^2}{x^2 + (y-a)^2}. \tag{9.12}$$

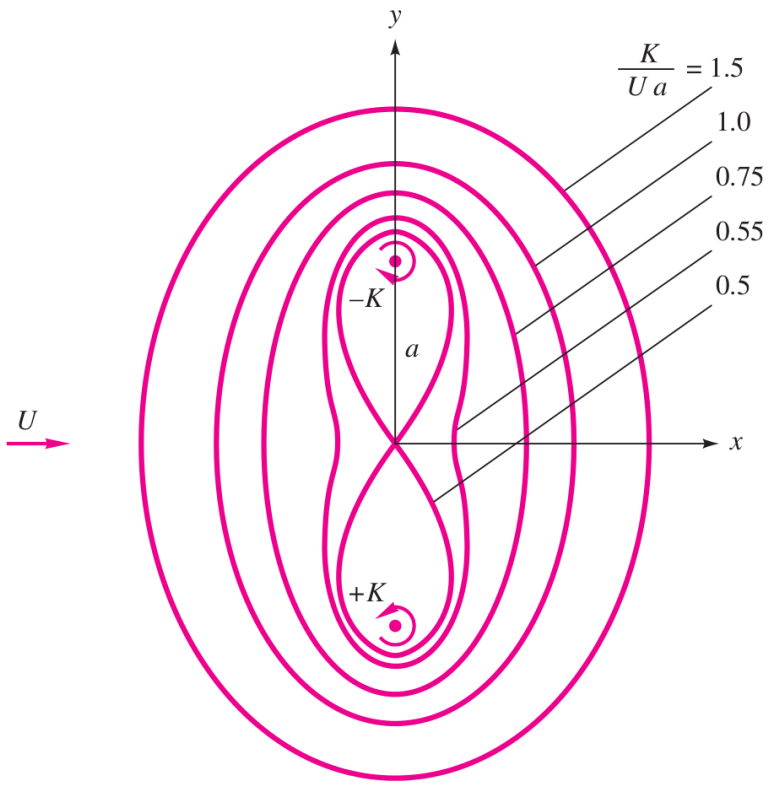


Figure 9.3: Flow generated by the superposition of two vortices $\pm K$ located at $(x, y) = (0, \mp a)$ and a uniform stream $U\hat{\mathbf{x}}$. This configuration creates a closed streamline around the vortex pair called Kelvin oval. The closed streamline is represented for several values of $K/Ua$. After White, *Fluid Mechanics* (2011).

We can obtain the half-length $L'$ of the Kelvin oval by setting $x = 0$:

$$UL' = \frac{1}{2}K \ln \frac{(L'+a)^2}{(L'-a)^2}, \tag{9.13}$$

$$\Rightarrow \quad \frac{2UL'}{K} = \ln\left[1 + \frac{4aL'}{(L'-a)^2}\right], \tag{9.14}$$

$$\Rightarrow \quad \exp\left(\frac{2UL'}{K}\right) = 1 + \frac{4aL'}{(L'-a)^2}, \tag{9.15}$$

$$\Rightarrow \quad \frac{L'}{a} = \frac{1}{4}\left(\frac{L'}{a} - 1\right)^2 \left[\exp\left(\frac{2Ua}{K}\frac{L'}{a}\right) - 1\right]. \tag{9.16}$$

The half-width $h'$ of the Kelvin oval can also be obtained by assuming $y \ll 1$. We recall that for $z \ll 1$, $\ln(1+z) \approx z + \mathcal{O}(z^2)$, which gives:

$$\frac{2Uy}{K} \approx \frac{4ay}{h'^2 + a^2}, \tag{9.17}$$

$$\Rightarrow \quad h'^2 + a^2 \approx \frac{2aK}{U}, \tag{9.18}$$

$$\Rightarrow \quad \frac{h'}{a} \approx \sqrt{\frac{2K}{Ua} - 1}. \tag{9.19}$$

### 9.1.3 Comparison between Rankine and Kelvin ovals

It is interesting to compare the shapes of the Rankine and Kelvin ovals. At large $m/Ua$ (small $Ua/m$), expression (9.6) yields:

$$\frac{L}{a} \approx \sqrt{\frac{2m}{Ua}}, \tag{9.20}$$

while expression (9.16) at large $K/Ua$ (small $Ua/K$) yields:

$$\frac{L'}{a} \approx \frac{1}{4}\left(\frac{L'}{a} - 1\right)^2 \frac{2Ua}{K}\frac{L'}{a}, \tag{9.21}$$

$$\Rightarrow \quad \frac{L'}{a} \approx \frac{1}{4}\left(\frac{L'}{a} - 1\right)^2 \frac{2Ua}{K}\frac{L'}{a}, \tag{9.22}$$

$$\Rightarrow \quad \left(\frac{L'}{a} - 1\right)^2 \approx \frac{2K}{Ua}, \tag{9.23}$$

$$\Rightarrow \quad \frac{L'}{a} \approx \sqrt{\frac{2K}{Ua}}. \tag{9.24}$$

The half-width can also be compared. Under the same conditions, expression (9.9)

yields:

$$\frac{h}{a} \approx \frac{1}{2}\left[\left(\frac{h}{a}\right)^2 - 1\right]\left(\frac{Ua}{m}\right)\frac{h}{a}, \tag{9.25}$$

$$\Rightarrow \quad \left(\frac{h}{a}\right)^2 - 1 \approx \frac{2m}{Ua}, \tag{9.26}$$

$$\Rightarrow \quad \frac{h}{a} \approx \sqrt{\frac{2m}{Ua}}, \tag{9.27}$$

while expression (9.19) yields:

$$\frac{h'}{a} \approx \sqrt{\frac{2K}{Ua}}. \tag{9.28}$$

Therefore, when $m/Ua$ and $K/Ua$ are taken large, we observe identical limits for the size of the ovals in relations (9.20) and (9.24) as well as for their width in relations (9.27) and (9.28).

## 9.2 Flow past a circle

If we consider the limit of large values of $m/Ua$, i.e., of large source strength (or weak incoming flow, or close enough source and sink), expressions (9.20) and (9.27) indicate that the Rankine oval tends to a circle. A similar statement can be made for a large values of $K/Ua$, based on expressions (9.24) and (9.28), for which the Kelvin oval tends to the Rankine oval, hence to a circle.

The radius of the circle is large compared to the spacing between the source and the sink, as indicated by expression (9.20) or (9.27). As we are interested in what happens outside the circle, we can unzoom the same way as when we looked at the source-sink pair in Chapter 8 to unveil a doublet. The Rankine oval viewed from afar is then the superposition of a uniform stream with a doublet:

$$\psi = Uy - \frac{\lambda y}{x^2 + y^2}, \tag{9.29}$$

where $\lambda = 2am$. In polar coordinates, this becomes:

$$\psi = Ur\sin\theta - \frac{\lambda \sin\theta}{r}. \tag{9.30}$$

For convenience, we set $\lambda = Ua^2$ such that

$$\psi = U\sin\theta\left(r - \frac{a^2}{r}\right), \tag{9.31}$$

for which $r = a$ is an obvious streamline ($\psi = 0$): the circle. Note that due to the new definition of $\lambda$, $a$ does no longer have any link with the half-distance between the source and sink, nor has to be small.

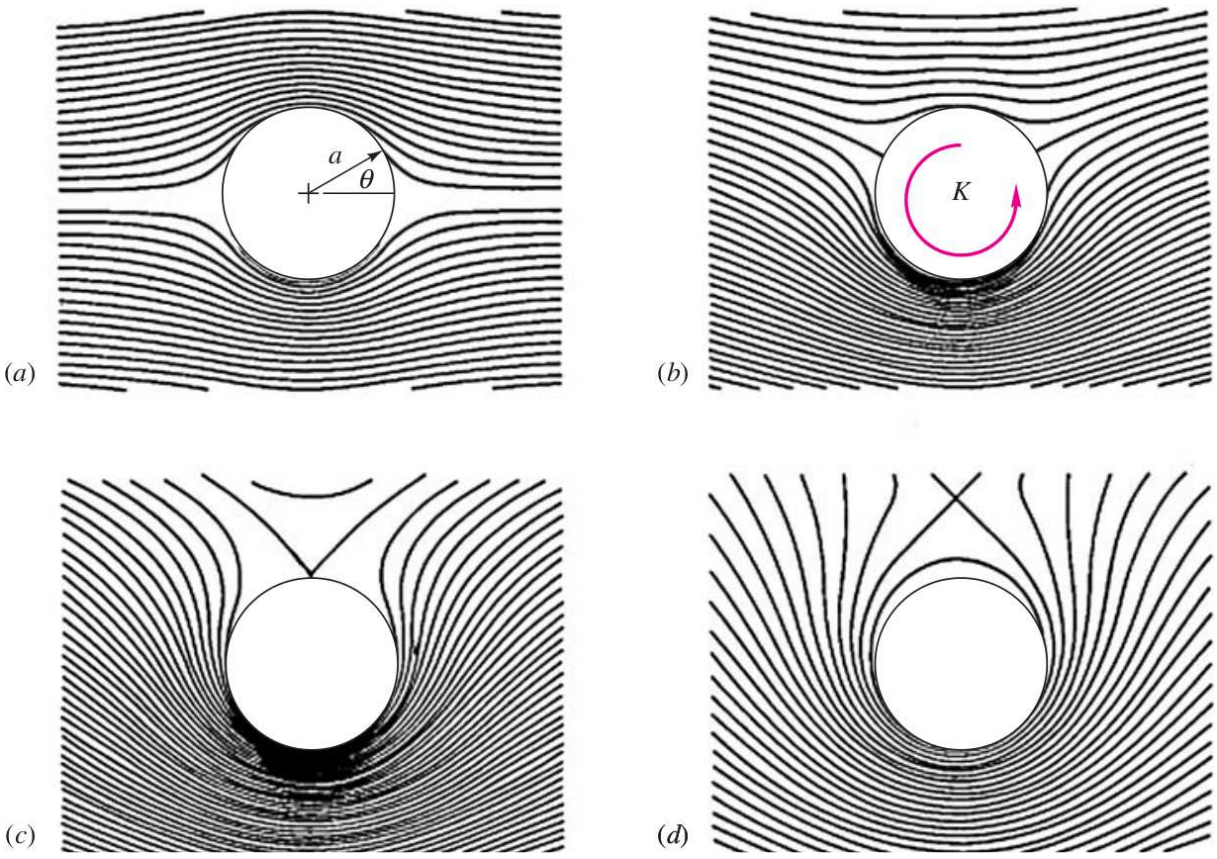


Figure 9.4: Flow around a rotating circle or radius $a$ generated by the superposition of a uniform stream $U\hat{\mathbf{x}}$, a doublet and a vortex of strength $K$. The streamlines are shown for $K/Ua = 0$ (a), $K/Ua = 1$ (b), $K/Ua = 2$ (c), $K/Ua = 3$ (d). After White, *Fluid Mechanics* (2011).

### 9.2.1 Rotating circle

The effect of rotation of the circle can be modelled by adding a free vortex of strength $K$ to the center of the configuration just described. The new streamfunction reads

$$\psi = U \sin\theta \left( r - \frac{a^2}{r} \right) - K \ln \frac{r}{a}, \tag{9.32}$$

where $r$ is divided by $a$ in the vortex contribution to the streamfunction so that the circle still corresponds to the streamline $\psi = 0$.

Figure 9.4 shows the streamlines around a rotating circle for different values of the dimensionless parameter $K/Ua$.

To understand these figures, we calculate the velocity components:

$$u_r = \frac{1}{r}\partial_\theta \psi \tag{9.33}$$

$$= U\cos\theta\left(1-\frac{a^2}{r^2}\right), \tag{9.34}$$

$$u_\theta = -\partial_r \psi \tag{9.35}$$

$$= -U\sin\theta\left(1+\frac{a^2}{r^2}\right)+\frac{K}{r}. \tag{9.36}$$

Expressed at the surface of the circle $r = a$, these yield:

$$u_r(r=a)=0, \qquad u_\theta(r=a) = -2U\sin\theta + \frac{K}{a}, \tag{9.37}$$

confirming that there is no radial flow on the circle.

We can calculate the location of the stagnation points on the circle:

$$0 = -2U\sin\theta_s + \frac{K}{a} \tag{9.38}$$

$$\Rightarrow \quad \sin\theta_s = \frac{K}{2Ua}. \tag{9.39}$$

So, for $K/Ua = 0$, i.e., no rotation, the flow is fully symmetric with two stagnation points on the circle: $\theta_{s1} = 0$ and $\theta_{s2} = \pi$, as confirmed by figure 9.4(a). As $K/Ua$ departs from 0, the flow looses the top/bottom symmetry and the stagnation points move at the same rate (figure 9.4(b)) to meet at $\theta_s = \pi/2$ for $K/Ua = 2$ (figure 9.4(c)). At larger values of the relative rotation rate, there is no stagnation point at the surface of the circle: it is rotating too fast and is surrounded by a layer of fluid rotating with it (figure 9.4(d)).

### 9.2.2 Circulation

We define the circulation as the closed line integral of the tangential velocity:

$$\Gamma = \oint_{\mathcal{C}} \mathbf{u}\cdot\mathbf{ds}, \tag{9.40}$$

where **ds** is the oriented line element on the closed contour $\mathcal{C}$. In the rotating circle case studied here, the circulation around the circle quantifies how much the fluid rotates around the body. The velocity is only azimuthal and the line element in this direction is $ad\theta$, so the circulation writes:

$$\Gamma(r=a) = \int_0^{2\pi}\left(-2U\sin\theta+\frac{K}{a}\right)ad\theta \tag{9.41}$$

$$= 2\pi K. \tag{9.42}$$

Unsurprisingly, this quantity is related to circle's rotation rate in a linear fashion.

### 9.2.3 The Kutta–Joukowski theorem

Heinrich Gustav Magnus (1802–1870), German physicist, University of Berlin
Nikolay Zhukovsky (1847–1921), Russian aeronautical engineer, Moscow State Technical University
Wilhelm Kutta (1867–1944), German mathematician, University of Stuttgart

We can investigate the Magnus effect generated by the rotation of the circle by calculating the lift force $L$ acting on it. Such a force is created by a non-trivial profile of pressure around the body and has to be counted positively if upwards. We then write:

$$L = -\int_0^{2\pi} (p_s - p_\infty) \sin\theta \, a d\theta, \tag{9.43}$$

where $p_s$ stands for the pressure at the surface of the circle and $p_\infty$ for that far away from the circle.

The surface pressure can be calculated on a streamline using the Bernoulli law and velocity (9.37):

$$p_\infty + \frac{1}{2}\rho U^2 = p_s + \frac{1}{2}\rho \left(-2U\sin\theta + \frac{K}{a}\right)^2 \tag{9.44}$$

$$\Rightarrow \quad p_s = p_\infty + \frac{1}{2}\rho U^2 \left[1 - 4\sin^2\theta + \frac{4K}{Ua}\sin\theta - \left(\frac{K}{Ua}\right)^2\right]. \tag{9.45}$$

Replacing the pressure in expression (9.43), we obtain:

$$L = -\frac{1}{2}\rho U^2 \int_0^{2\pi} \frac{4K}{U} \sin^2\theta d\theta, \tag{9.46}$$

$$= -2\rho U K \pi, \tag{9.47}$$

$$= -\rho U \Gamma. \tag{9.48}$$

This result is known as the Kutta–Joukowsky theorem and shows that the lift generated on a circle due to its spinning is linearly proportional to the incoming flow velocity and the circulation around the circle. It is independent of the radius $a$ of the circle.

### 9.2.4 The D'Alembert paradox

Jean Le Rond d'Alembert (1717–1783), French polymath, University of Paris.

In a similar way as that we used to calculate the lift force and derive the Kutta–Joukowsky theorem, we can compute the drag force acting on the circle. This force is still due to the pressure profile, but it is horizontal. We write:

$$D = -\int_0^{2\pi} (p_s - p_\infty) \cos\theta \, a d\theta, \tag{9.49}$$

where once again the pressure has to be replaced by expression (9.45):

$$D = -\frac{1}{2}\rho U^2 \int_0^{2\pi} \left[1 - 4\sin^2\theta + \frac{4K}{Ua}\sin\theta - \left(\frac{K}{Ua}\right)^2\right] \cos\theta \, a d\theta, \tag{9.50}$$

$$= 0. \tag{9.51}$$

Thus, according to potential flow theory, the drag of the circle, rotating or not, within a uniform stream is identically zero. This statement can even be generalised to any body of any shape and is known as the D'Alembert paradox.